Analysing Hybrid Drive System Topologies

Karin Jonasson

To know when you know,
and to know when you do not know,
that is knowledge.

Konfucius

Abstract

In this thesis a simulation model is presented that enables a comparison of different hybrid topologies, with respect to fuel consumption, emissions and performance. The obtained results stress the properties of the different topologies and form a foundation for the choice of hybrid topology.

The simulation models included in this thesis are the result of collaboration with Petter Strandh at the Division of Combustion Engines, Department of Heat and Power Engineering, Lund University.

The studied hybrid electric vehicles (HEVs) are restricted to those with an internal combustion engine (ICE), an electrical energy storage and at least one electric machine in the driveline.

The goal with the work presented in this thesis is to:

1. Model hybrid topologies as comparable as possible regarding motor models, battery models, control laws, major energy converters and relevant limitations due to speed and torque.
2. Compare the number of possible topologies, which increase drastically when adding more clutches, electric machines and other components. Therefore only four, however essential, topologies are chosen for the comparison. The four topologies that have been selected are series, parallel, strigear and power split hybrid.

The hybrid topologies have been simulated in two different cycles, the demanding highway cycle US06 and the slower urban cycle ECE15 with its much smoother accelerations.

The reference vehicle in the simulations has been a Toyota Prius, an electric hybrid family car, which is available on the market today. As input for the ICE, measured values from a SAAB naturally aspirated gasoline engine has been used, but scaled to better correspond to the ICE in the real Prius.

There are many possible parameters in the simulation models, that are adjustable; vehicle chassis parameters, engine, electric machine(s) and battery size and types, losses models, charging strategies and driver behaviour etc. To investigate all of them is possibly interesting but not realistic in this survey. It is not the aim and the result flow would be overwhelming. Therefore six key parameters are chosen and thereafter adjusted one by one. The chosen ones are ICE dynamic response time constant, battery inner resistance, ICE charging gain, engine and motor sizes and finally maximum vehicle speed.

The work presents a limited number of results. The results presented have been chosen to illustrate the impact the individual parameter has to the behaviour of the single topology.

The results of the simulated topologies have been compared with measurements made by MTC in Sweden and EPA in USA on a Toyota Prius.

The received results can be evaluated with the help of different criteria. Two different criteria are shown as an example of how the chosen criteria influence the results; the price of fuel consumption and produced emissions respectively a mutual comparison using weight factors.

The results from the simulations made, show that the parallel topology is the most efficient alternative. It is also the topology with the lowest complexity. It should be observed that the differences between the strigear and the parallel hybrid do sometimes not exist or turn to be of advantage to the strigear. The parallel topology however turns to be the preferred choice due to its lower complexity.

Acknowledgements

This thesis marks the end of a journey. It has, once in a while, been made up on a bumpy road. When looking in the rear-view mirror there are several persons who have made a contribution by travelling together with me for a distance, given me guidance during the journey and have encouraged me to continue despite the arisen difficulties.

My supervisor, Prof. Mats Alaküla at Dep. of Industrial Electrical Engineering and Automation, has been a patient guide, a source of inspiration and a long-suffering travelling companion. I would like to thank him for all encouragement and help he has provided me with during this work.

Prof. Gustaf Olsson, my co-supervisor, at Dep. of Industrial Electrical Engineering and Automation, has made a valuable contribution, first of all as a patient listener but also with a lot of encouragements.

I owe Dr Joeri Van Mierlo at Vrije University in Belgium great thanks for helping me in my information retrieval.

Tech. Lic. Anders Lasson at ABB Utilities in Göteborg, Sweden and Dr Anders Malmqusit at ABB Motors in Västerås, Sweden, have also contributed to my literary survey and furthermore with valuable points of view.

Dr Kanehira Marou at Dep. of Machine and Vehicle Design, division of Vehicle Dynamics has also been a reliable information source.

Tech. Lic. Petter Strandh at the Dep. of Heat and Power Engineering, division of Combustion Engines, has contributed with fruitful discussions and has also served as my private Matlab$^{®}$ support in times of difficulties.

I would also like to thank Dr Lars Vedmar and Dr Anette Andersson at Dep. of Mechanical Engineering, division of Machine Elements, for their help with explaining the complex world of gears.

At the Dep. of Industrial Electrical Engineering and Automation there are especially some of my colleagues I would like to mention; Tech. Lic. Christian Andersson for his mixture of teasing and support that keep up one's spirits and MSc EE Sabine Marksell for understanding my struggle and being a sounding board.

There is a life outside the office as well, without its existence I would never have been able to full fill this journey. The interest in my work, shown by family and friends, has been very valuable.

Last, but definitely not least: mum, dad and Lars, tack!

<div align="right">

Helsingborg, May 2002
Karin Jonasson

</div>

Contents

Chapter 1 Introduction

This thesis concerns a comparative study of hybrid electric vehicles (HEVs). Modelling and simulation are key tools in this effort.

1.1 Hybrid Electric Vehicles – a definition

A hybrid is an offspring of two animals, plants etc of two different varieties. A more modern use of the term has come to include man made inventions as well;

… something (as a power plant, vehicle, or electronic circuit) that has two different types of components performing essentially the same function. (Your dictionary, 2001)

Any vehicle, that combines two or more sources of power, is a hybrid. Power sources can be, for instance, ICE, fuel cells, electric machines or muscle power. The HEV studied in this thesis are restricted to those with an internal combustion engine (ICE), an energy storage and at least one electric motor. The intention is that this should lead to improved fuel consumption and lower emissions compared to conventional vehicles. (U.S. Department of energy, 2001 and How stuff works, 2001a)

1.2 Problem Framing

There are many different HEV topologies available, each one with its own pros and cons. The question is how does one compare them? The task in this thesis is to form a model that enables a comparison of different hybrid topologies, with respect to fuel consumption, emissions and performance. The obtained result will then stress the properties of the different topologies and form a foundation for the choice of hybrid topology.

The simulation models included in this thesis are the result of collaboration with Petter Strandh at the Division of Combustion Engines,

Department of Heat and Power Engineering, Lund University. The ICE sub model included in the HEV models is a freestanding section and a part of Strandh's licentiate thesis. (Strandh, 2002)

1.3   Research Goal

There are several hybrid configurations commercially available, that all combine a battery, an ICE, a vehicle propulsion system, required control system etc. There are several vehicles available on the commercial market today, using a number of these various topologies. Usually there is no possibility to make a fair comparison of the topologies since there are too many parameters that differ, as vehicle weight, ICE size and type, control laws, fuel, etc.

The goal with the work presented in this thesis is to:

3. Model hybrid topologies as comparable as possible due to for instance, motor models, battery models, control laws, major energy converters and relevant limitations due to speed and torque.
4. Compare the number of possible topologies, which increase drastically when adding more clutches, electric machines and other components. Therefore only four, however essential, topologies are chosen for the comparison. The four topologies that have been selected are series, parallel, strigear and power split hybrid.

The comprehensive hybrid models consist of detailed sub models of the included units, such as electric machines, ICE, power distribution, transmission etc. The ICE model simulates not only the stationary operation, but also the transient operation. This facilitates to take into account the consequences of different control laws in the fuel consumption and the emissions, even in transient operation.

The aim with the models is not to execute the economic consequences of the selected topologies. They can vary drastically, due to new research results and political decisions etc. Rather, the aim is to demonstrate a systematic way of comparing different topologies and give a framework for such a work.

The simulation models are furthermore made disregarding the long-term effects that, can, affect the vehicle components.

1.4   Criticism of the sources

There is a major obstacle in the comparison of commercial systems. Often there is a great difficulty to get comparable data for the included components. Often the manufacturers do not wish to reveal certain parameters, and

sometimes the parameter values are not comparable. In order to overcome this available vehicle data have been completed with data measured in lab and then scaled it to suitable size. In other cases the data has been estimated. The assumption used for this is separately accounted for.

1.5   Main Results

Four different HEV topologies have been investigated in this comparison; parallel-, series-, strigear- and power split HEV. The results from the simulations made, show that the parallel topology is the most efficient alternative. It is also the topology with the lowest complexity.

Fast ICE dynamics, i.e. short charging time constant, load the battery less and leads to a lower fuel consumption.

The gain factor, which controls the power demand as a function of the deviation in battery SOC, influences the fuel consumption too. A large gain factor does not utilize the battery as a power buffer. A small gain factor leads to large battery losses.

1.6   Outline

A definition of the conception hybrid is presented in Chapter 1, together with a problem framing and a brief summary of the results.

In Chapter 2 details are given about the advantages with hybrid electric vehicles. The main behaviours of an internal combustion engine are also described. The four hybrid topologies that will be investigated in this thesis are presented. The chapter ends with a presentation of the criteria that will constitute the basis for forming a judgement of the topologies.

Chapter 3 contains the fundamental equations, used in the simulation models. The sub models are described one by one, including the distribution of the demanded traction power, which is unique for each topology.

The simulation platform is presented in Chapter 4 and the implementation of the models described.

The chosen driver cycles are presented in Chapter 5. The reference vehicle is also described and the variables and parameters selected. Thereafter follow the simulation results.

The conclusions are given in Chapter 6. They are followed in Chapter 7 by future work and references in Chapter 8. At the end, as Chapter 9, are the appendixes.

Chapter 2 Hybrids

2.1   Motivations for Hybrid Systems

The pure electric vehicles (EV) are still not ready to conquer the market from the conventional vehicles. The main reason is the shortcoming of the batteries. The energy supply is simply not enough for longer trips. Therefore a hybrid of today combines the extended range of a conventional vehicle with the environmental benefits of an electrical vehicle. This results in a vehicle with improved fuel economy and lowered, yet not zero, emissions (How stuff works, 2001a). The main drawback with a HEV is the price that is higher due to increased complexity.

When following a drive cycle, the ICE of a non-hybrid vehicle uses a lot of different torque - speed combinations, i.e. operation points. The hybrid vehicle control laws forces the traction system to chose operating points leading to e.g. the highest efficiency possible or the lowest emissions. Studying the time spent at different operating point and weighting them against the ICE efficiency, gives a hint of how efficiently the vehicle uses the added fuel. This is shown in Figure 2-1. Figure 2-1 a) shows the ICE from a conventional car, driving a very demanding drive cycle (US06) with the best possible choice of gear ratio at any time. The upper curve illustrates the ICE efficiency at different operating points. Figure 2-1 b) shows a HEV ICE in the same drive cycle. The main difference shown in the two figures is the absence of operation points at low efficiency for the HEV.

The goal, to minimize the use of non-efficient operating points, is more or less easy to achieve depending on the chosen hybrid topology.

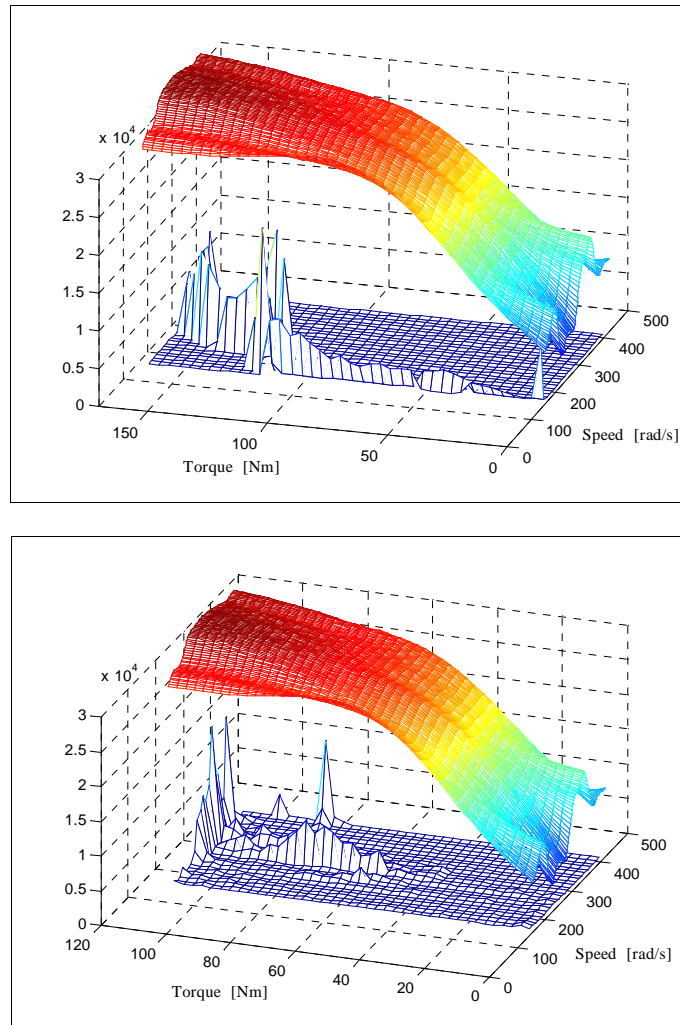Figure 2-1:   Operating diagram for ICEs. The upper figure is from a conventional
              car and the lower figure is from an electric hybrid vehicle. The upper
              curves in the figures are the ICE efficiency at different operation points.
              The lower curve shows the time spent by the engine at different
              working points, divided with the present efficiency.

2.2 Key Characteristics of Hybrid Electric Vehicles

Emissions

At certain conditions ideal combustion can occur in an ICE. This means that all hydrocarbons are transformed into carbon dioxide (CO_2) and water (H_2O). This is called stoichiometric combustion. $(A/F)_S$ is the stoichiometric air (A) to fuel (F) mixture, i.e. the mixture that leads to complete combustion. The ratio between the amount of actual and stoichiometric fuel-to-air mixture is better known as λ, defined in equation 2-1.

$$\lambda = \frac{\left(\dfrac{A}{F}\right)_{actual}}{\left(\dfrac{A}{F}\right)_s} \qquad (2\text{-}1)$$

When $\lambda \neq 1$, all fuel is not transformed properly and residual products, emissions, occur. Some emissions are governed by legislative regulations and some are not. Hydrocarbon (HC), carbon monoxide (CO) and nitrogen oxide (NO_x) are included in the regulated ones. Among the unregulated residues there are formaldehyde and polyaromatic hydrocarbons.

At combustion with a deficiency or surplus of oxygen incomplete combustion causes HC to be formed. The hydrocarbons are poisonous to human and can cause cancer.

Oxygen and nitrogen in the air react at high temperatures at combustion (> 1800 K) and forms NO_x. The NO_x reacts with water and causes acid rain, which is detrimental to the environment. It also causes choking and can cause cancer.

CO is formed at imperfect combustion from CH to CO_2 with a deficiency of oxygen or at uneven fuel mixture. CO outlet blocks the ability to absorb oxygen in any air-breathing body.

Mostly vehicles today are equipped with a three-way catalytic converter (TWC) to reduce the emission. The TWC is coated on the inside with a noble metal that causes the CO to convert to CO_2 and the HC into CO_2 and water. Furthermore the TWC converts the NO_x back to N_2 and O_2.

This emission reduction is strongly dependent on the λ value. There is only a small λ–window where this works.

Figure 2-2 shows the variations of HC, CO and NO_x before TWC and Figure 2-3 shows the emission after reduction in the catalyst (Haywood, 1988). Note the small λ-window. The exact shapes of the graphs are depending on the engine configuration.
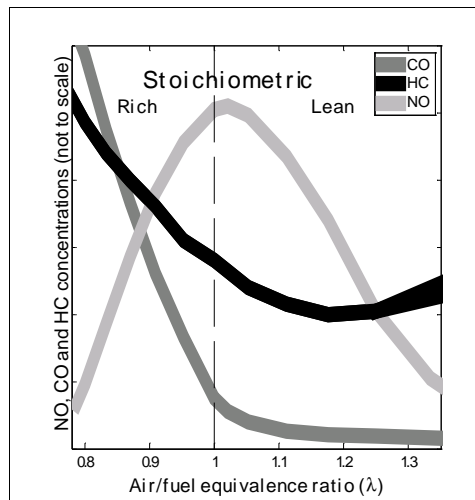

Figure 2-2:   The figure shows the variation of HC, CO and NO concentration in the exhaust of a conventional spark-ignition engine with air/fuel equivalence ratio.
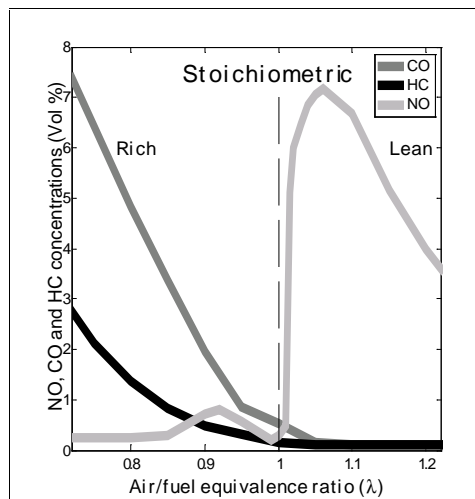

Figure 2-3: Remaining emissions after a three-way-catalyst.

At fast acceleration, the power demand changes transiently and forces the λ value outside the λ-window, since the TWC-control algorithm is too slow.

In a HEV it is possible to achieve λ=1 by choosing a control law that uses the electric machines for transient power demand. The ICE strain is therefore controllable and neither to little nor to much oxygen is available at fuel combustion. (Andersson et al, 2000, Johansson, 1999, Bäckström, 2000, Heywood, 1988) A good popular description can be found in (How stuff works, 2001b).

Fuel consumption

The fuel consumption, or brake specific fuel consumption (bsfc), during combustion is depending on several elements. The ICE speed and torque demand on the traction power demand and the ICE control laws affect the bsfc. The specific engine's design influences the consumption as well as the fuel energy contents and finally the driver's behaviour.

The chosen combination of torque (T) and speed (ω) is influenced of different losses. At high ω the mechanical friction losses increases but at low ω the cooling losses are dominating. The flow losses are dominating at high T. At lower values the pump losses are prevailing. The T/ω characteristic of an ICE is shown in Figure 2-4.
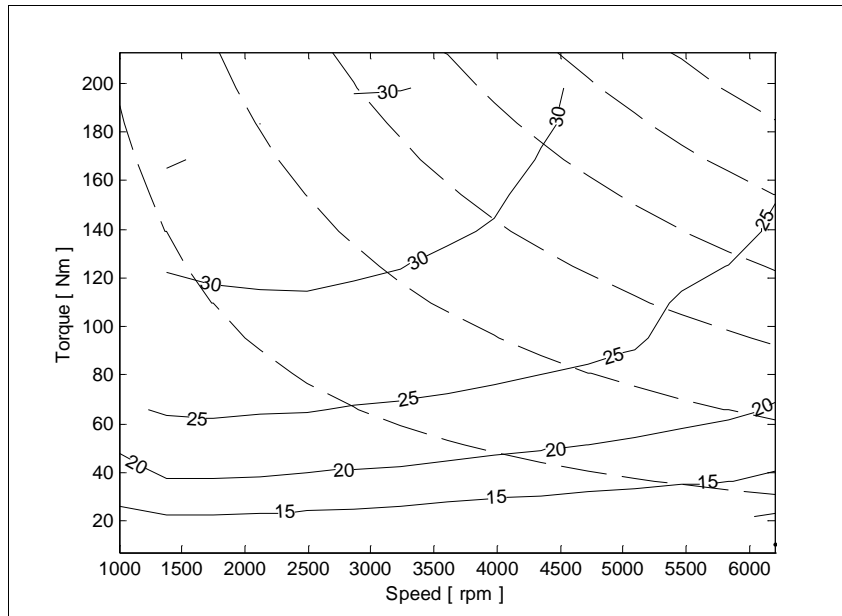
Figure 2-4:   Efficiency diagram. The ISO lines (dashed) indicate where a certain
               power will be supplied by the highest efficiency.

Efficiency

Efficiency is a standard of the relation of the capability to transform input
to output, such as fuel to kinetic energy. The theoretical efficiency of a spark
ignition engine (Otto) is given in equation 2-2. An ordinary Otto engine has
maximum efficiency of around 33%, while the efficiency of a Diesel engine is
approximately 45% (due to higher compression ratio, ε).

$$\eta_t = 1 - \frac{1}{\varepsilon^{\kappa-1}}$$

(2-2)

η_t = theoretical efficiency of a piston engine (ICE), ε = compression ratio of an
ICE, κ = the adiabatic exponent (= c_p/c_v), c_p = specific heat of a gas at constant
pressure, c_v = specific heat of a gas at constant volume

Increasing ε involves increasing friction losses. Therefore the results do not
necessarily lead to higher efficiency. The temperature also affects the
efficiency. The mechanical efficiency is described in equation 2-3.

$$\eta_m = 1 - \frac{p_f}{p_i} \tag{2-3}$$

η_m = mechanical efficiency of an ICE, p_f = mean pressure to overcome the mechanical friction loses, p_i = indicated mean pressure of a combustion engine

As p_i is increased, η_m increases too. This is possible by increasing the load, which implies a higher torque. The ICE efficiency is therefore higher at high torque and not too high rotational speed. The latter is due to friction losses.

The efficiency of a hybrid is not only depending on the ICE but also on the electric machines, the battery, the transmissions and the power electronics etc. The specific choice of the single components and system control makes up the total efficiency. The total efficiency is inversely proportional to the bsfc. (Heilig, 1985, Johansson, 1999, Bäckström, 2000)

Dynamic behaviour

To accelerate the vehicle the driver will step on the gas. This causes increased torque since the throttle, to which the gas pedal is connected, controls the airflow to the inlet manifold.

To minimize the emissions the mixture of air and fuel is carefully adjusted to be within the λ-window. If the mixture is allowed to get too lean the engine will start to misfire. The sudden increase of air in connection with acceleration has to be counteracted with fuel, so that λ remains constant. To manage this the engine controller usually orders injection of sufficient amount of fuel to avoid misfire. On the other hand, this can cause the engine to run fuel rich.

The suddenly increased amount of fuel jeopardizes in its turn the temperature in the cylinder since the amount of heat, produced by the engine and used to vaporize the fuel, will not be sufficient. The increased fuel injection has thereby a cooling effect on the cylinder and the fuel will condense at the cylinder walls. The vaporizing of the fuel will hereby be delayed and the λ-control will be unstable, that is the amount of emission will increase since $\lambda \neq 1$. (Johansson, 1999)

In Figure 2-5 the airflow through the throttle and the obtained torque are shown at stationary conditions. The figure displays the torque while the engine runs at $\lambda=1$. Tuning effects at transient load changes are not included.

It should be mentioned that the high torque at low speed is not achievable during normal conditions. This is due to the fact that the airflow will be

insufficient. The pressure in the manifold is limited and can't get higher than the ambient pressure. However, the airflow can be increased with a supercharger, resulting in an increased torque.
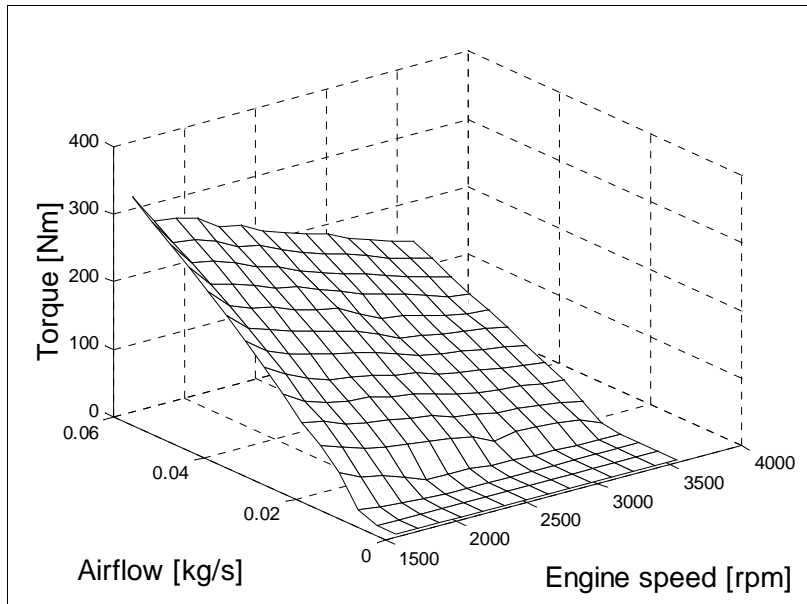

Figure 2-5: The air map of an ICE.

During transients, the engine will *not* run at $\lambda = 1$. This affects in its turn the achieved torque, which has to be corrected for the actual λ value. (Equation 2-4.) Figure 2-6 shows an example of such correction. (Standh - Egnell, 2001)

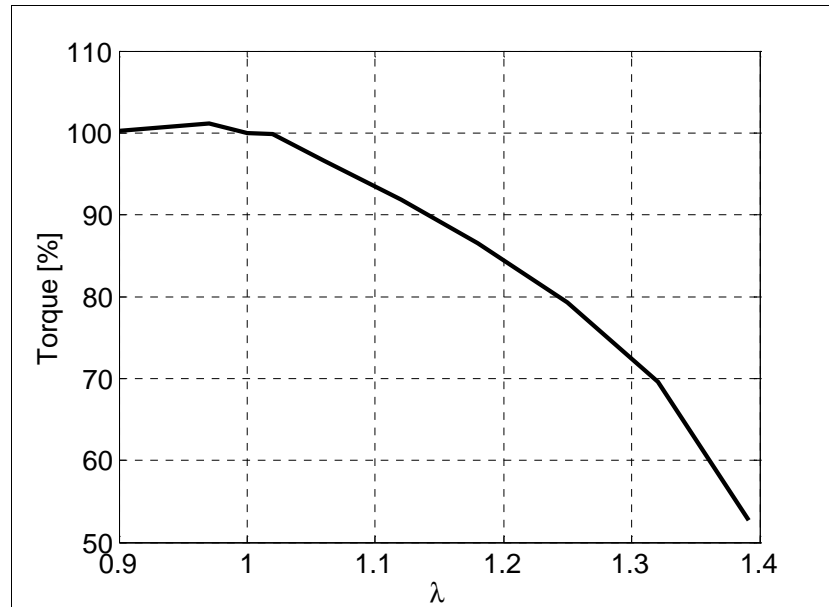$$T_{actual} = f\left(T_{air\_flow}, \lambda_{actual}\right)$$

(2-4)

Figure 2-6: Torque reductions as function of λ.

The λ-control is possible to manage as long as the changes of the torque demand aren't too large or at least not too rapid. Expressed as a bandwidth, operating point-changes that are slower than approximately 2 Hz can be handled by the λ-control system. The torque changes can be seen as settled by feed forward of fuel injection and tardiness in the system, i.e. the demanded torque is low pass filtered by the system itself.

When mounting an electric machine in an ordinary vehicle one of the primary advantages is the possibility to let the electric machines handle the transient changes and thereby reduce requirement on the fast dynamics in the ICE. The transients are instead loaded on the batteries, which of course causes electric losses. In return, the emissions can be controlled within desired limits, while this strategy keeps $\lambda \approx 1$.

2.3   Topologies

The tractive system of a hybrid electric vehicle includes both an ICE and, at least, one electric machine. There are many ways of combining the included components and consequently the number of possible hybrid topologies is very large, considering the combinations of electric machines,

gearboxes, clutches etc. (Harbolla, 1992) The two main solutions, series and parallel hybrid, can be supplemented in a numerous amount of combinations, each one with its pros and cons. The topology efficiency is depending on the chosen vehicle solution with its unique characteristics and the actual working condition.

The topologies chosen in this work are commented in the following sections 2.4 - 2.7.
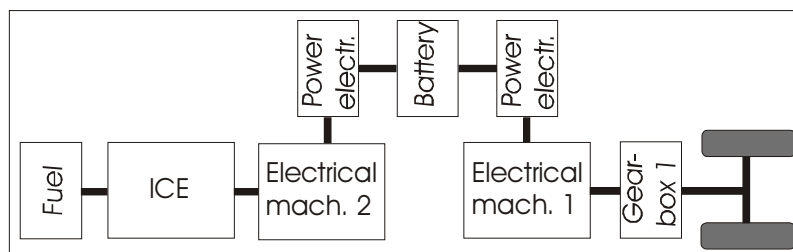
2.4   Series

Figure 2-7: Series hybrid topology.

The series hybrid has no mechanical connection between the ICE and the wheels. The ICE working point, i.e. speed and torque, can therefore be chosen freely, but at the expense of many energy conversions. The thermal energy is converted into mechanical energy in the ICE, and thereafter, in the generator, turned into electric energy. The generator charges the battery that in its turn supplies the electric traction motor(s). On its way the energy also passes power electronics twice. These many energy conversions cause the topology a significant reduction of the system efficiency. In the simulations made, the ICE of the series hybrid is controlled to work at the best possible efficiency. The ICE efficiency is depending on the average power demand.

The electric machine 1 in Figure 2-7, i.e. the traction motor, has to be designed for peak power and the generator is designed for the ICE power. The simplest series hybrid vehicle is an electric vehicle, equipped with a range extender.

An advantage with the topology is that the ICE can be turned off when the vehicle is driving in a zero-emission zone. Yet another merit of the topology is that the ICE and the electric machine can be mounted separately. This involves a possibility to distribute the weight of the vehicle drive system and in buses an opportunity to use low floor. (Hemmingsson, 1999, Van Mierlo et al, 1998)

2.5   Parallel
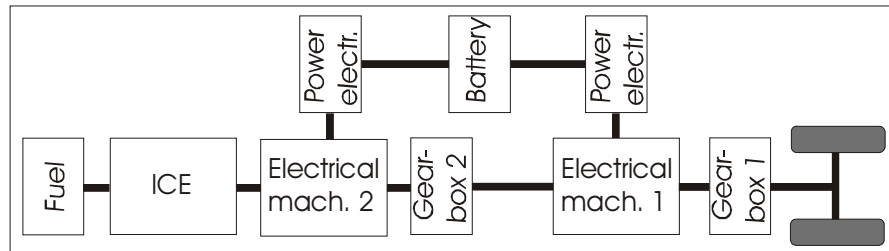
Figure 2-8: Parallel hybrid topology with one optional electric traction motor.

The parallel hybrid is a combination of drive systems (see Figure 2-8). The ICE is mechanically connected to the wheels via a gearbox. The gearbox (no.2) used in the simulations, is made variable into 5 steps. Gearbox 1 is given a fixed gear. The reduced amount of power conversions can potentially increase the efficiency of the vehicle as compared to a series hybrid.

The working point of the hybrid can be chosen freely with the help of the electrical machines, i.e. the speed of the ICE is chosen with the gearbox(es) and the torque with the electric machine(s). There are four options available: pure electric operation, pure ICE operation, electric operation but ICE is charging the battery and finally operation with all power sources. To achieve peak tractive power, both ICE and electric machine 1 are used. The parallel topology is also possible to achieve with only one electric machine.

A relative to the parallel topology is the dual mode hybrid where the electric motors drive the vehicle via one axle each. (Van Mierlo, 2000)

2.6   Strigear

Figure 2-9: Strigear hybrid topology.

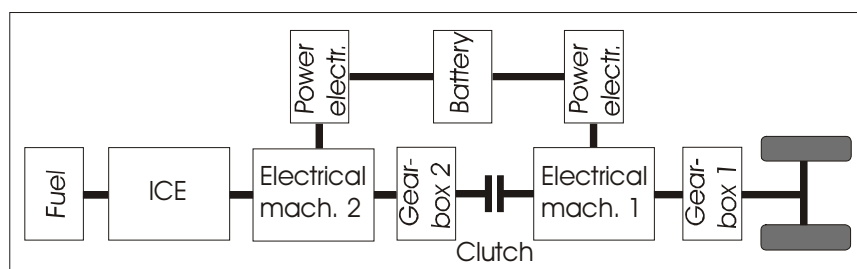The strigear hybrid is actually a combination of a parallel and a series hybrid vehicle (see Figure 2-9). (Stridsberg, 1998) By adding a clutch in between the electric machines in a parallel HEV equipped with two electric machines, it is possible to switch from parallel to series mode. The onboard computers are given the task to compare the predicted over all losses from the two hybrid concepts. The best solution is chosen, i.e. the clutch is engaged or disengaged.

The name s*trigear* is a short form of "sequentially run, triple gearbox connected engine/motor hybrid". (Powertrain, 2001) This demands two electric machines, one extra clutch and computer capacity to handle the momentary loss comparison that is made. The benefit is the ability to choose the best configuration at any time with respect to e.g. losses.

Van Mierlo, who designates all topologies different from series and parallel complex hybrid vehicle, also refers to this solution as combined hybrid. (Van Mierlo et al, 1998, Van Mierlo, 2000)

2.7   Power Split
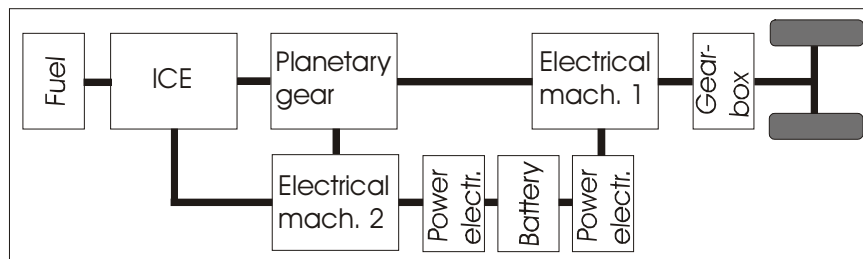
Figure 2-10: Power split hybrid topology.

The Power Split Hybrid (PSH) has a blurred transformation between the series and parallel hybrid state (Figure 2-10). The PSH is even called complex, combined or dual hybrid vehicle.

A planetary gearbox (Figure 2-11) connects the two electrical machines and the ICE. The traction motor (electric machine 1) is connected to the ring wheel, the generator (electric motor 2) to the solar wheel and finally the ICE is connected to the carrier and thereby possible to switch off and the vehicle can drive in a pure electric mode. Owing to the connection of the sun wheel and the planet wheels the speed of the engine can simply be adjusted by varying the speed of the generator.

At most operating points some of the prime energy flows from the ICE to the wheels via the gearbox as in a parallel hybrid, and some flows via the electrical machines as in a series hybrid. The proportion between these two energy flows is speed dependent and at a certain speed it works as a pure parallel hybrid. In most other operating points it's partially a parallel hybrid and partially a series hybrid. The latter means several conversions of the energy that flows the "series" way from the prime energy source to the wheels. This hints that it is difficult to get the system efficiency lower than the parallel hybrid efficiency.

There are many possible combinations of a PSH. While using reduction gears, CVT, advanced planetary gear, clutches and different numbers of motors the possible number of combinations grows rapidly. The drawback with the topology is that it can cause a power vicious circle that cost unnecessary high transmission losses.

Planetary gear

The planetary gear (Figure 2-11) has three shafts, which are connected to the sun-, carrier- and the ring wheel. They are connected to the electrical machine 2, the ICE and the electrical machine 1 respectively. The size and number of the wheels, number of pinions, number of planets, wheel inertia, rotational friction etc influences the behaviour of the gear.
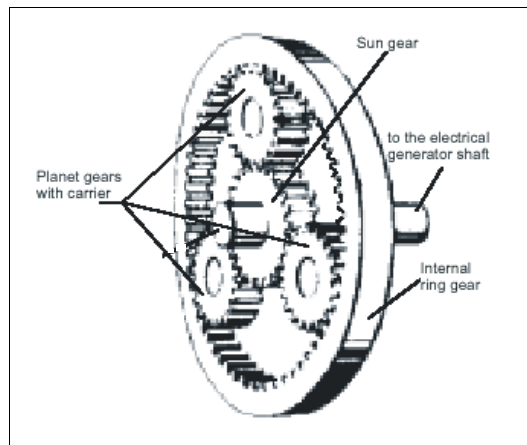

Figure 2-11:   Planetary gear. The numbers of planet wheels are variable but influence the equations.

In the simulation model the fundamental dynamic equations for the planetary gear have been used, see equation 2-5 - 2-9. (Vedmar, 1998)

$$A = \frac{J_p}{g_p} - \frac{J_p}{g_p}\frac{z_r}{z_p} - \frac{J_s}{g_s}\frac{1+\frac{z_r}{z_s}}{n} \tag{2-5}$$

$$B = m_p\rho^2 + \frac{J_c}{n} + J_s\frac{1+\frac{z_r}{z_s}}{n}(1+\frac{z_p}{z_s}) \tag{2-6}$$

$$\dot{\omega}_r = (T_r\frac{1-\frac{z_p}{z_r}}{n} + T_s\frac{1+\frac{z_p}{z_s}}{n} + \frac{T_c}{n})A - (\frac{T_r}{ng_r} - \frac{T_s}{ng_s})B \Bigg/$$

$$(J_r\frac{1-\frac{z_p}{z_r}}{n} - J_s\frac{z_r}{z_s}\frac{1+\frac{z_p}{z_s}}{n}(A - (\frac{J_p}{g_p}\frac{z_r}{z_p} + \frac{J_r}{ng_r} + \frac{J_s}{ng_r}\frac{z_r}{z_s})B \tag{2-7}$$

$$\dot{\omega}_c = \frac{1}{A}\left((-\frac{J_p}{g_p}\frac{z_r}{z_p} - \frac{J_r}{ng_s} - \frac{J_s}{ng_s}\frac{z_r}{z_s})\ddot{\Phi}_r + \frac{T_r}{ng_r} - \frac{T_s}{ng_s}\right) \tag{2-8}$$

$$\dot{\omega}_s = -\frac{z_r}{z_s}\dot{\omega}_r + \left(1+\frac{z_r}{z_s}\right)\dot{\omega}_c \tag{2-9}$$

c = carrier wheel, g = a radius (see Figure 2-12), J = moment of inertia, m = mass, n = grasping of teeth with the planet wheel(s), p = planet wheel, r = ring wheel, s = sun wheel, z = number of tooth, ρ = a radius on which the circumferential forces $n \cdot T$ acts, T = torque
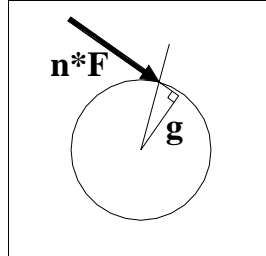
Figure 2-12: The figure shows a schematic picture of forces of a cogwheel (n = grasping of teeth with the planet wheel(s) and F = tooth load) and the location of the radius g.

By forming a matrix and replacing the expressions formed by invariables (moment of inertia, numbers of teeth, number of planet-wheels and mass of the planet wheel etc) with k_{11}, k_{12} and k_{13} etc, the equations are given the following structure where T_{frict} is the load on the ring wheel due to road and rolling friction on the car (Vedmar, 1998, Eiraku et al, 1998). See equation 2-10.

$$\frac{d}{dt}\begin{bmatrix} \omega_r \\ \omega_c \\ \omega_s \end{bmatrix} = \begin{bmatrix} k_{11} & k_{12} & k_{13} \\ k_{21} & k_{22} & k_{23} \\ k_{31} & k_{32} & k_{33} \end{bmatrix} \cdot \begin{bmatrix} T_r \\ T_c \\ T_s \end{bmatrix} + \begin{bmatrix} k_{11} \\ k_{21} \\ k_{31} \end{bmatrix} \cdot T_{frict} \qquad (2\text{-}10)$$

2.8   A   Qualitative   Comparison   of   Different Topologies

The configuration in the series hybrid involves an increased amount of components in the vehicle compared to a parallel HEV, for example two units with power electronics. The number of possible losses increases with increased amount of components as well as the EMC is increased. In Table 1 the number of components needed for each topology is quantified. In the parallel topology it is possible to model with one or two machines. Depending on the chosen solution the number of components will vary. It should also be mentioned that the amount of components could be increased further with additional clutches, CVTs, gears, ISG and new control algorithms.

Table 1:   Number of components included in the presented topologies. Figures in parenthesis mark possibility for divergent number of components.

Component:	Series:	Parallel:	Strigear:	Power split:
ICE	1	1	1	1
Electric machine	2	1 (2)	2	2
Battery	1	1	1	1
Gearbox	1	1 (2)	2	1
Power electronics	2	1 (2)	2	2
Clutch	-	-	1	-
Planetary gear	-	-	-	1

The power losses are a key parameter. The more transformations the tractive power has to pass, the higher the losses will be. The straightest power path is found in the parallel topology. The worst power path is found in the series topology. The other two are a mixture of the previously mentioned two topologies. Then the losses are more difficult to define. Their losses will nevertheless fall short of the losses in parallel topology.

Some of the most important pros and cons of the four investigated topologies are presented in Table 2.

Table 2: Pros and cons with the four investigated hybrid topologies.

Topology:	Positive qualities:	Negative qualities:
Series	ICE working point can be chosen freely ICE can be turned off ICE can be mounted with or separated from the electric tractive motor → distribute weight and facilitates low floor	Many energy conversions → low efficiency Electric machine 1[1] must handle peak power
Parallel	ICE directly connected to the wheels → few power conversions Due to the electric machine and the gear boxes the ICE working point can be chosen freely	ICE and electric machine must be mounted together → no low floor
Strigear	Offers the most efficient solution possible at any time regarding losses Reduces the amount of power transformations	The components size etc are fixed, i.e. it is working as a series hybrid equipped as a parallel hybrid Demands many components (electric machines, power electronics, etc) Switching modes can't be performed infinitely fast.
Power split	ICE can be turned off ICE speed can be chosen by adjusting the generator speed	A power vicious circle can occur → low efficiency

To sum up the pros and cons, it can be said that a hybrid topology including fewer power transformations will result in a higher efficiency. An increased amount of components involved will also result in an increased vehicle price. The parallel hybrid includes the purest solution and the series the one with highest amount of losses. The other two topologies are more blurred in their transition of topologies. The chosen control law is, to some extent, determining the power losses. Consequently, the efficiency is not easy to calculate in advance.

---

[1] See Figure 2-7.

Hybridisation

To define, categorize and better understand HEV there are some possible definitions to use. *The Order of Hybridisation* is equal to the number of different systems that are necessary to build the specific drive train. A pure electric vehicle is of first order, a parallel hybrid with one engine and one electric motor is of second order and a power split or a strigear hybrid is of third order of hybridisation. (Baretta, 1998)

To get an indication of the range and performance of a hybrid vehicle the concept *the Electric Hybridisation Rate* (EHR) can to be used. It is a ratio between the electric power and the total traction power, expressed in percentage. (Equation 2-11.) A higher ratio indicates that the hybrid is to a higher degree an electric vehicle, i.e. the hybrid is equipped with a large traction motor. (Maggetto et al, 1997)

$$EHR = \frac{electric\_power}{traction\_power} \qquad\qquad (2\text{-}11)$$

A similar way to validate a vehicle is *the Combustion Hybridisation Rate* (CHR). This concept renders the contribution from the ICE to the hybrid. The ratio is expressed in percentage and a higher value indicates that the vehicle tends to be a pure thermal vehicle. See equation 2-12.

$$CHR = \frac{thermal\_power}{traction\_power} \qquad\qquad (2\text{-}12)$$

The sum of EHR and CHR is always one and each concept is just an indication whether the vehicle lends towards a pure electric or a pure thermal vehicle. To investigate the relative contribution of each energy source to the traction system *the Ratio of Hybridisation* (RH) has to be defined. As the systems contribute equally the rate is one. The concept is only valid for HEV of the second order. First order vehicles have the ratio zero. For hybrids more complex than of second order is the RH not useable, since it is not straightforward. (Van Mierlo, 2000) See equations 2-13 and 2-14.

$$\text{If } P_{el} < P_{th} \qquad RH_{th} = \frac{P_{el}}{P_{th}} \qquad\qquad (2\text{-}13)$$

$$\text{If } P_{th} < P_{el} \quad RH_{el} = \frac{P_{th}}{P_{el}} \tag{2-14}$$

2.9   Criteria

When deciding which topology that stands out as the best choice, "the best" has to be decided. That is which variables are to be chosen to mould the crucial criteria since the output variables available are overwhelming.

There is yet another question to answer: why are these variables chosen instead of others available. By defining these key values, there is a foundation to point out a single topology that will suite our goals better than the others investigated.

There are many possible criteria to use as a base for judging the topologies, such as purchase price, operative expenses, emissions, observable performances and ride comfort. Some criteria are imperative like legislation, some are subjective, others are strongly fluctuating depending on location and political decisions and yet others are immediately measurable.

Fuel

Consumption

For a vehicle, especially a heavy vehicle operating in traffic, the purchase price is by far surpassed by the operating expenses. The fuel consumption is one of the main items among the working expenses. An established value for vehicle comparison has become the fuel consumption, or rather just because of its impact of the running costs.

The fuel consumption is depending on engine design, aerodynamic design, drive cycle, driver behaviour etc. The vehicle weight has an important impact. There is a method available to calculate the effect that a revised vehicle design will have at the fuel consumption. From a general point of view 50 kg extra vehicle weight is equivalent to 100 W losses. (Miller – Nicastri, 1998)

Pricing

In the light of these facts, it is of interest to obtain a more upright price of the total vehicle working expenses. Though fuel prices are varying depending on political decisions, the world situation etc, there is a possibility to use a "fixed price", *knowing* that is fluctuating depending on definable reasons. In Figure 2-13 the fuel price in Sweden during 2001 is shown. The graph shows

a monthly average, since there were more then one hundred price changes during 2001. The price represents the 0-zon, which are costal areas. Inland areas demand longer transportations, which leads to more cartage.

The average cost 2001, for 1 litre petrol, were 9.52 SEK (Euro 1.02). The peak in April and May is mainly depending on the habit among the fuel distributors to create a buffer before the summer season. (Preem, 2002)
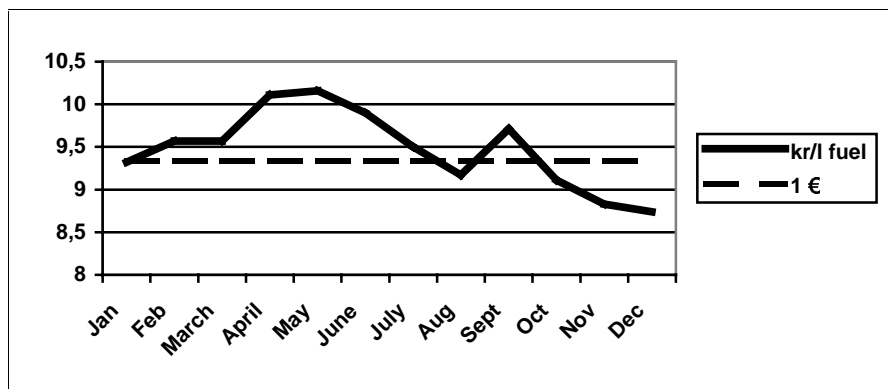

Figure 2-13: Fuel price, mean value for each month during 2001. The price is from 0-zon, i.e. coastal areas in Sweden. Source: Preem petroleum AB. 1 Euro= 9.34 SEK. Source: Forex AB, 2002-02-20.

Emissions

Measuring

The environmental impact the use of a vehicle has is also an interesting variable. The emissions are not linearly dependent on fuel consumption or mileage. The construction of machinery, in connection with vehicle design, drive cycle, driver behaviour, choice of fuel etc is together founding the total emissions. Last but not least, the emissions are affecting the environment from the very first pollution.

When measuring emissions, it is important to keep in mind that the result can vary from time to time. One reason is the temperature, both the outdoor temperature, but also the temperature of the engine. The measuring methods are another cause. Hereby is it wise to handle the absolute emission figures with care. However using the emission results, as an instrument for reciprocal comparison, where the mutual order of magnitude is in focus, is on the other hand not suffering from possible sources of errors to the same extent.

The emissions in this survey are specified in g/km. The emissions during a drive cycle are accumulated and a mean value for the cycle is created. By using an average value instead of the sum of emissions from a cycle, is it possible to compare cycles with different length.

Pricing

The damage of the green house gases, toxic pollutions etc are priceless. Even though there are price labels possible to use and their correctness can be questioned.

Authorities have their opinion of the "price" of emissions and by introducing taxes they endeavour to reduce the emergence of emissions. The taxes are often used as a control instrument and are influenced by occurrence in the world around, i.e. international environment agreements. The tax levels are not an easily defined function of the environmental impact.

As a result of taxes, emission quota assigned to companies by authorities, and penalty fees when the outlet figures are exceeded, a market for emission quota has arisen. This brings about another emission price, assigned by the market and fluctuating as like stock-exchange prices (Emissionstrading, 2002).

The EPS system, that is a systematic approach to *E*nvironmental *P*riority *S*trategies in product development, is developed to assist designers and product developers to find which of two product concepts that has the least negative impact on the environment. The system is based on Life Cycle Assessment methodology. EPS is also founded on ISO standard frameworks (ISO 14040-43).

As validation in the EPS system the unit ELU (Environmental Load Unit) is used. 1 kg fish or meat is considered as 1.0 ELU. This is meant as 1 kg protein grazing in the enclosed field or swimming in the lake. Not the steak sold by the butcher. The economic value of 1 ELU is about equal to 1 Euro. The emissions are then estimated as environmental load and given an index in ELU/kg (Steen, 1999, Steen – Ryding, 1992). The EPS values for the investigated emissions are shown in Table 3.

Table 3: Default impact indices for emissions.

Emission:	Cost [ELU / g]:	Source:
NO_x	$2.13*10^{-3}$	EPS
CO	$0.331*10^{-3}$	EPS
HC	$2.14*10^{-3}$	EPS

There are assessments made on air emissions. These estimations are strongly discussed and once in a while revised. SIKA (Statens Institut för Kommunikations Analys) has made cost estimations for effects of emissions on behalf of the Swedish government. Their reports from 1999 and 2000 account some emission pricing. The NO_x validation became quite controversial, and the pricing has therefore been revised since the reports were published. (SIKA 1999 and 2000)

The validation of NO_x is, among other things, depending on location. In this case the NO_x pricing for larger urban area (Stockholm) has been used, and it is the value of their regional effects that have been used.

SIKA does not estimate the cost for CO anymore, but they have done. The pricing of CO ordinates from calculations carried out by Banverket (the Swedish National Rail Administration), by recommendations from SIKA. (Banverket, 1992) It should however be mentioned as addendum that Banverket does not use pricing for CO anymore. See Table 4.

Table 4: Validation of regional effects of emissions in urban areas.

Emission:	Cost [/ g]:	Source:
NO_x	$2.57*10^{-3}$	SIKA
CO	$0.21*10^{-3}$	SIKA
HC	$3.22*10^{-3}$	Banverket

There are other quotations available also. The European Commission has carried out some estimation for pricing emissions (ExternE, 1999). Two of the authors of that report have also published a separate paper, which includes validation of external costs in urban transports in the city of Baden-Württenburg (Friedrich – Bickel, 2002). Their estimations include highway driving, rural- and urban traffic. See Table 5.

Table 5:   Emission costs in Baden-Württenberg. The original table was written in DM/ton. In the conversions 1 DM is considered as 0.485 Euro. Source: Forex AB 2002-02-28.

Emission:	Highway [Euro / g]:	Rural [Euro / g]:	Urban [Euro / g]:	Source:
NO_x	$5.87*10^{-3}$	$5.87*10^{-3}$	$5.87*10^{-3}$	Friedrich - Bickel
CO	$0.82*10^{-6}$	$0.92*10^{-6}$	$2.13*10^{-6}$	Friedrich - Bickel
HC	$1.57*10^{-3}$	$1.57*10^{-3}$	$1.57*10^{-3}$	Friedrich - Bickel

Performance index

Ranking

Four of the possible outputs are used as output variables from the simulation models. These are bsfc, NO_x, CO and HC. Since this is a comparison with above defined four HEV topologies, and no other model or existing vehicle, only relative results are of interest.

One possible criterion is therefore that the emission and fuel consumption are placed in mutual order of rank. The best topology, i.e. lowest emission or fuel consumption, is given the best rank (1) and the worst topology is given rank 4, and so forth. This is then done with all four variables.

Weighting

The different topologies included in this comparison will deliver different values on the measured items. It is therefore important to find a way of weighting these results mutually. There are many ways to do this, each one with its pros and cons. The chosen one is done with the above shown argumentation as its base.

Since there is uncertainty to some extent concerning the measuring of the emissions, they are given a smaller weight than the fuel consumption. The uncertainty among the three emissions is considered being equal. By taken these argument into consideration, the variables are given the following weight; $\alpha_{bsfc} = 1.0$, $\alpha_{NOx} = 1/3$, $\alpha_{HC} = 1/3$ and $\alpha_{CO} = 1/3$.

These weighting factors are not absolute figures. They can be adjusted when the circumstances are changed, driving in an emission sensitive area for instances, or the reliability of the figures has been updated. This gives us a base to found a criteria table, usable in our comparison.

Criteria options

There are, as above discussed, foundation for many different criteria. In this comparison two different criteria are going to be used, pointing out the importance of the chosen weighting factors.

The first criteria have the price as weighting factor (equation 2-15) and in the second criteria is the order of rank weighted with a presumed reliability factor (equation 2-16).

$$criteria_1 = bsfc \cdot price + NO_X \cdot price + CO \cdot price + HC \cdot price \qquad (2\text{-}15)$$

$$criteria_2 = 1 \cdot rank_{bsfc} + \frac{1}{3} \cdot rank_{NO_X} + \frac{1}{3} \cdot rank_{CO} + \frac{1}{3} \cdot rank_{HC} \qquad (2\text{-}16)$$

The criteria result from the different topologies, simulated with the chosen drive cycles and are summarized in Table 6 and Table 7. In Chapter 5.4, the true results are presented in these tables.

Table 6:   Comparison table, using the criteria 1. Lowest result figure gives "the best" topology, when using criteria 1.

Topology	Bsfc [l/10 km]	NO$_x$ [g/10 km]	CO [g/10 km]	HC [g/10 km]	Drive cycle	Result Criteria 1
Price [Euro]						
Parallel						
Series						
Strigear						
Power split						

Table 7:   Comparison table, using the criteria 2. Lowest result figure gives "the best" topology, when using criteria 2.

Topology	Bsfc [l/10 km]	NO$_x$ [g/10 km]	CO [g/10 km]	HC [g/10 km]	Drive cycle	Result Criteria 2
Weight factor						
Parallel						
Series						
Strigear						
Power split						

As changes occur, legislation, fuel prices, new valuation of emission costs etc, the criteria can be adjusted to fulfil the new conditions. Thereafter the tables can be determined once again.

Chapter 3 Hybrid Modelling

3.1   Modelling Purpose

The aim with this study is to compare four specified topologies with each other in terms of handling performance, losses and emissions. For this purpose simulation models are built, that describe the entire vehicle for different topologies.

The single sub models in the simulation models are chosen with care. The intensions with the models are to model each component that significantly affects fuel consumption and emissions separately. Hereby consist electric machines, ICE, battery, transmission etc of separate simulation blocks. All control algorithms, i.e. the onboard computers, are gathered in one block called power distribution. This mode of procedure facilitates the study of the most important energy transformations in the HEV thoroughly. The time scaling is chosen to facilitate a closer study in the matter of transient behaviour of the ICE.

To be able to simulate and compare the four chosen topologies as fairly as possible, the models are built as similar as possible. That is that three of the models, series, parallel and strigear, are even simulated in the very same simulation model. By changing the model parameters the model switches between the three topologies. The power split topology has to constitute its own simulation model due to the presence of the planetary gear and its diverged power distribution and the involved transmission.

3.2   Key Modelling Parameters

Parameters that have a significant influence on performance, power consumption and emissions, are chassis dynamics, efficiency of the electric machines and ICE and theirs maximum torque at different working points, battery state of charge (SOC) and temperature, driver behaviour and last but

not least control of the power distribution between the sources of traction power.

The dynamic behaviour of the ICE is crucial when determining the emissions and the fuel consumption. Hence the time scaling is chosen with respect to the wall wetting and other dynamic sources in the ICE.

The simulation models are only simulating longitudinal movements of the vehicle, thus road slope, lateral and vertical forces have not been taken under consideration.

The following part of this chapter will describe the equations that the simulation models consist of. The vehicle sub models are presented in an intuitive order; the chassis first and the largest traction power sources thereafter. After that comes a description of the driver modulation. Finally the control systems are discussed in details.

3.3   Chassis dynamics

The sub model describing the chassis includes both the transmissions and the friction forces in a vehicle. In the transmission sub model are torques and resistances added and the vehicle speed is obtained. The transmission models are varying depending on chosen hybrid topology. The vehicle speed for the series and parallel topology is described by equations 3-1 and 3-2.

$$\frac{dv_{series}}{dt} = \left(\left(T_{brake} + T_{resistance} + T_{em1}gr_1\right)\frac{1}{r_{wheel}}\frac{1}{m_{vhicle}} \right) \tag{3-1}$$

$$\frac{dv_{parallel}}{dt} = \frac{1}{r_{wheel}}\frac{1}{m_{vhicle}}\left(T_{brake} + T_{resistance} + T_{em1}gr_1 + gr_1 gr_2\left(T_{ICE} + T_{em2}\right)\right)$$

$$\tag{3-2}$$

The strigear topology switches between the series- and parallel mode. This is carried out with the clutch (see Figure 2-9). In this manner the vehicle speed is derived from one of the two above expressions.

In the case of power split topology the speed of the ring wheel is obtained by equation 3-3. The *k*-matrix consists of moment of inertia, numbers of teeth, number of planet wheels and mass of the planet wheel. To then obtain the vehicle speed a gain factor, $K_{\omega_{r\_to\_speed}}$, is used. See equation 3-3 - 3-5.

$$
\begin{bmatrix} \omega_r \\ \omega_c \\ \omega_s \end{bmatrix} = \int \left(\begin{bmatrix} k_{11} & k_{12} & k_{13} \\ k_{21} & k_{22} & k_{23} \\ k_{31} & k_{32} & k_{33} \end{bmatrix} \cdot \begin{bmatrix} T_r \\ T_c \\ T_s \end{bmatrix} + \begin{bmatrix} k_{11} \\ k_{21} \\ k_{31} \end{bmatrix} \cdot T_{frict} \right) \tag{3-3}
$$

$$
v_{powersplit} = \omega_r \cdot \frac{1}{K_{\omega_{r\_to\_speed}}} \tag{3-4}
$$

$$
K_{\omega_{r\_to\_speed}} = \frac{gr_1}{r_{wheel}} \tag{3-5}
$$

The sub model describing vehicle friction forces are based on the following relations. The friction force, i.e. the resistance torque $T_{resistance}$, is one of the inputs in the equations above (Haywood, 1988) (Equation 3-6 - 3-7).

$$
P_r = \left(C_r M_v g + \frac{1}{2} \rho_a C_d A_v S_v^2 \right) S_v \tag{3-6}
$$

$$
T_{resistance} = \frac{P_r}{S_v} r_{wheel} \tag{3-7}
$$

P_r = resistance power, C_r = rolling resistance, M_v = vehicle mass, g = gravity, ρ_a = air density, C_d = air resistance, A_v = vehicle front area, S_v = vehicle speed

3.4   Internal Combustion Engine

As earlier mentioned the Internal Combustion Engine (ICE) sub model is made by Petter Strandh at Combustion Engines, Department of Heat and Power Engineering, Lund University, as a part of his licentiate thesis (Strandh, 2002). A detailed description of the ICE model is available in his thesis. Here follows though a brief description of the ICE model.

The ICE model describes a naturally aspirated gasoline engine. Input data consist of engine speed and torque demand. Outputs are composed by actual torque, fuel consumption and emissions (HC, NO_x and CO).

The model tries to deliver the demanded torque as accurately as possible during a simulation. This has to be done while taking the different dynamic phenomena in the inlet manifold and fuel flow characteristics into

consideration. A concise description of the inlet manifold is a low pass filter with a time constant of about 0.1s.

The fuel calculations include equations that describe the wall-wetting model. That is how much of the injected fuel that instantaneously enters the engine and how much of the injected fuel that is stuck to the walls of the inlet port.

There is also a closed loop model for adjusting the fuel injection to achieve the desired stoichiometric air/fuel mixture ($\lambda = 1$).

To form the engine torque the airflow and engine speed are needed. The engine speed is known and the airflow is derived from the manifold and throttle sub model. By using these two variables as input in a look up table, the torque at stoichiometric conditions is derived. This torque is thereafter corrected to achieve the torque at the current λ-value.

An interesting variable in a study like this is the engine size. The size is depending on dominating load point of the application and engine efficiency. The maximum efficiency for a naturally aspirated SI engine can be found at full torque and about the middle of the engines operating speed range. So in order to minimize the fuel consumption, the engine size should be chosen in such way that the dominating load points of the application, in this case the hybrid vehicle, are found within this region.

The scaling of the ICE has been achieved by changing the number of cylinders. By this procedure it is reasonable to assume that the engine maintains its main characteristics, apart from the torque.

A real engine has been run in transient operation and logged. Afterwards the model engine has been run according to the same cycle. These measured and calculated data are shown in Figure 3-1. The upper curve shows how the air fuel ratio differs between the real engine and the simulated engine. The lower curve is the torque change. Conclusions from the graph is that the wall-wetting model, to some extent describes the wall wetting that occurs in the real engine. (Strandh, 2002)
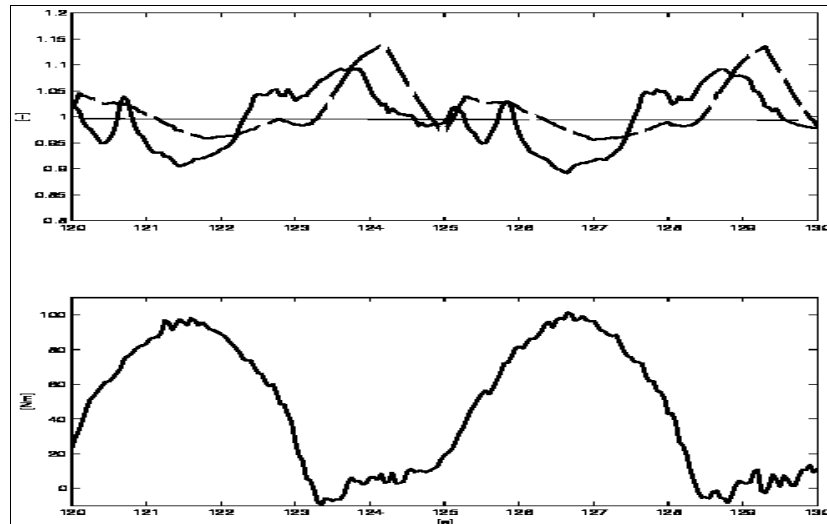
Figure 3-1:   Upper graph: Dashed line is the simulated air fuel ratio and the solid
                line is taken from real engine tests. Lower graph: Torque change.

The way that the model has been built makes it possible to simulate other naturally aspirated makes and sizes of engines. This is achieved by modification of the air map, the inlet manifold size and the exhaust manifold size combined with control parameters from the engine control unit.

In the present model, emissions are calculated using values that have been measured after the catalyst. When the engine operates in a transient mode, during a fast load change and when the fuel/air ratio is deviated from $\lambda=1$, the emissions are assumed to increase by the same percentage as the emissions increase before the catalyst. Thus, it is assumed that the conversion efficiency of the catalyst is maintained outside the λ-window. This could be the case for fast and not so large lambda deviation, due to the storage capability of the catalyst.

3.5   Electric Machines and Power Electronics

The power supply, from each electric machine, is obtained through equation 3-8 (electric machine 1 is used as example). The two machines, in each topology, are modelled in the same manner, but with unique figures. The figures are furthermore adjusted depending on the chosen topology. The two most important properties of the machines are the efficiency and the

torque limitations. In equation 3-9 the torque is limited concerning the maximum torque and in equation 3-10 according to field weakening.

$$P_{em1} = \begin{cases} \dfrac{\omega \cdot T_{em1}^*}{\eta_{em1}} & when \quad \omega \cdot T_{em1}^* > 0 \\ \omega \cdot T_{em1}^* \cdot \eta_{em1} & when \quad \omega \cdot T_{em1}^* < 0 \end{cases} \tag{3-8}$$

$$T_{em1}^* = \begin{cases} T^{'} & when \quad T^{'} < T_{max} \\ T_{max} & when \quad T^{'} > T_{max} \end{cases} \tag{3-9}$$

$$T^{'} = \begin{cases} T_{em1}^* & when \quad T_{em1}^* \cdot \omega < P_{max} \\ \dfrac{P_{max}}{\omega} & when \quad T_{em1}^* \cdot \omega > P_{max} \end{cases} \tag{3-10}$$

The efficiency of the electric machine, η_{em1}, is dynamically adjusted with respect to speed and torque. Depending on the instantaneous torque and speed, a look-up-table will deliver the efficiency at the present working point.

The power electronic losses are represented in Figure 3-2 (upper) as a normalized efficiency table. In Figure 3-2 (lower) the normalized values for efficiency in an electric machine are shown.
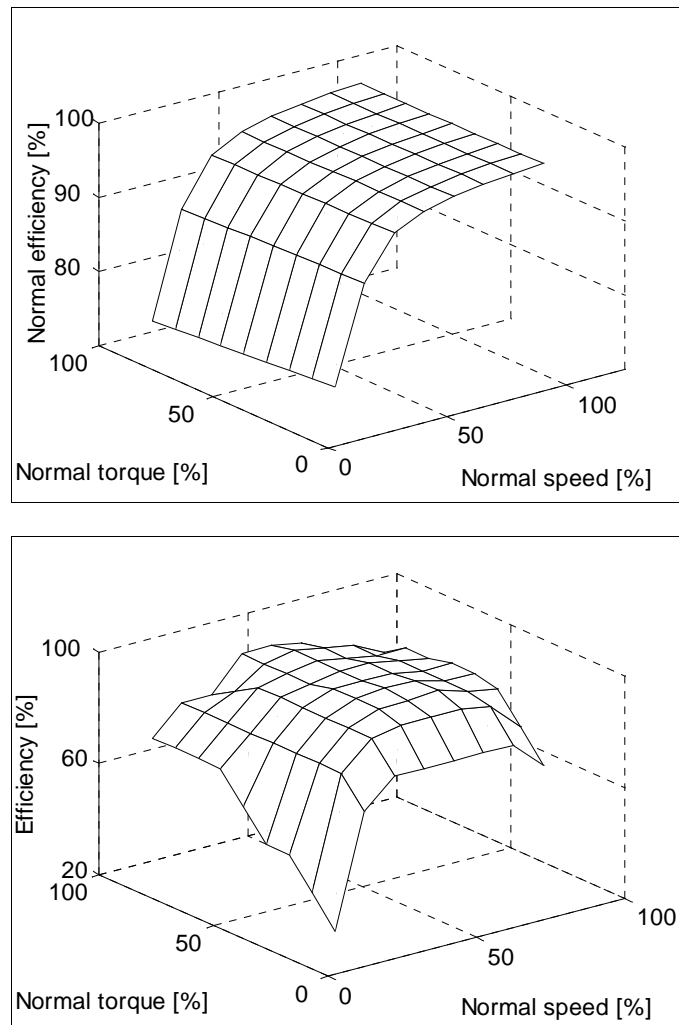
Figure 3-2:   The upper figure shows the normalized value for power electronic
losses. The lower figure shows the normalized values for efficiency in an
electric machine.

These two efficiency tables can be multiplied into one, i.e. the efficiencies
are multiplied with each other and a new table is obtained. This table,
representing efficiency in the electric machine including the power electric
losses, is shown in Figure 3-3. This table is then used in the simulation mode
to represent the entire drive. This table also includes the influences from the

power electronics. This is possible since the speed is roughly proportional to the voltage and the torque is nearly proportional to the current. In other words, the simplified battery model is not made voltage dependent.

The maximum torques of the electric drive is limited, taken field weakening into account. This is schematically viewed in Figure 3-4.
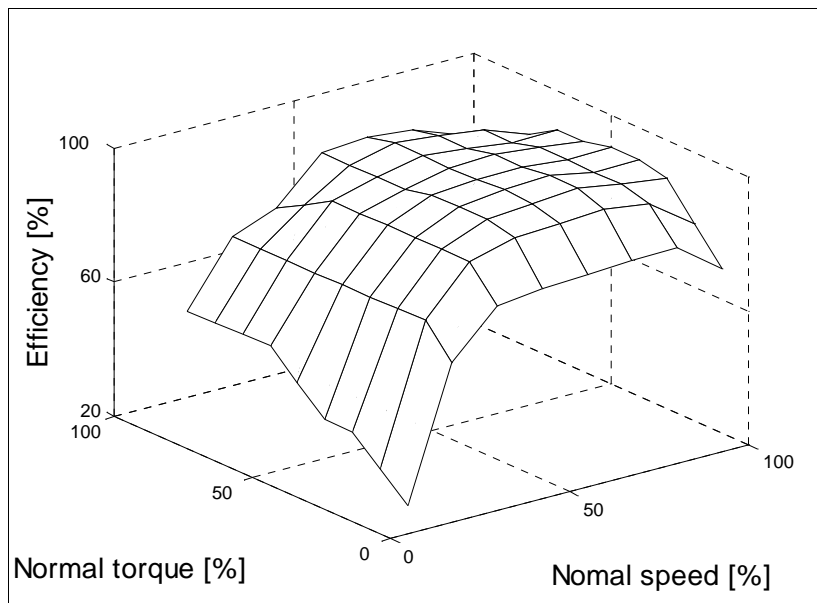

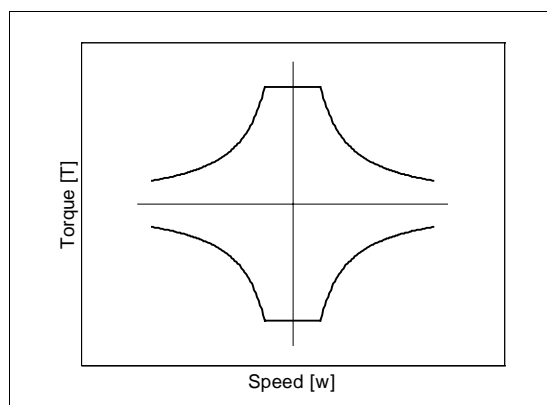Figure 3-3:   The normalized value for efficiency in an electric machine, including the power electric losses.

Figure 3-4: Diagrammatic view of field weakening used in the electric machines.

The timescales in the electric machines are much faster than those in the engine and in the chassis dynamics. Before the changes in the ICE are executed, the transients in the machines have died out since long. Therefore the timescales are chosen with regards to the ICE, not the electric machines.

Battery

The battery model represents the battery losses that act on the deviation of power, ΔP. ΔP is the sum of electric power that flows out of the battery. See equation 3-11.

$$\Delta P = P_{em1} + P_{em2} + P_{aux} \tag{3-11}$$

P_{em1} = power to electric motor 1, P_{em2} = power to electric motor 2 and P_{aux} = power needed to auxiliary, that is air condition, fan etc.

The power used to charge or discharge the battery, P_{batt}, and the battery losses, P_{loss}, are calculated in the following way (equation 3-12 and 3-13), when ΔP is positive, i.e. the battery is discharged:

$$P_{loss} = \left| \Delta P - \Delta P \eta_{batt} \right| \tag{3-12}$$

$$P_{batt} = \Delta P \eta_{batt} \tag{3-13}$$

η_{batt} is the battery efficiency and $\eta_{batt} < 1$ when $\Delta P < 0$ and $\eta_{batt} > 1$ when $\Delta P > 0$ (see Figure 3-6).

The battery efficiency, η_{batt}, is dynamically adjusted depending on the present SOC, battery current and voltage and also the demanded ΔP. The total battery efficiency consist actually of two separate parts, one depending on the prevailing SOC and one depending on the battery power electronics (*PE*). See equation 3-14.

$$\eta_{batt} = \eta_{batt(SOC)} \cdot \eta_{batt(PE)} \tag{3-14}$$

In the simulation model, the battery is modelled as a resistance model (see Figure 3-5). The fundamental battery equations are shown in equation 3-15 - 3-17.
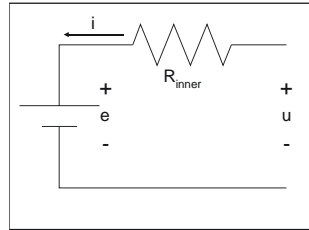

Figure 3-5:   The figure shows a schematic model of the battery model, used in the simulation model.

$$\Delta P = u \cdot i \tag{3-15}$$

$$P_{batt} = e \cdot i \tag{3-16}$$

$$e = u - R_{inner} \cdot i \tag{3-17}$$

where $R_{inner} = f(SOC)$ and $e = f(SOC)$

The battery model is based on physical data originating from the Toyota Prius, when such have been available. Supplementary data have been used from battery measurements (Johnson et al, 2001). These data are mould together into a look-up-table with ΔP and SOC as inputs and the battery efficiency, $\eta_{batt(SOC)}$, depending on SOC as the output. See Figure 3-6.
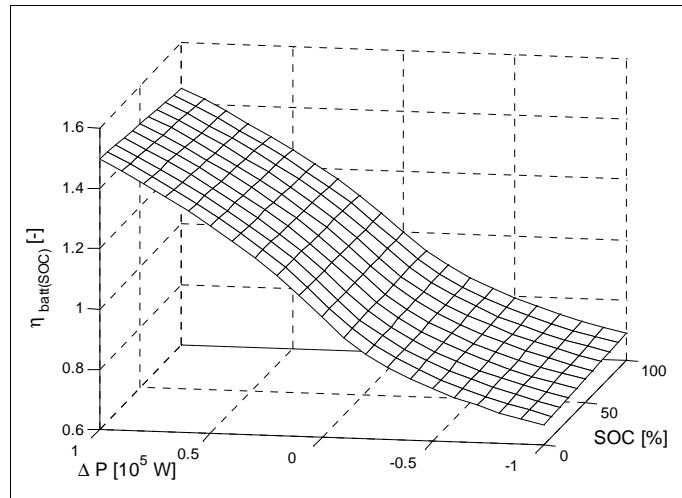
Figure 3-6: Battery efficiency as function of ΔP and SOC.

The influence of the power electronics in the battery has been modelled as a normalized efficiency table, see Figure 3-7.
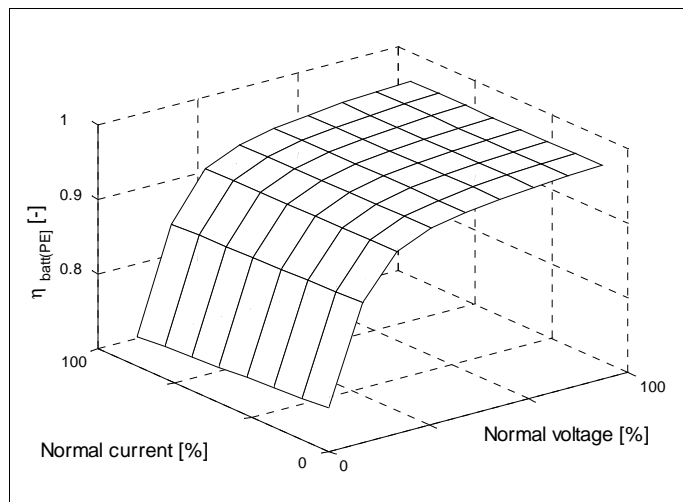

Figure 3-7: The normalized value for power converter efficiency.

Figure 3-6 and Figure 3-7 represent together η_{batt} in equation 3-12 and 3-13.

The SOC of the battery is calculated as an integral of the power, reduced by the battery losses according to equation 3-18 and 3-19. P_{loss} is depending on whether ΔP is positive or negative, i.e. if the battery is charging or discharging.

When the battery is charging:

$$SOC = \frac{1}{W_{batt,max}} \int (P_{batt} - P_{loss})dt \qquad (3\text{-}18)$$

When the battery is discharging:

$$SOC = \frac{1}{W_{batt,max}} \int (P_{batt} + P_{loss})dt \qquad (3\text{-}19)$$

A thermal model is included with one thermal node inside the battery pack for a rough estimate of the battery temperature with the various topologies and control methods. The battery temperature arises from the assumptions and premises described below.

The thermal equilibrium in a homogenous body can be expressed by equation 3-20.

$$\frac{dT_{emp}}{dt} = \frac{(P_{loss} - P_{cool})}{C_{batt\_thermal}} \qquad (3\text{-}20)$$

C = thermal capacity

The cooling losses in a homogeneous body can bee described in the manner shown in equation 3-21.

$$P_{cool} = \frac{T_{emp} - T_{outer}}{R_{batt\_thermal}} \qquad (3\text{-}21)$$

That gives the expression in equation 3-22.

$$\frac{dT_{emp}}{dt} = \left(\frac{1}{C_{batt\_thermal}} \left(P_{loss} - \left(\frac{(T_{emp} - T_{outer})}{R_{batt\_thermal}} \right) \right) \right) \qquad (3\text{-}22)$$

This simple battery temperature model is present in the simulation model, but not used in the analysis made in this thesis.

3.6   Driver Model

The driver is designed as a simple *PI*-controller with anti-windup on the integrator to prevent saturation in the actuator. (Årzén, 2000) The necessary amount of torque to achieve the requested vehicle speed is received with equation 3-23 and 3-24. The requested speed is given by drive cycles as look-up-tables.

$$F_{tot}^* = K\left((v^* - v) + \frac{1}{s\tau_i}(v^* - v) \right) + \frac{1}{\tau_t}(u - v_{controller}) \qquad (3\text{-}23)$$

F_{tot}^* = total requested force, $v_{controller}$ = output of the controller, u = actuator output

$$T_{tot}^* = F_{tot}^* r_{wheel} \qquad (3\text{-}24)$$

T_{tot}^* = total requested torque, r_{wheel} = wheel radius

With no saturation the expression (u-$v_{controller}$) approaches zero, i.e. no windup and hence no use for the tracking time constant, τ_t.

The tracking time constant is supposed to be larger than τ_d and smaller than τ_i. In the model it has been sized by the rule of thumb that is shown in equation 3-25.

$$\tau_t = \sqrt{\tau_i \tau_d} \qquad (3\text{-}25)$$

It is important to keep in mind that the model is a rough and conscious simplification of the behaviour of a driver. This simplified driver is suitable for comparative studies, though less accurate for absolute studies of specific driver behaviour.

3.7   Power Distribution

The traction and auxiliary torque references have to be distributed to the ICE, the electric machine(s) and the battery. The considerations that controls the power flows are taken in the sub model called the power distribution block.

The power distribution block represents the computer force onboard the vehicle. Its output is therefore controlling the electrical machines, ICE and so forth. It calculates the references for the required torque from each of the main energy converters. These torques are calculated as a function of the instantaneous tractive power demand, the auxiliary power demand, the deviation of SOC in the battery and finally the actual speed of the vehicle and the different machines. This is done differently depending on the chosen topology and described in detail further on.

A fundamental consideration within this block is that the dynamic operation of the ICE must be limited. It can be argued that an ICE consumes fuel and generates emissions out of proportion when making changes of operating point with a certain rate, compared to the fuel consumption and emissions in stationary operation (Andersson, 2001).

The simplest way to limit the dynamic operation of the ICE is to low pass filter the power requirement from the ICE. See Figure 3-8. The time constant of the filter must thus be selected to ensure quasi-stationary operation of the ICE. The ICE power requirement is thus given by equation 3-26.
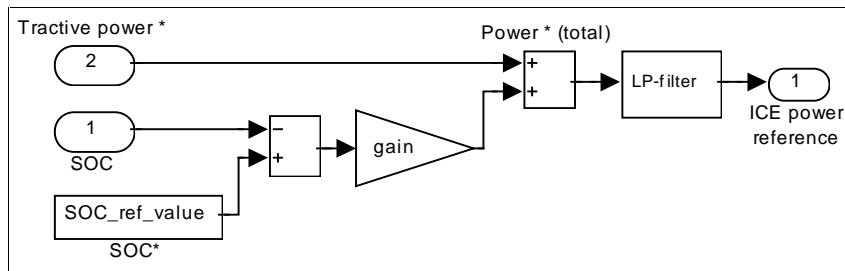

Figure 3-8:   A generalized view of the part of the power distribution block in the simulation models that handles the calculation of ICE power reference.

$$\frac{dP_{ice}*}{dt} = \frac{P_{tractive} + P_{aux} + k(SOC* - SOC) - P_{ice}*}{\tau_{ice}}$$

(3-26)

The stationary efficiency or emissions of an ICE can be expressed in a map as a function of speed and torque. This disregards dependence of temperature and ageing etc. From this map the best operating point for any power level within the ICE's operating range can be selected. Figure 3-9, the upper, shows the efficiency map and the optimum torque and efficiency as a function of the requested power derived from the efficiency map.
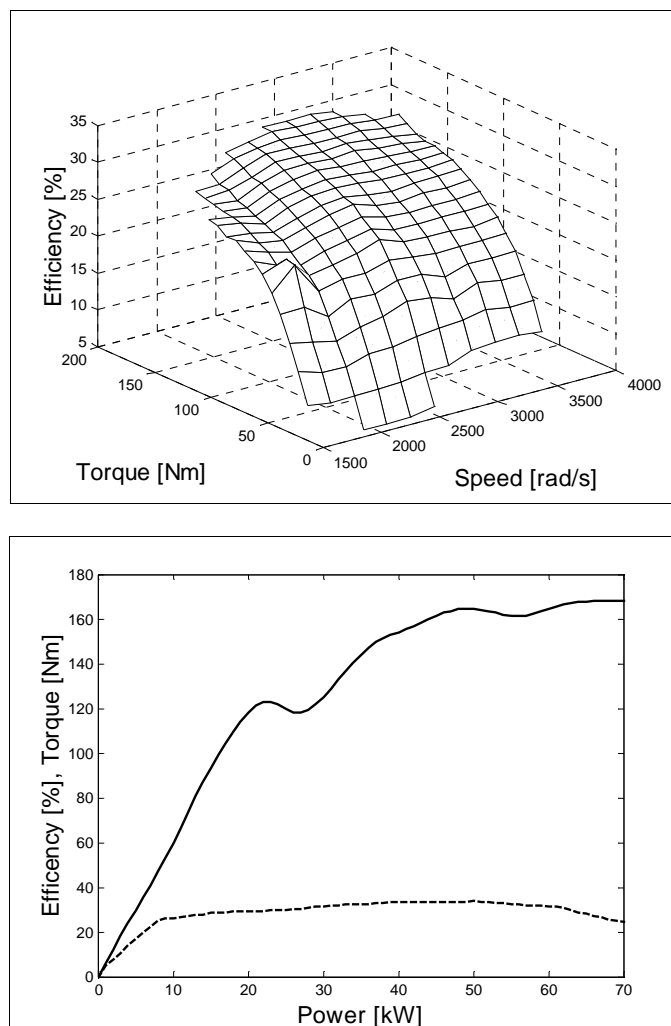

Figure 3-9:   Upper: Efficiency map for ICE. Lower: Efficiency at optimal working point for the ICE.

The torque and speed references for the ICE are calculated from the demanded power, $P_{ice}*$, via a look up table like the one in Figure 3-9, the lower, in the hybrid models. The references are being denoted $T_{ICE}*$ and $\omega_{ice}*$. The ways to realize these references are slightly different for the different hybrids. Equations 3-27 and 3-28 display how the reference torque and speed are selected.

$$T_{ice}^{*} = "look-up-table" \text{ (See Figure 3-9.)} \tag{3-27}$$

$$\omega_{ice}^{*} = \frac{P_{ice}^{*}}{T_{ice}^{*}} \tag{3-28}$$

To increase the efficiency of the ICE, it is controlled to only operate at efficiencies above a predetermined limit. The limit is controlled with hysteresis, to avoid a nervous behaviour of the ICE. The ICE torque demand is then switched on at $\eta_{ICE} = 23\%$ and switched off at $\eta_{ICE} = 22\%$. This procedure is implemented for the parallel-, series- and strigear topology.

Series hybrid strategy

The tractive torque is entirely supplied by electrical machine 1 (em1) in Figure 2-7, and its reference can be calculated directly from the wheel torque reference given by the driver according to equation 3-29 where gr_1 is the gear ratio in the final gear of the drive train.

$$T_{em1}^{*} = \frac{T_{wheel}^{*}}{gr_1} \tag{3-29}$$

The torque reference for the second electrical machine (em2) is calculated to obtain the desired speed of the ICE, according to equation 3-30 where K_s is the proportionality gain of the em2 and the ICE speed controller.

$$T_{em2}^{*} = K_s \cdot \left(\omega_{ice}^{*} - \omega_{ice}\right) - T_{ice}^{*} \tag{3-30}$$

K_s = speed regulation device gain

Parallel hybrid strategy

Since the ICE in the parallel hybrid is mechanically connected to the wheels (Figure 2-8), the speed reference for the ICE can only be reached if the gearbox is able to set up a suitable gear ratio (gr_2) given the instantaneous combination of vehicle speed and ICE speed reference. The most suitable gear ratio is selected and a set of new references for the ICE torque and speed are calculated by equations 3-31 and 3-32.

$$gr_{2,min} < gr_2 = "\frac{V_{vehicle}}{r_{wheel} \cdot \omega_{ice}^* \cdot gr_1}" \text{ in } 5 \text{ fixed steps} < gr_{2,max} \tag{3-31}$$

$$\omega_{ice}^{*\,'} = \frac{\dfrac{V_{vehicle}}{r_{wheel}}}{gr_1 \cdot gr_2} \quad \text{and} \quad T_{ice}^{*\,'} = \frac{T_{ice}^* \cdot \omega_{ice}^*}{\omega_{ice}^{*\,'}} \tag{3-32}$$

Given the new set of ICE torque and speed references, the torque references for the electrical machine(s) are calculated according to equation 3-33 and 3-34. Since the simulation model contains two electric machines, the torque demand is distributed proportional to the best of their ability given the operating conditions. Consideration is taking to the two gearboxes included in the model.

$$T_{em1}^* = \frac{T_{wheel}^* - \left(T_{ice}^* \cdot gr_1 \cdot gr_2\right)}{gr_1} \cdot \frac{T_{em1,max} \cdot gr_1}{T_{em1,max} \cdot gr_1 + T_{em2,max} \cdot gr_1 \cdot gr_2} \tag{3-33}$$

$$T_{em2}^* = \frac{T_{wheel}^* - \left(T_{ice}^* \cdot gr_1 \cdot gr_2\right)}{gr_1 \cdot gr_2} \cdot \frac{T_{em2,max} \cdot gr_1 \cdot gr_2}{T_{em1,max} \cdot gr_1 + T_{em2,max} \cdot gr_1 \cdot gr_2} \tag{3-34}$$

If only one machine is used, the specification for the other of the two in the model is set to zero maximum torque in equation 3-34 and 3-33. The maximum torque values, used in equation 3-34 and 3-33, are momentary values taking field weakening into account, and do thus vary continuous with speed.

Strigear hybrid strategy

The strigear hybrid is able to run as a series or a parallel hybrid depending on the position of the clutch (Figure 2-9). The selection of the clutch position is based upon a comparison of two loss estimates, one for each topology. The loss estimates are calculated from equation 3-35 and 3-36.

$$\hat{P}_{loss,serie} = \hat{P}_{loss,em1} + \hat{P}_{loss,em2} + \hat{P}_{loss,ice} + P_{em1} \cdot (1 - \eta_{gr_1}) +$$
$$(P_{em1} + P_{em2}) \cdot (1 - \eta_{batt}) \tag{3-35}$$

$$\hat{P}_{loss,parallel} = \hat{P}_{loss,em1} + \hat{P}_{loss,em2} + \hat{P}_{loss,ice} + (P_{em1} + P_{em2}) \cdot (1 - \eta_{batt}) +$$
$$P_{em1} \cdot (1 - \eta_{gr_1}) + (P_{ice} + P_{em2}) \cdot (1 - \eta_{gr_1} \cdot \eta_{gr_2}) \tag{3-36}$$

η_{gr1} and η_{gr2} are the efficiencies of the gear boxes 1 and 2 respectively. The selection rule is simple; the configuration with the lowest estimated losses is used. The losses in each mode are simultaneously calculated. For this purpose the optimal speed and torque combination is used for the demanded power, and they differ between the two modes. This affects in its turn the speed and torque when switching between the two modes.

The comparison of the two loss estimates is then low pass filtered and a small hysteresis is used to limit the number of clutch position changes.

Power split strategy

In this case the ring motor (*em1* in Figure 2-10) is used to produce the instantaneous torque for traction. The combination of the ICE and the solar motor (*em2*) are used to supply the low pass filtered power demand by using em2 to speed control the ICE.

Since the torque demand for the ICE is known through the look up table in Figure 3-9, equation 3-37 can be used to calculate the additional torque references, see also equation 3-38 - 3-40.

The *k*-matrix consists of, as mentioned above, moment of inertia, numbers of teeth, number of planet wheels and mass of the planet wheel.

$$
\begin{bmatrix} T_{em1}^* \\ T_{em2}^* \end{bmatrix} = \begin{bmatrix} k_{11} & k_{13} \\ k_{31} & k_{33} \end{bmatrix}^{-1} \cdot \begin{bmatrix} \dfrac{\left(\omega_{em1}^* - \omega_{em1}\right)}{\tau_x} \\ \dfrac{\left(\omega_{em2}^* - \omega_{em2}\right)}{\tau_z} \end{bmatrix} - \begin{bmatrix} k_{12} \\ k_{32} \end{bmatrix} \cdot T_{ice}^* + \begin{bmatrix} 1 \\ 0 \end{bmatrix} \cdot \dfrac{T_{wheel}^*}{gr_1} \quad (3\text{-}37)
$$

where

$$
\omega_{em1}^* = \frac{gr_1}{r_{wheel}} v^* \tag{3-38}
$$

$$
\omega_{em2}^* = R_{planet} \cdot \omega_{em1}^* + (1 - R_{planet}) \cdot \omega_{ice}^* \tag{3-39}
$$

$$
R_{planet} = \frac{\omega_{solar} - \omega_{carrier}}{\omega_{ring} - \omega_{carrier}} \tag{3-40}
$$

Chapter 4 Implementation in Simulink

4.1 Simulation Platform

To model HEV systems is quite a complex task. The dynamics are varying from less than µs to long-term effects of wear and ageing. It is necessary to limit the modelled dynamics with regard to the purpose of the simulations.

There are several software environments suitable for analysing such systems. For this task the Matlab®/Simulink® environment has been used. It is at present a widely spread simulation program both in industry and in academia. The vehicle models are designed in Simulink® and thereafter fed with input parameters via Matlab®. This facilitates rapid simulations with an adjustment in examined variables. A not unimportant advantage in Simulink® is its graphical user interface, which facilitates an easy overview of the complex systems.

Other accessible programs are Modelica, Advisor, CRUISE, Vehicle Simulation Program (VSP) (Van Mierlo, 2000), SIMPLEV and EHVSP, just to mention the most important ones.

The topmost level in the simulation model is shown in Figure 4-1.
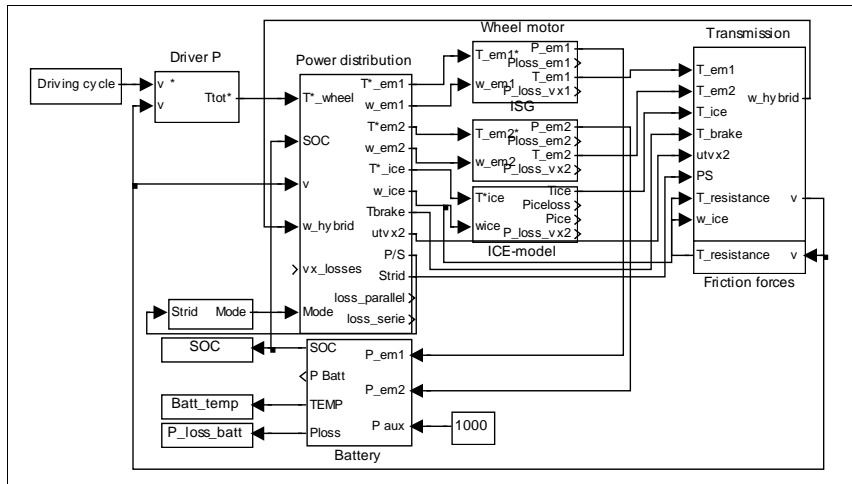
Figure 4-1:   The topmost level in the simulation model. Each modelled subsystem is
              forming a separate block, such as battery, engine etc.

The implementations of the sub models in Simulink® are described below
one by one.

4.2   Chassis Dynamics

The chassis dynamics include both the transmissions and the friction
forces, i.e. the air- and roll resistances etc.

The transmission model includes the basic equations for the gearboxes,
including a fixed efficiency (99%) of each gear step. In the parallel hybrid a 5
speed automatically shifted "manual" gearbox is used.

In the planetary gear the ICE is connected to the carrier, the electrical
machine 2 to the sun wheel and finally the electrical machine 1 and the
wheels of the vehicle are connected to the ring wheel.

The model inputs are torques and in the series-, parallel and strigear
topology the ICE speed. The model outputs are speed of the hybrid aggregate
and vehicle speed. The power split model also delivers the speed of the
different shafts in the planetary gear and the gear losses. See Figure 4-2 and
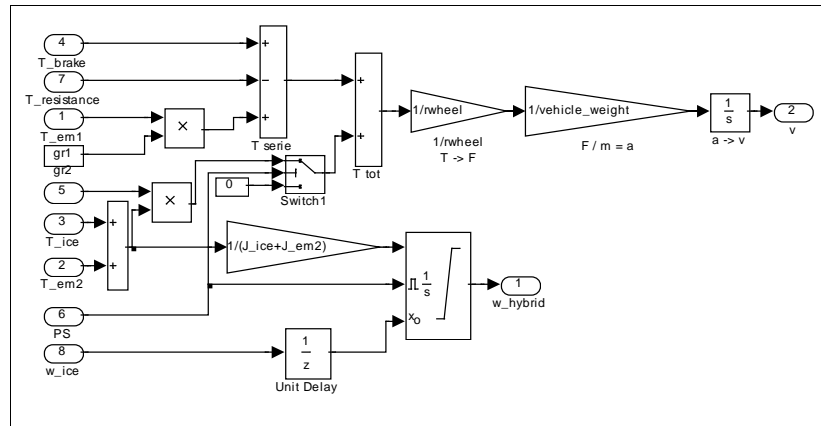Figure 4-3 respectively.

Figure 4-2: The transmission block in the series-, parallel or strigear topology.
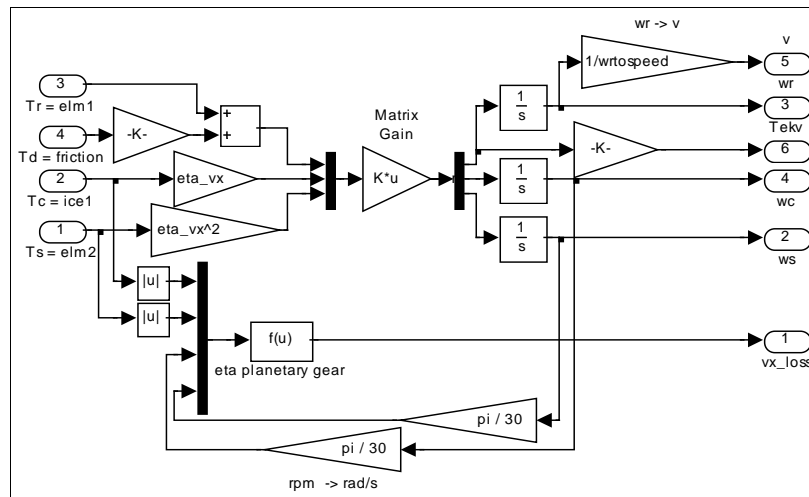

Figure 4-3: The transmission block in the power split hybrid.

The friction losses are equal to the air- and roll resistance. The losses are simulated in Simulink® as shown in Figure 4-4.
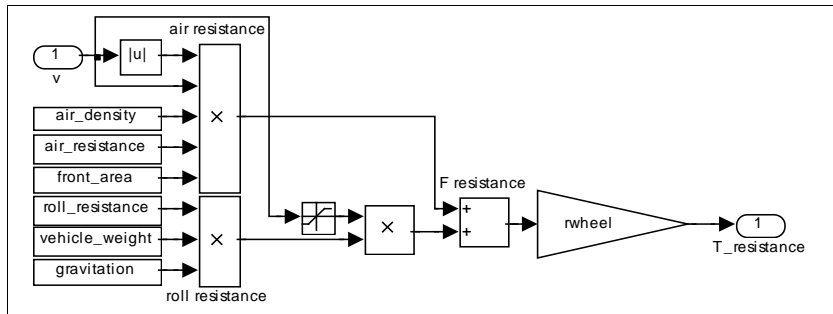
Figure 4-4: The simulation block that considers the air- and roll resistance.

Input value in the block is the vehicle speed and output value is the resistance torque. The output signal, $T_{resistance}$, is thereafter inserted in the transmission block as a negative torque contribution. The physical quantities (C_r, M_v, C_d and A_v) represent the Toyota Prius as far as possible.

Road slope, lateral and vertical forces have not been taken into consideration in the simulation model.

4.3   ICE

The ICE model included in the simulation models is built with input data from a SAAB-engine. As previous mentioned the ICE sub model is made by Petter Strandh and further details are available in (Strandh, 2002). The topmost level is shown in Figure 4-5.
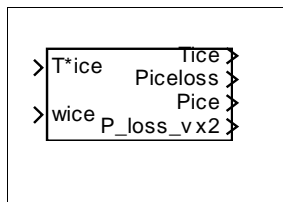

Figure 4-5: The topmost level of the ICE-model.

The ICE model contains a quasi-stationary model with transient behaviour. This means that it is basically built by using tables, but has also dynamic equations for describing inlet manifold states, fuel delivery and wall wetting as well as closed loop control of air/fuel ratio. This makes it behave like a naturally aspirated gasoline engine, with a three-way catalyst. However, the catalyst as such is not modelled in the present version of the sub model.

Inputs in the model are revolutions per minute and required torque. Output values are torque, power and losses. The model also calculates fuel consumption and emissions, which are the key parameters for comparing the topologies in this study. The block for calculation the emissions is shown in Figure 4-6 where the look-up-tables for the emissions NO_x, CO and HC are clearly visible in the middle of the model.
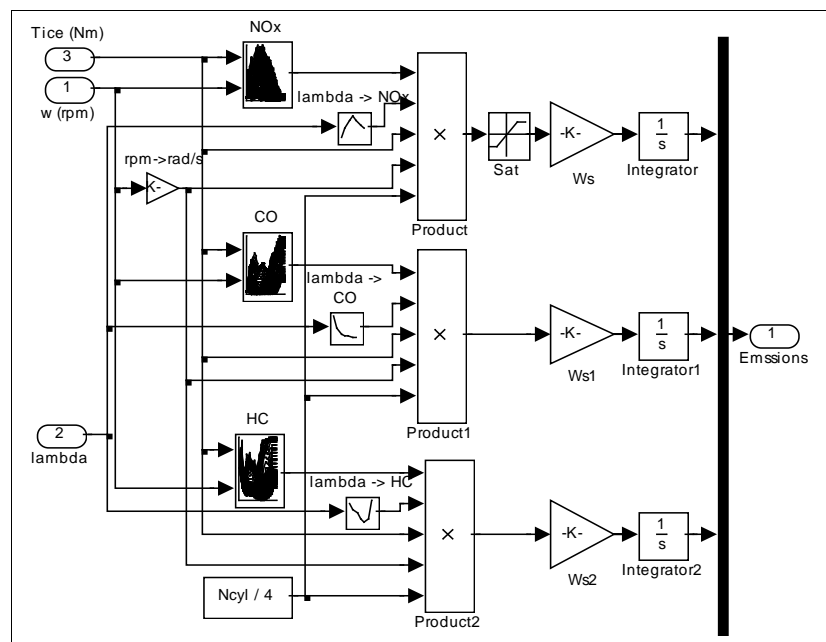

Figure 4-6: The simulation block for calculation of emissions.

4.4   Electric Machines and Power Electronics

In these models the electrical machines and corresponding power electronics are represented together as a look up table of efficiency depending on speed (~ voltage) and torque (~current). In addition the maximum torque is limited taking field weakening operation into account. Transient torque boost is not represented.[2]

---

[2] Torque boost is the ability to transiently boost the torque from the electric machine at low speeds, above the actual maximum torque. This is only possible at limited time periods. The electric machine will otherwise obtain injurious temperatures due to the increased current.

The electrical machines are modelled as a look up table with efficiency, where also the power electronic losses are included. This is motivated by the fact that speed and voltage are almost proportional in stationary operation. Moreover, current and torque are also almost proportional in stationary operation. Each electrical machine is given the efficiency characteristic shown in Figure 4-7, but the speed and torque axes that are scaled according to the specifications following each topology.
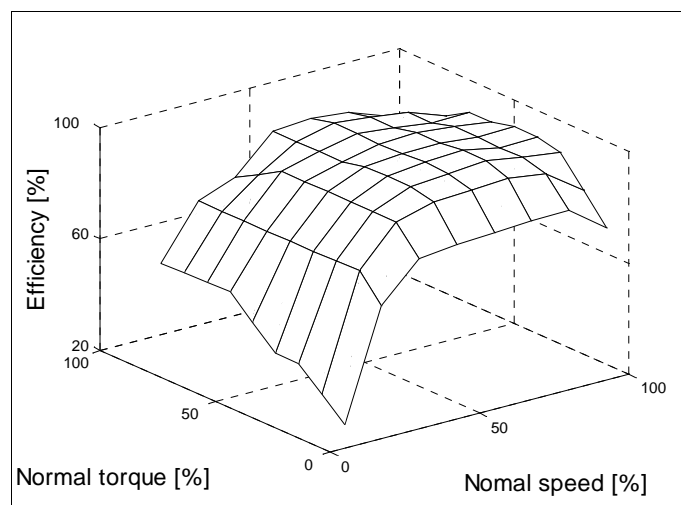

Figure 4-7:   The normalized value for efficiency, including the power electric losses, used in the electric machines.

The block inputs are the torque requirement, which originate from the power distribution block, and the present speed of the machine. The outputs consists of real supplied torque, power, gear- and machine losses. The block can be seen in Figure 4-8, where the look-up-table (shown in Figure 4-7) is visible in the centre of the simulation model.
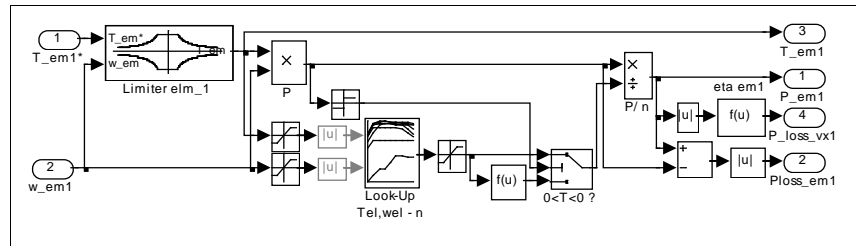
Figure 4-8: The Simulink® block describing one of the electric machines.

4.5   Battery

The input values in the battery model are the power from the electric machines and the auxiliary that is a constant power representing light, air condition, fan etc. The size of P_{aux} is chosen with consideration to the power consumption from the air condition published by Idaho National Engineering and Environmental Laboratory (INEEL, 2002). Depending on if the sum of power is positive or negative, the battery is charged or discharged.

Outputs from the sub model are battery temperature, battery losses, battery power and SOC, which has a reference value of 70% allow variations in SOC. See Figure 4-9. The SOC level is a result of the ICE control, i.e. the ICE is run at the best efficiency possible at any time and the battery is used as power compensator.
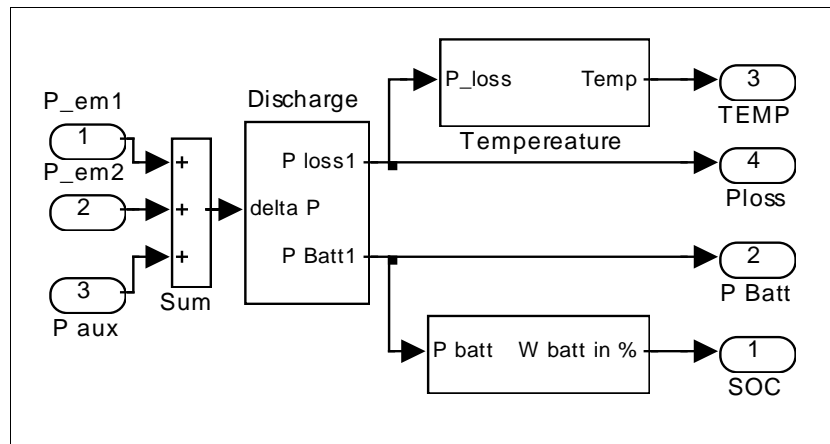

Figure 4-9: The battery model.

The battery efficiency is dynamically adjusted depending on present values from SOC, battery current and voltage and the demanded ΔP. The battery inner resistance, R_{inner}, is depending on temperature and SOC. The temperature is assumed to be stable at $+25°C$. That means that R_{inner} is made only SOC dependent.

A thermal model is included in the sub model. It contains one thermal node inside the battery pack for a rough estimate of the battery temperature with the various topologies and control methods.

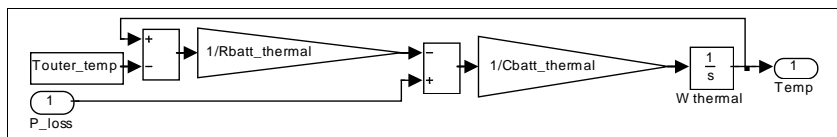This is then implemented in the following way in Simulink® (Figure 4-10):

Figure 4-10: The sub model to determine the battery temperature.

4.6   Driver model

In reality the driver reacts on a speed error and steps on the gas or the break depending on the sign of the speed error. The driver is modelled as a simple PI-controller, which reacts on the speed error, with anti-windup on the integrator to prevent saturation in the actuator.

There are three types of drivers to choose from in the simulation model; slow, normal and nervous. The differences between these driver types are the time before they react on a speed error (the time step) and the amplitude of the power demand. The "mode-factor" is a scaling factor of the size 0.5, 1.0 or 2.0.

The model is a rough and conscious simplification of the behaviour of a driver. The model is not checked against recorded driver behaviour, but this simplified driver is suitable for comparative studies, where the aim is the mutual results, not the definite figures.

The input values to the sub model are the driving cycle, i.e. the speed set point and the measured speed value. The output is the torque needed to minimize the speed error, i.e. if the driver needs to step on the gas or maybe break. See Figure 4-11 and Figure 4-12.
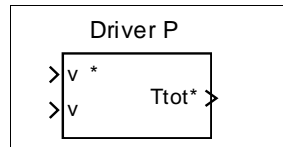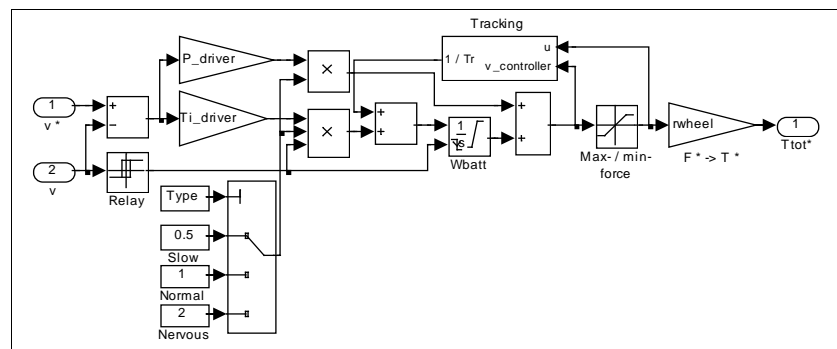
Figure 4-11: Driver model.

Figure 4-12: Inside the driver block consisting the PI-controller.

4.7   Power distribution

This sub model represents the computing power used for control of the tractive energy flows onboard. All relevant quantities such as speeds, SOC etc. are used for calculation of the torque references for the ICE and the electrical machines, which are the model outputs.

The requested torques are depending on, i.e. the block inputs are, requested total torque, vehicle speed, speed of the ICE, SOC and last but not least, which topology that is chosen.

The two simulation models have power distribution blocks that differ from each other. Inside these two blocks there is a hidden control system that calculates, optimises and distributes the requested torque for the electric machines and the ICE. This is dynamically calculated and the different boundaries are dynamically adjusted with respect to field weakening, efficiency etc. The complexity in the block makes showing the inside of the blocks more confusing than clarifying. Figure 4-13 shows consequently only the topmost level of the power distribution block in the two models.
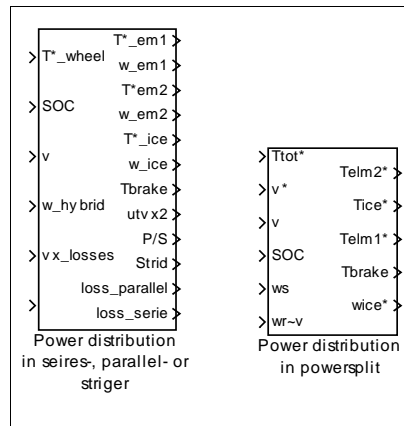
Figure 4-13: Power distribution blocks; the left most is from the series-, parallel- or strigear HEV. The right most is from the power split simulation model.

Strigear mode control

In the strigear hybrid there is also an instantaneous comparison of the estimated total losses in the series and the parallel hybrid mode. Based on this estimate, the most suitable configuration (series or parallel) is selected and the clutch is operated accordingly. The selected signal is low pass filtered and is given a suitable hysteresis so the system won't get too spasmodic.

The estimated total losses are the input in the Figure 4-14. The output signal is the control signal when manoeuvring the clutch in Figure 2-9, i.e. choosing between parallel or series mode in the strigear topology.
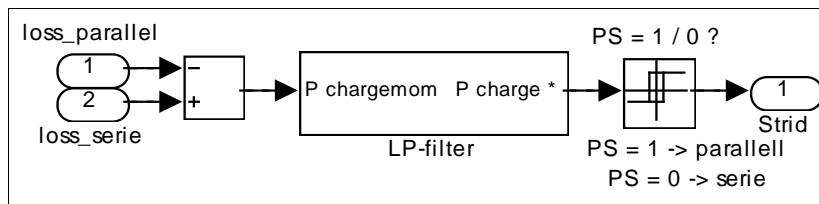

Figure 4-14: A concentrated view of the strigear mode control.

When operating the strigear topology it is important to remember that it is neither a series nor a parallel HEV. It is just a strigear. This means that it is bringing a history (SOC for instance) of a strigear and is equipped as a strigear. Comparisons with a parallel or a series HEV should only be made with outmost care.

4.8   Driving cycle

This driving cycle block contains 12 driving cycles to choose from. Some of the cycles are internationally accepted standard cycles developed in different continents, and some are recorded locally in Sweden. Some are for buses and yet others are for private cars, see Figure 4-15. In this survey not all cycles are used. The chosen cycle is the model input, as the simulated vehicle's attempt is to achieve the cycle speed. The single cycle consists of a look-up-table, where vehicle speed is a function of time.
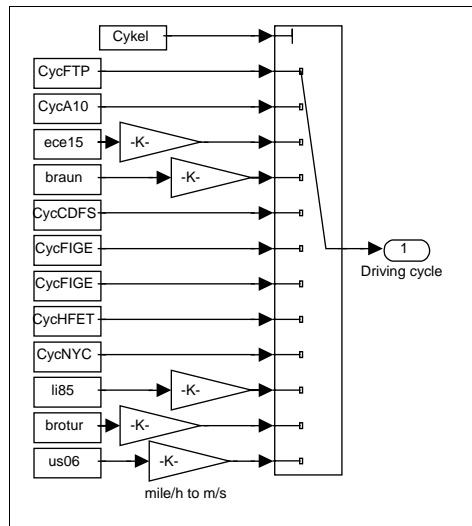

Figure 4-15: The driving cycle options.

4.9   Conclusion of Implementation

The Simulink® sub models described above form themselves into two, quite similar, models. They have been used for comparative simulations of two of the included driving cycles. Parts of the models are, as previous mentioned, just a rough estimation, but detailed enough to be used for this mutual comparing purpose. The particular case study will be presented in the following chapter.

Chapter 5 Case Study

The models described in the previous chapter have been used for a case study. The four topologies have been implemented as like a Toyota Prius as possible and thereafter compared with each other in terms of performance and emissions for various driving conditions. The quantities of the vehicles have been adjusted to suit the demands from the single topology respectively. This chapter describes the prevailing circumstances for the comparative study.

5.1 Driving Cycles

The simulations made in this thesis have been made with the US06 and the ECE 15 cycles. US06 describes a demanding highway driving including aggressive accelerations and high speed driving. The cycle is 12.8 km long and has a mean speed of 77.8 km/h, maximum speed of 130 km/h and a maximum acceleration of 3.24 m/s^2 (Figure 5-1 and Figure 5-2).
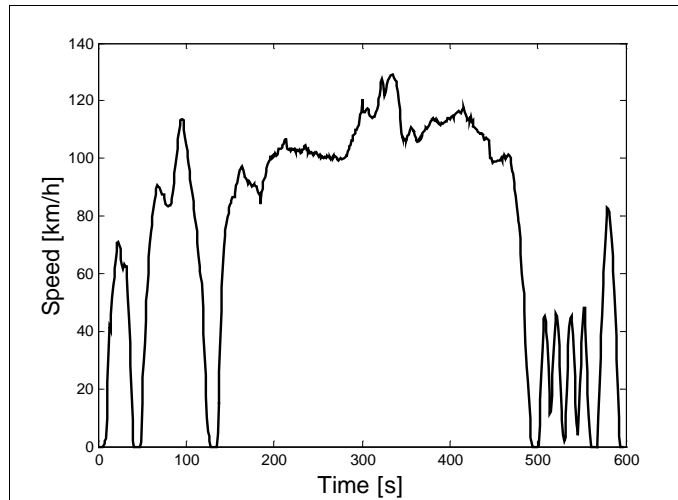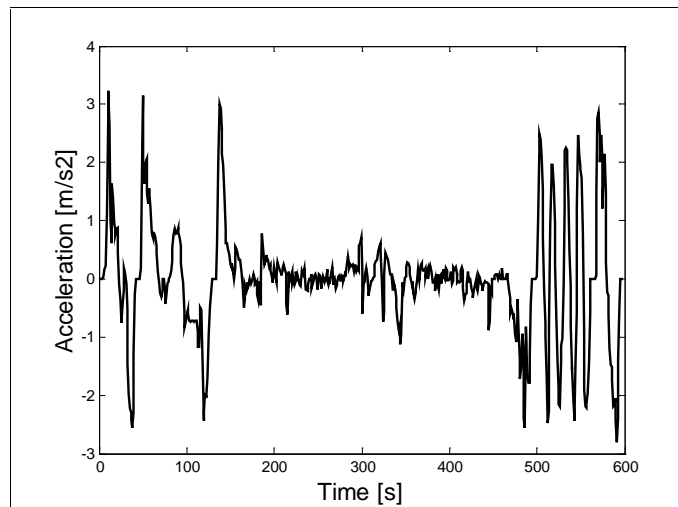
Figure 5-1: Drive cycle US06, velocity.

Figure 5-2: Drive cycle US06, acceleration.

The US06 Supplemental Federal Test Procedure (SFTP) is developed to address the shortcomings with the FTP-75 test cycle in the representation of aggressive, high speed and/or high acceleration driving behaviour, rapid speed fluctuations and driving behaviour following start up.

The reason to include the US06 cycle in the survey is that its demanding accelerations expose the transient behaviour in fuel consumption and emission.

The drive cycle ECE 15 has also been used in the survey to make a fair comparison of the topologies. The ECE 15 drive cycle is not as demanding as the US06 cycle. Car manufacturers that aim to measure fuel consumption use the ECE 15 cycle. The cycle is theoretical and includes relatively low accelerations. The ECE cycle is an urban driving cycle, also known as UDC. It was devised to represent city driving conditions. It is characterized by low vehicle speed, low engine load, and low exhaust gas temperature (Dieselnet, 2002).

For light duty vehicle the speed limit is 90 km/h. The cycle is 10.8 km long and its average speed is 31.7 km/h. The accelerations are considerably lower than the US06 with 1.04 m/s^2 (Figure 5-3 and Figure 5-4).
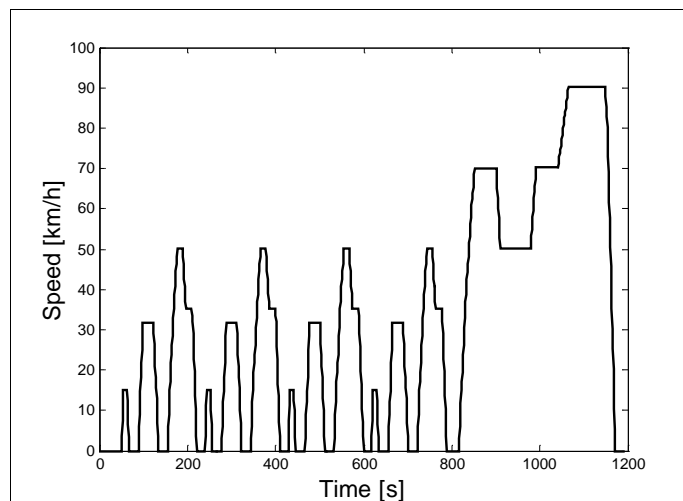

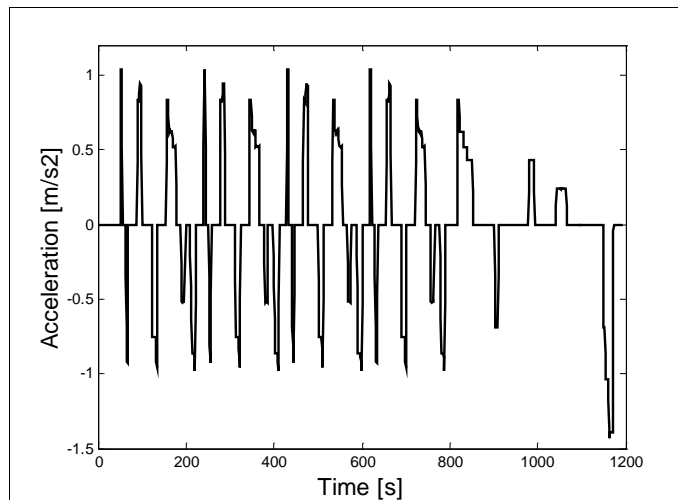Figure 5-3: Drive cycle ECE 15, velocity.

Figure 5-4: Drive cycle ECE 15, acceleration.

There is a possible variation of the cycle. For heavy-duty vehicles the top speed is limited to 70 km/h. This affects also cycle distance and average speed.

5.2   Reference Vehicle

To make the survey fair and relevant to a large market segment, a medium sized family car was chosen as simulation input. The specific vehicle became Toyota Prius, an electric hybrid family car, available on the market today. The advantages with the choice are that input data are accessible and there are measured data available as well. (See appendix 9.2 and 9.3.)

The chosen Toyota Prius is the one marketed in Europe. It is equipped with a larger engine then the ones earlier sold in the USA and at the Japanese market. Further details about Toyota Prius can be found in appendix 9.1.

As input in the ICE-simulation model data from a SAAB engine has been used. This is due to lack of sufficient detailed information about the Toyota Prius engine.

The SAAB engine is a naturally aspirated gasoline engine, 2.3 l and 16 valves. Its max torque is 212 Nm at 3800 rpm and its max power is 110 kW at 5500 rpm. The engine data used in the model are all measured at Lund University, department of Heat and Power Engineering, Combustion Engines division.

The SAAB engine data is thereafter adjusted through cylinder reduction to suite the size of the Prius ICE (PRIUS, 2000). Input data in the simulation

model are the engine speed and the torque demand. Outputs are the actual torque, the fuel consumption and the emissions. The emission output is derived from scaled emission maps, as based on the SAAB engine measurements.

The sizes of the machines are selected to correspond to the Prius data, as well as possible and adjusted to suit the demands following the single topology. (See Table 8.) Note that the pure series hybrid has a smaller ICE and a larger em1, with preserved total installed power.

Table 8: Vehicle data.

Property:	Unit:	Prius:	Series:	Parallel:	Strigear:	Power split:
$P_{max\ em1}$	kW	33	43	33	33	33
$T_{max\ em1}$	Nm	350	547	419	839	323
$\omega_{max\ em1}$	Rad/s	585	157	157	157	551
fwf[3]	-	5.4	2.0	2.0	4.0	5.4
$P_{max\ em2}$	kW	33	33	33	33	33
$T_{max\ em2}$	Nm	68	79	140	140	140
$\omega_{max\ em2}$	Rad/s	471	419	471	471	471
fwf	-	1.0	1.0	2.0	2.0	2.0
$P_{max\ ICE}$	kW	53	43	53	53	53
$T_{max\ ICE}$	Nm	115	103	112	112	112

5.3   Parameters

There are many possible parameters that are adjustable in the simulation models; vehicle chassis parameters, engine, motor and battery size and types, losses models, charging strategies and driver behaviour etc. To investigate all of them is possibly interesting but not realistic in this survey. It is not the aim and the result flow would be overwhelming.

Since different driving cycles involve varying demands and consequently different results it has been of interest to simulate differently demanding driving cycles. The chosen ones are described above.

In Table 9 the varied parameters are displayed including their original values.

---

[3] fwf = field weakening factor

Table 9:   The table shows the investigated parameters, which have been used for
            simulations with 4 different topologies and 2 driving cycles.

Parameter	Notation	Default value	Unit	Alternatives
Time constant	τ_{ICE}	1	s	1, 10
Battery inner resistance	R_{inner}	100	%	100, 500
Battery size	-	1705	Wh	1705, 853
Charging gain	K_{Pice}	0.1	-	0.01, 0.03, 0.1, 0.3
Engine and motor sizes	-	ICE = 53, em1 = 33 and em2 = 33	kW	53/33/33, 43/15/61
Maximum vehicle speed	-	160	km/h	100, 160

To make the results comparable to such a great extent as possible, the deviation in SOC at start and at stop has been accounted for. This means that the fuel consumption has been adjusted so the SOC ends at the same level as it starts at.

In a strict point of view this leads to a slightly incorrect level of emissions. The emissions are therefore adjusted with the same percent as the fuel consumption has been adjusted with.

5.4   Results

In the simulations, carried out in this comparison and presented below, no other parameters have been adjusted than those explicitly mentioned. Furthermore only one parameter at a time has been varied, if not stated otherwise. This is done since there are several parameters available in the simulation models. To simulate all those parameters, in all different combinations, would result in hundreds of simulations. Such a result flow would be impenetrable.

This chapter presents a limited number of the results, in a selection of parameters, which has been varied. The presented results have been chosen to illustrate the impact the individual parameter has to the behaviour of the single topology.

Comparable results

MTC in Sweden and EPA in USA have made measurements on Toyota Prius. Their results for fuel consumption are displayed in Figure 5-5. For

further details about the measurements, vehicles, SOC deviations, emissions etc, see appendices 9.2 and 9.3.

As a conclusion of the performed investigation of the Prius, the fuel consumption has ended in the range 0.48 – 0.69 l/10 km at ECE 15 and 0.67 – 0.75 l/10 km at US06 for MTC and 0.63-0.72 l/10 km at US06 for EPA.
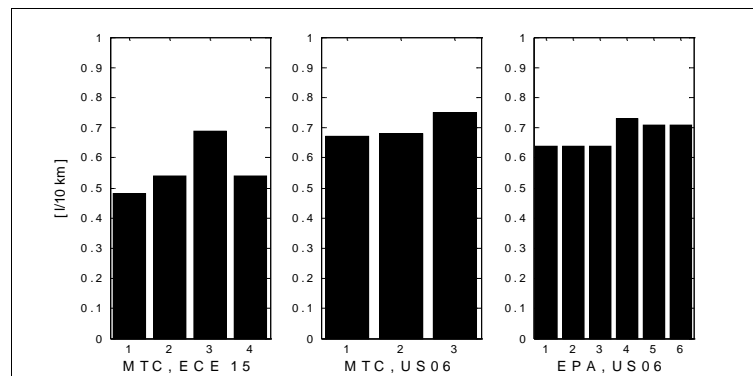

Figure 5-5:   These graphs show the fuel consumption from different measurements, made on a Toyota Prius by MTC and EPA respectively.

Time constant, τ_{ICE}

In Chapter 3.7 the power distribution is described, including its main equations. It is argued that the simplest way to limit the dynamic operation of an ICE is to low pass filter the power requirements from the ICE. The choice of time constant therefore significantly affects the vehicle behaviour.

All four topologies have been simulated with a time constant of 1 and 10 seconds to illustrate the importance of the time constants. The results of the simulations are presented in Figure 5-6.
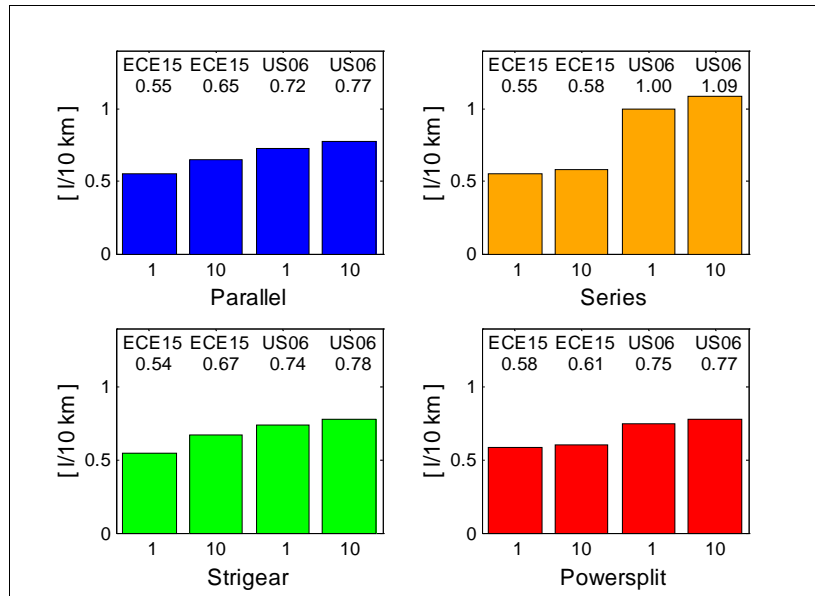
Figure 5-6:   The graphs show the fuel consumption when the time constant, τ_{ICE}, is either 1 or 10 seconds combined with the driving cycles ECE 15 and US06.

As can be seen in Figure 5-6 the slower ECE15 results in lower fuel consumption than the rapid US06. The series topology results in a significantly higher consumption, while the rest are rather similar.

With τ_{ICE} theoretically set to zero, the vehicle is behaving like an ordinary combustion vehicle. No power will then be supplied from the battery, if the ICE can deliver the demanded power. The drawback is that a transient behaviour of the ICE that involves an increased amount of emissions.

When τ_{ICE} increases, the battery has to supply an increased amount of transient power. In Figure 5-7 SOC in the parallel topology, driving ECE 15, are shown. In Figure 5-8 the emissions are also shown for ECE 15, parallel topology.
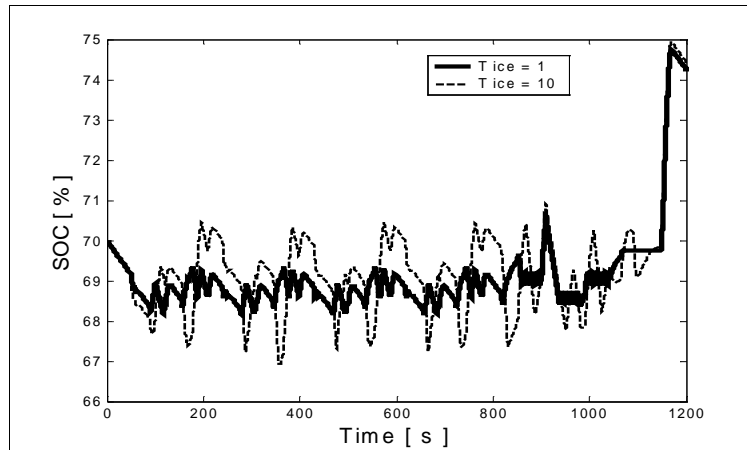
Figure 5-7:   SOC in parallel hybrid, driving ECE 15. Solid line τ_{ICE} = 1 and dashed, thin line τ_{ICE} = 10.

With an increased time constant, the battery has to supply more power. This leads to a smoother use of the ICE at the price of larger battery losses. When the losses get too large, this will be visible in increased fuel consumption.
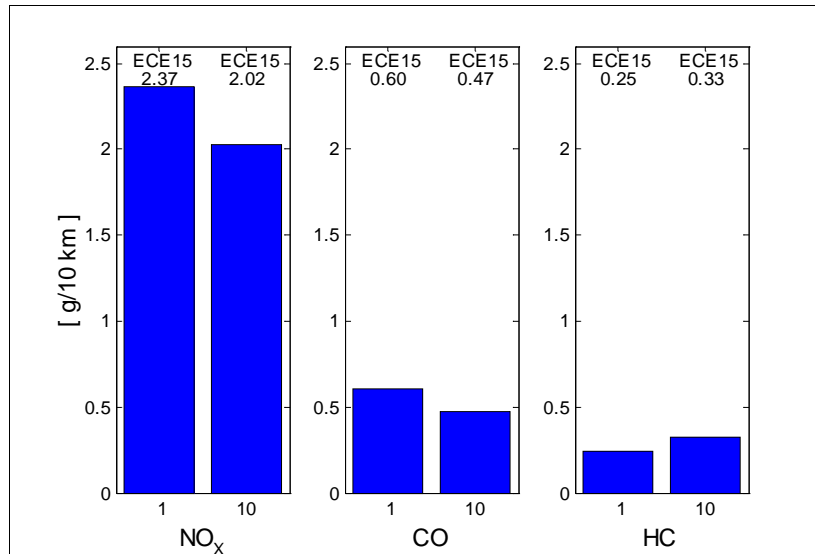
Figure 5-8:   Emissions in g/10 km, while driving the parallel topology in ECE 15
               and varying τ_{ICE} 1 and 10 seconds. The values are adjusted to
               correspond to SOC_{stop} equal to SOC_{start}.

With a large time constant (10 seconds), the engine works smoothly and causes lower amounts of emissions. The price for this is increased fuel consumption, due to losses in battery, electric machines and their power electronics.

The chosen speed and torque combinations while driving the parallel topology in both drive cycles are shown in Figure 5-9. The time constant is 1 second, in both simulations. The rapid highway driving demands higher torque than the slower urban cycle.
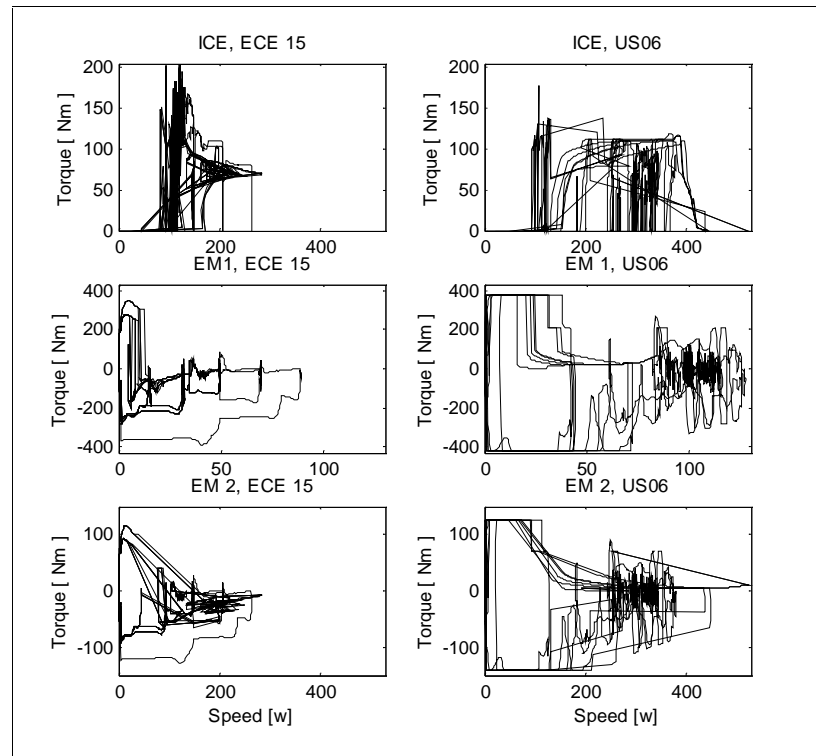
Figure 5-9:   The graphs display speed vs torque for the parallel topology driving
                ECE 15 and US06, with τ_{ICE} = 1. The graphs show, from top to
                bottom, ICE, electric motor 1 and electric motor 2.

   Figure 5-9 gives an indication of where the machines operate in relation to
their maximum ratings. It can be seen that higher and efficient operating
points are reached with US06, as that driving cycle fit better to the vehicle
design.

   In Figure 5-10 are both the ICE- and the total vehicle efficiency are shown
for all four topologies.

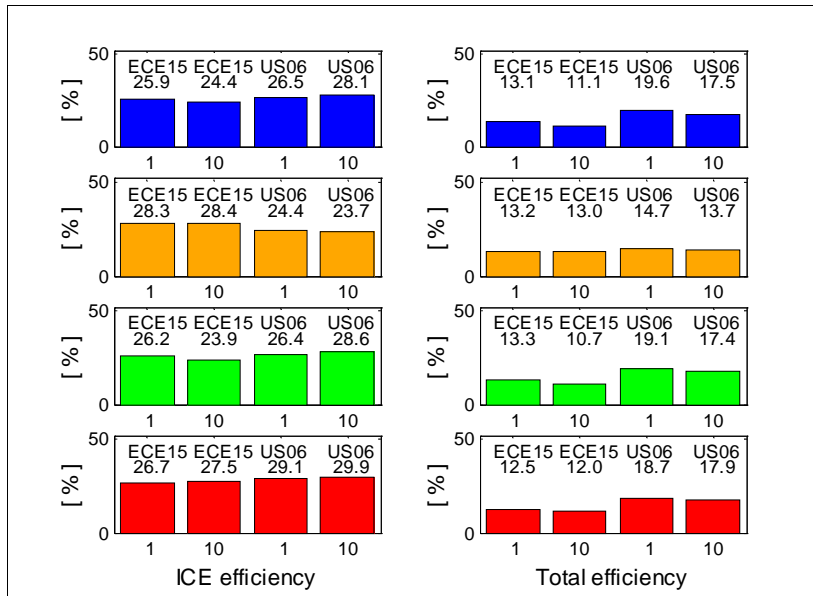Figure 5-10: The graphs show the ICE- and the total efficiency for the four topologies. The efficiency values are corrected to correspond to SOC_{start} = SOC_{stop}. The graphs represent, from top to bottom; parallel-, series-, strigear- and power split topology.

In the way the Toyota Prius is equipped, the total efficiency at high velocities exceeds the one at more moderate speeds (US06 vs ECE 15). The ICE efficiency is strongly controlled and therefore not speed dependent to the same extent.

Battery inner resistance, R_{inner}

When charging and discharging the batteries, there are losses. In the model these losses are not temperature dependent, as they are in reality. The losses are, however, related to the battery inner resistance, R_{inner} (see Figure 3-5). To stress the importance of R_{inner}, the models have been simulated with R_{inner} at 100% and 500% of Prius battery inner resistance. The results are shown in Figure 5-11.
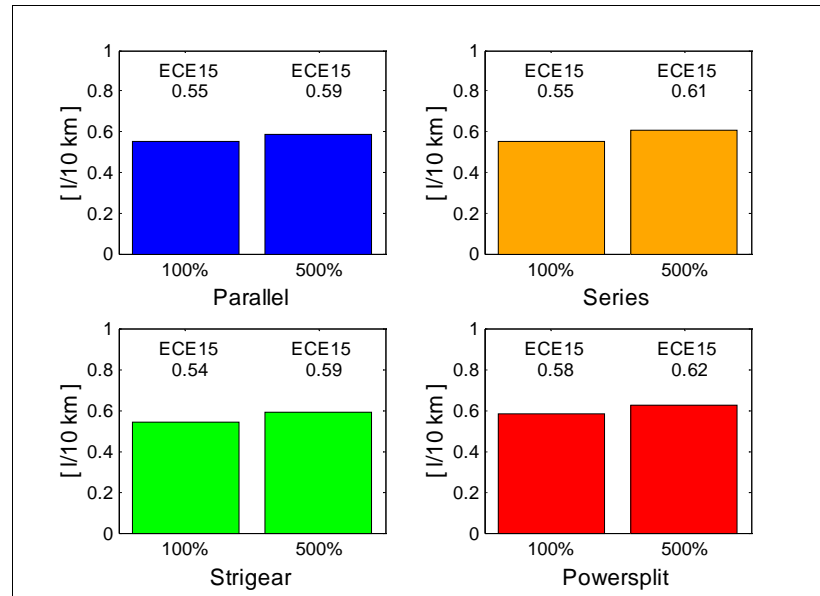
Figure 5-11: The graphs show simulations with variations of R_{inner} (100% and 500%), while driving ECE 15.

As expected, the fuel consumption is slightly higher with increased R_{inner}. Depending on topology, the fuel consumptions increased with 7-11%, when battery inner resistance increased from 100% to 500%.
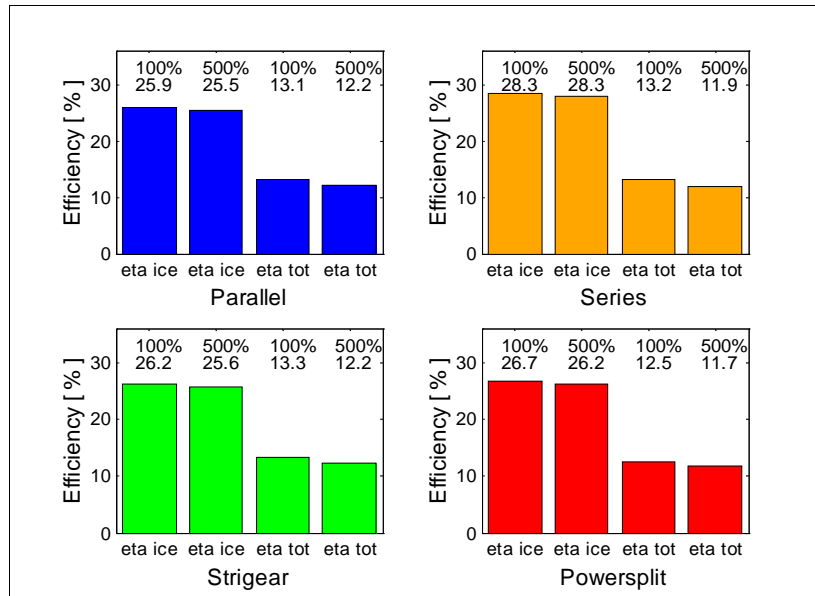
Figure 5-12: The graphs show the ICE- and the total efficiency for the vehicle, when simulated with R_{inner} = 100% and 500% respectively. The efficiency values in the figure are corrected to correspond to SOC_{start} = SOC_{stop}.

The ICE tends to work with the same efficiency independently of the battery inner resistance. For the total losses, the higher inner resistance of the battery is however clearly visible. The efficiency of the ICE is depending on the chosen control algorithm, not on the battery.

Battery size

The batteries in the simulation models are in the basic design chosen to be as equal to the ones in Toyota Prius as possible, i.e. with a specific energy of 44Wh/kg, 1.020 kg/module and 38 modules.

The parallel topology has, besides the Prius sized battery, also been simulated with a battery half the Prius size. The simulations have been carried out on both the ECE 15 and the US06 cycles. The results of these simulations are shown in Figure 5-13.
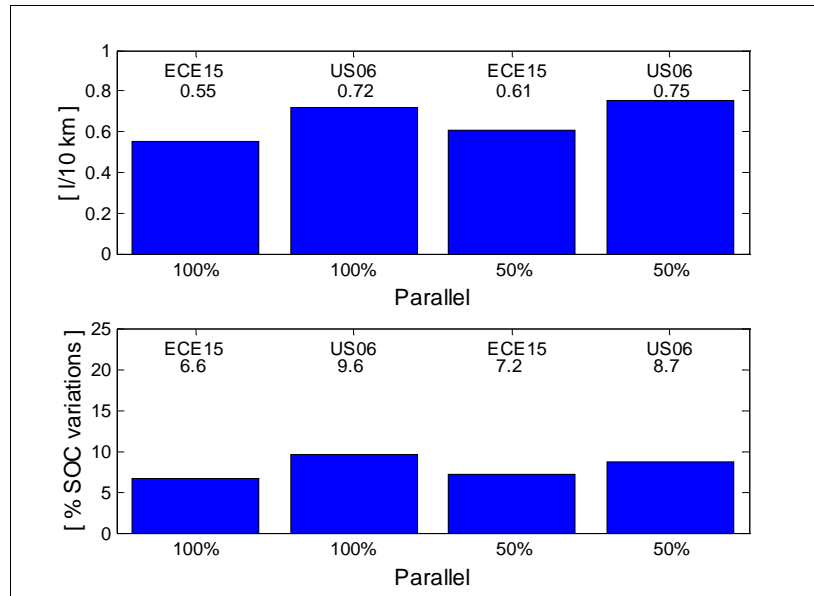
Figure 5-13: The upper graph shows the fuel consumption and the lower shows the variations of SOC (max - min value). The simulations are made on the parallel topology with variations of battery size, 100% and 50% respectively combined with ECE 15 and US06. It must be noted that the US06 cycle keeps the SOC at a relatively even deviation. The ECE 15 contains a powerful retardation before its stop, which diverge from the average SOC deviations in the cycle. This retardation results in a relatively high total SOC deviation the ECE 15 cycle, even though it is slightly lower than in the US06 cycle.

With smaller batteries the variations in the SOC are increasing. This leads to larger losses, but as can be seen this has only small influences on the fuel consumption. With a smaller battery, the absolute figures of the SOC deviations are increased. This is due to that the same amount of power still is requested, but from a smaller battery.

Figure 5-14: The figure shows the ICE- and the total efficiency for the vehicle, simulated with 100% and 50% battery, using both driving cycles. The efficiency values are corrected to correspond to $SOC_{start} = SOC_{stop}$.
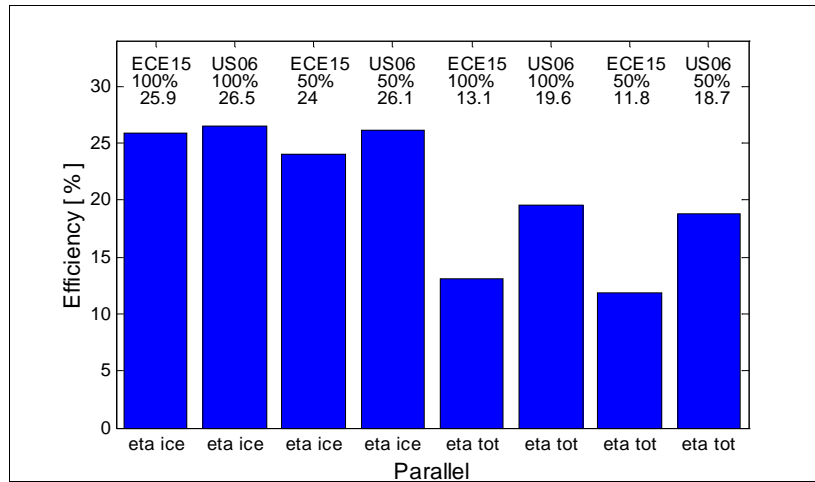
A reduced battery size leads to an increased fuel consumption and lower efficiency, but the deterioration of system performance is not proportional to the reduction of battery efficiency.

Charging gain, K_{Pice}

The ICE power demanded is a sum of power demands for traction, auxiliary power and a proportion of the deviation of the SOC.

When the SOC diverges from its reference value, a *P*-controller requests a correction (the battery can be overcharged as well). With a small gain factor, a SOC deviation is slowly corrected, i.e. the battery is permitted to compensate for a transient ICE power request. This will be done to the price of larger deviations of SOC. A larger gain factor adjusts the SOC deviation quicker, at the expense of higher ICE power and its associated emissions.

To investigate the influence of different gain factors, the parallel and the strigear topology have been simulated in both drive cycles and with different gains. The SOC deviation is multiplied with both the maximal ICE power and with a gain factor, called K_{Pice}, and thereafter added to the total ICE power demand. The gain factors investigated are 0.01, 0.03, 0.1 and 0.3 and the results can be seen in Figure 5-15.

As the default design in the simulation models in all other simulations K_{Pice} = 0.1 has been used. Facing the simulation results this did not turn out as the

best option. Therefore some of the parameters have been simulated with not only the default value, but also an alternative value of K_{Pice} (i.e. 0.03).
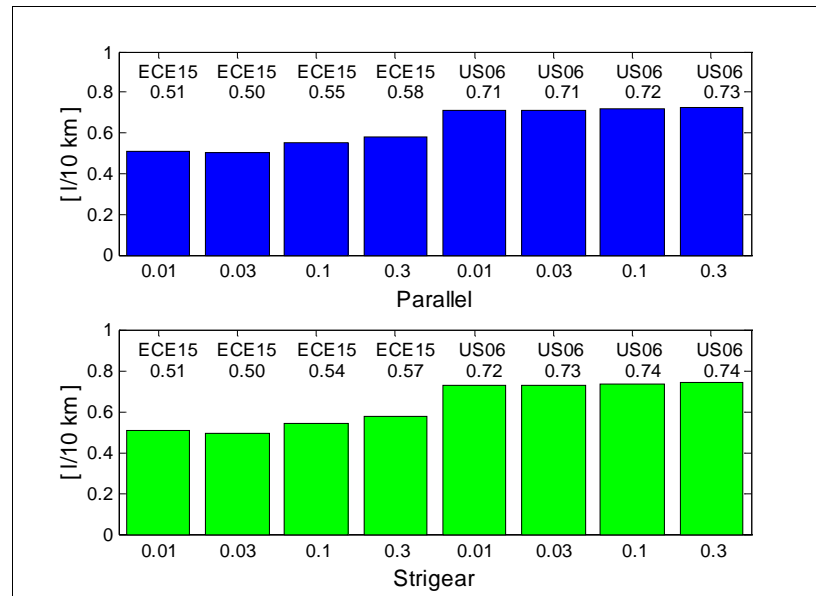
Figure 5-15: This figure shows the fuel consumptions when simulating the parallel and strigear topology with variations of the charging gain, K_{Pice} and driving cycle.

When choosing a larger gain it is accompanied with reduced utilization of the battery. As can be seen in Figure 5-16 the ICE has to supply the power demand on its own to an increasing extent when the gain is increased.
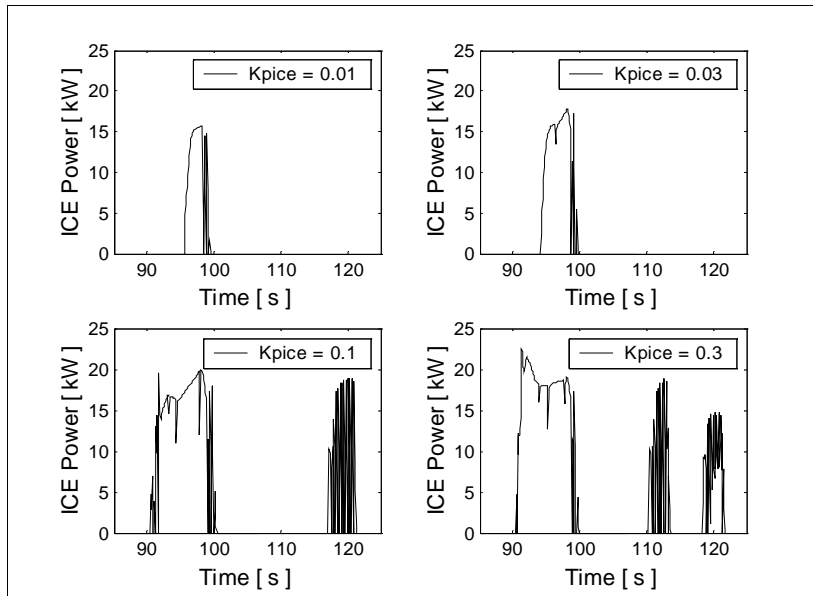
Figure 5-16: The figure illustrates the consequences that different K_{Pice} have for the ICE power supply. All four graphs are for the parallel topology driving ECE 15.

A small gain stresses instead the battery. In Figure 5-17 the SOC are shown for the same simulations. A large deviation in SOC reduces to battery lifetime and consequently ought to be avoided.
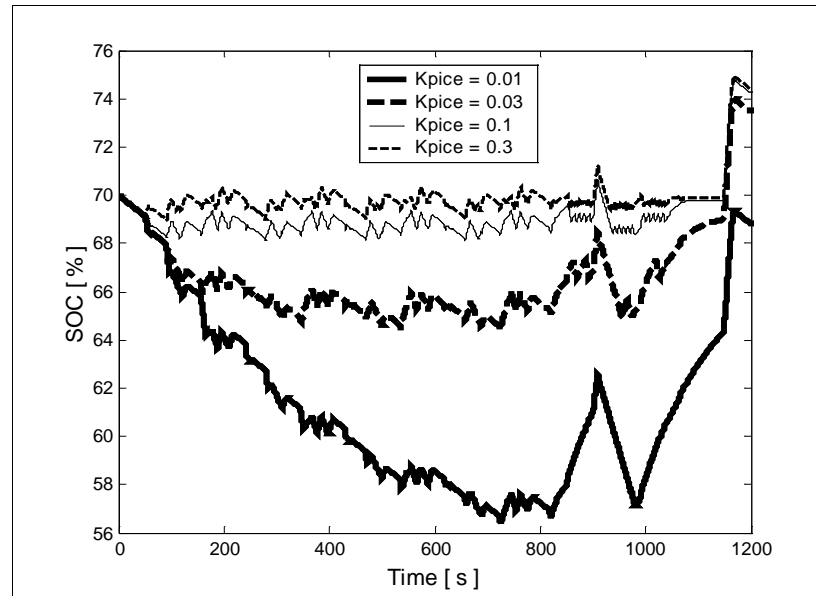
Figure 5-17: The figure shows SOC for the parallel topology when driving ECE 15 when varying K_{Pice}.

In Figure 5-18 the emissions for the very same simulations are shown. The emission levels cannot be used as foundation for motivating a larger stress of the battery, i.e. smaller gain.
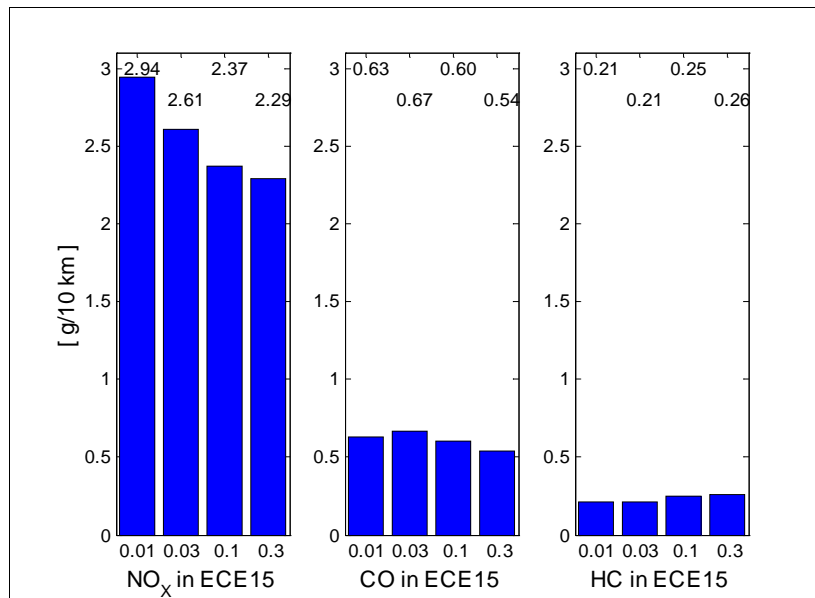
Figure 5-18: The graphs shows the emissions in g/10 km while driving the parallel topology in ECE 15 and varying K_{Pice} between 0.01, 0.03, 0.1 and 0.3. The values are adjusted to correspond to SOC_{stop} equal to SOC_{start}.

The emissions are depending on the control of the ICE. The ICE in its turn is controlled consider its efficiency. The ICE is therefore only working at a rather high efficiency.
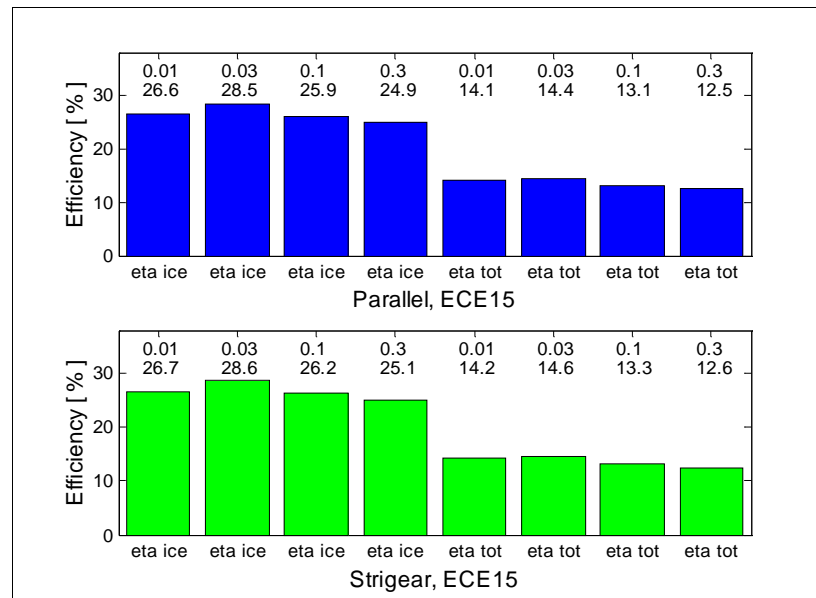
Figure 5-19: The figure shows the ICE- and the total efficiency for the vehicle simulated in ECE 15 and K_{Pice} varied between 0.01, 0.03, 0.1 and 0.3. The efficiency values are corrected to correspond to $SOC_{start} = SOC_{stop}$.

The simulations show that $K_{Pice} = 0.03$ is the best choice, i.e. at 10% deviation of SOC, the charge control requests 30% of ICE maximum power.

Varying size of electric machines and ICE

The simulated models are all equipped with the same engine and motor sizes as the Toyota Prius. To examine the chosen distribution of power, an alternative solution is simulated as well. This alternative is made with the same total power as in the Prius, but with another allocation of the power.

For this alternative solution the power demand for ECE 15 has been investigated and the traction motor (electric motor 1) was designed to *almost* be able to handle it. The ICE power was also reduced in size.

There are of course other possible ways to reallocate the total power supply and there are also opportunities to simulate with a different total power installed, but to limit the simulations, only one alternative solution is investigated. The two engine and motor sizes alternatives that have been simulated are shown in Table 10.

Table 10: Power distribution used in the simulations.

Case	P_{ICE} [kW]	P_{cm1} [kW]	P_{cm2} [kW]
Toyota Prius	53	33	33
Alternative solution	43	15	61

To keep the total power constant is only a crude way of creating comparable drive systems. To really design a comparable alternative would involve redesign of the machines and the power electronics. Thus, the results created in this section must be seen as indications only.

In Figure 5-20 the fuel consumption are shown for both driving cycles, both alternatives. One simulation has also been carried out with $K_{Pice}= 0.03$ (the charging gain) instead of 0.1.
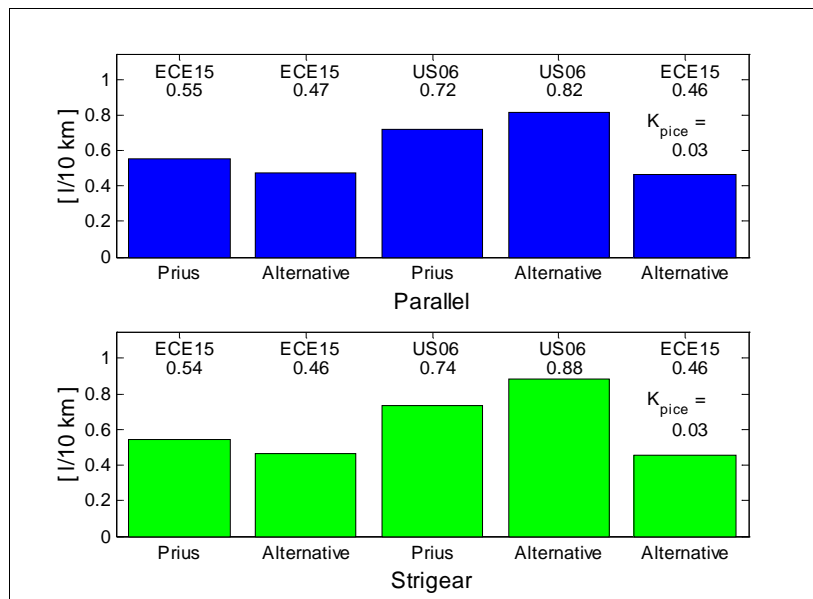
Figure 5-20: The figure shows the fuel consumption when simulating parallel and strigear topology, using different engine and motor sizes as well as varying the charging gain, K_{Pice}, in the last simulation.

The original motor and engine sizes are not the most suitable while driving ECE 15. When driving the more rapid US06 the original solution consumes less fuel then the alternative one. This might not be to surprisingly, since the alternative solution is chosen with considerations to ECE 15, not US06.

In Figure 5-21 the ICE- and total efficiency, for the simulations described above, is shown.
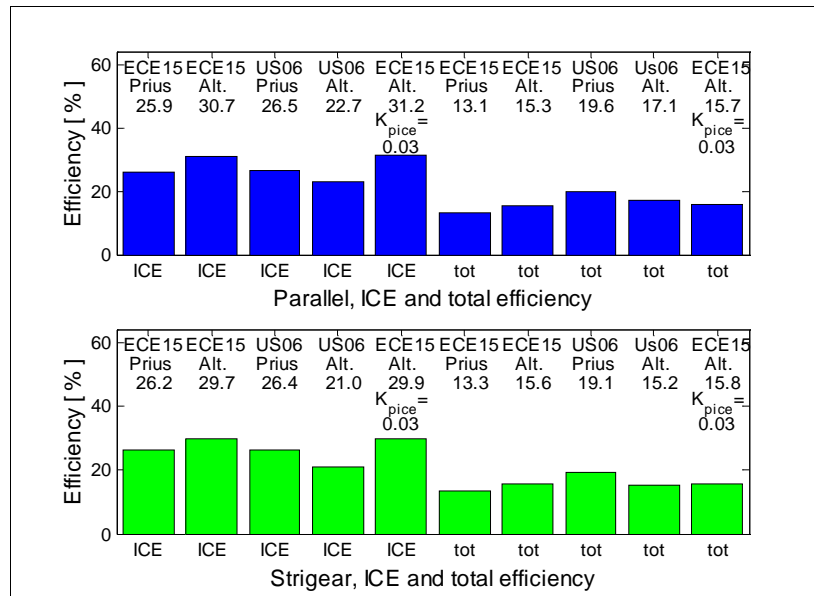
Figure 5-21:   The graphs show the ICE- and the total efficiency. The efficiency values are corrected to correspond to SOC_{start} = SOC_{stop}. In the simulations the engine and motor sizes, driving cycle and charging gain have been varied.

With the alternative sized engine and motors the efficiencies are notably raised, when driving the slower ECE 15. The alternative design allows the engine and motors to operate at higher efficiency and the chosen control algorithm switches off the ICE and/or electric motor 2 when their efficiencies are below a certain level.

In the simulations made with the rapid US06 cycle the efficiency is consequently lowered with the alternative design, since the engine and motors then will be sized to fit the a slower driving cycle.

The SOC for three of the parallel simulations are shown in Figure 5-22. The SOC is varying more in the case with the alternative engine/motor solution, ECE 15 and K_{Pice} = 0.03, but it is consuming a lower amount of fuel than the other two alternatives, as shown above.
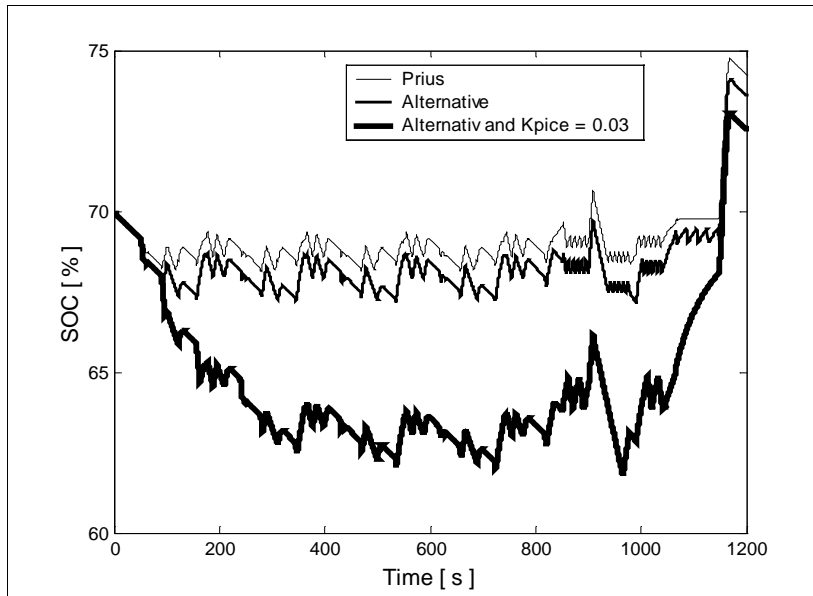
Figure 5-22: The figure illustrates the SOC while driving the parallel topology in ECE 15 as Prius, alternative design and alternative design with K_{Pice}=0.03.

The Figure 5-23 including the emission results shows that the emission levels are affected by the choice of engine and motor sizes.
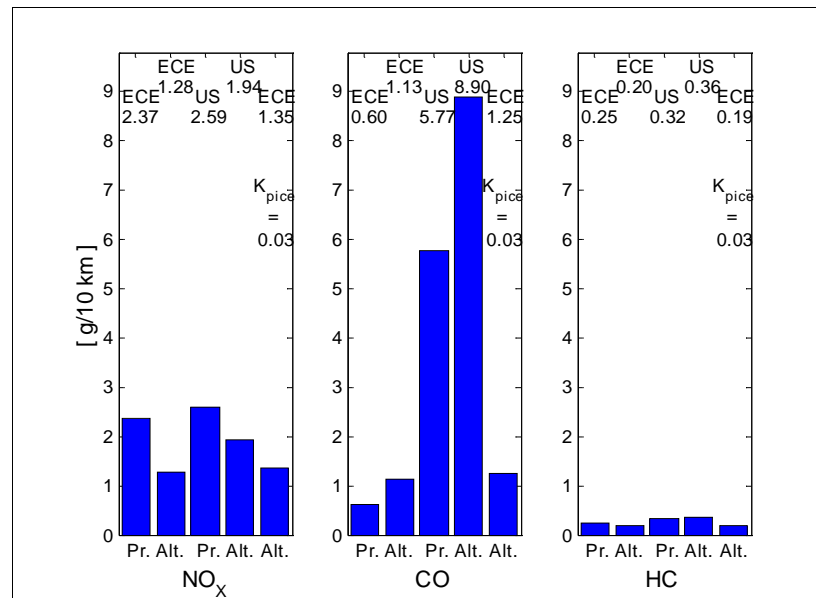
Figure 5-23: The figure displays the emissions in g/10 km for the parallel topology. The simulations have been done to the two engines/motors alternatives and with two different driving cycles. Finally has the charging gain, K_{Pice}, been given an alternative value (0.03).

Maximum vehicle speed

The ICE torque/speed distribution will be designed with a gear ratio suitable to the chosen maximum vehicle speed. This will lead to a limited efficiency at moderate speeds. The best efficiency is only reachable at speeds that are seldom, legally, used. Toyota Prius is designed for a maximum speed of 160 km/h and so are the simulation models in their default design.

There are vehicles available at the market, for instance pure electric vehicles, designed with maximum speed of 100 km/h. To investigate the impact that a lower maximum speed would have for the fuel consumption, such simulations have been carried out. Only the gear ratio has been redesigned. The power supplies are still the same. For this purpose only ECE 15 has been used, since the maximum speed of US06 is 130 km/h.

Yet one case has been added. The alternative engine and motor sizes design, in combination with reduced maximum speed are simulated as well. See Figure 5-24.

Figure 5-24: Variations of maximal vehicle speed (160 and 100 km/h) while driving
ECE 15. The simulations have been carried out for parallel- (3), series-
(2) and strigear (3) topology. The parallel- and strigear topology have
also been simulated with the alternative engine/motor design.

A lowered maximum speed, in combination with the alternative engine
and motor designs leads to a reduced fuel consumption. There is an
ambiguous connection between ICE- and total vehicle efficiency. This is due
to the control of the ICE. The engine is switched off if the efficiency is too
low and the switching on and off is limited with hysteresis, and allows hereby
some variations. The efficiencies for the eight simulated cases are found in
Figure 5-25.

The efficiency figures shows that there is a possibility to raise the efficiency
slightly, if combining a lowered maximum speed with an alternative engine
and motor design. A lowered maximum speed does not by itself reduce the
fuel consumption and results instead in a lowered efficiency.

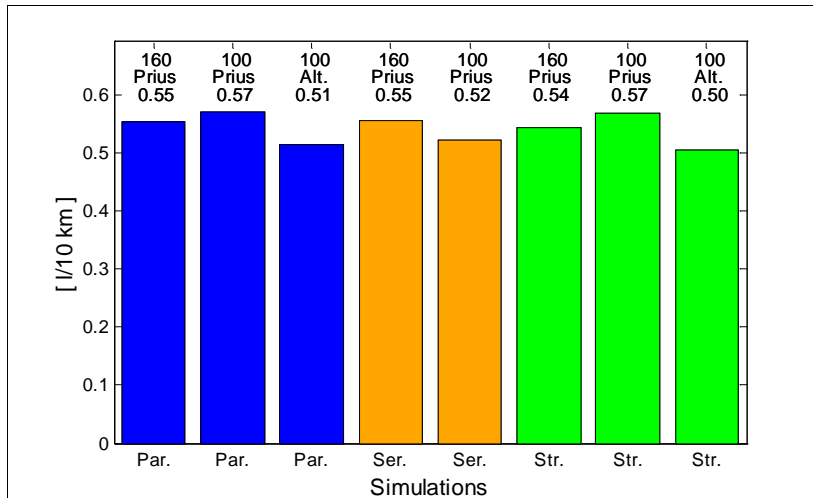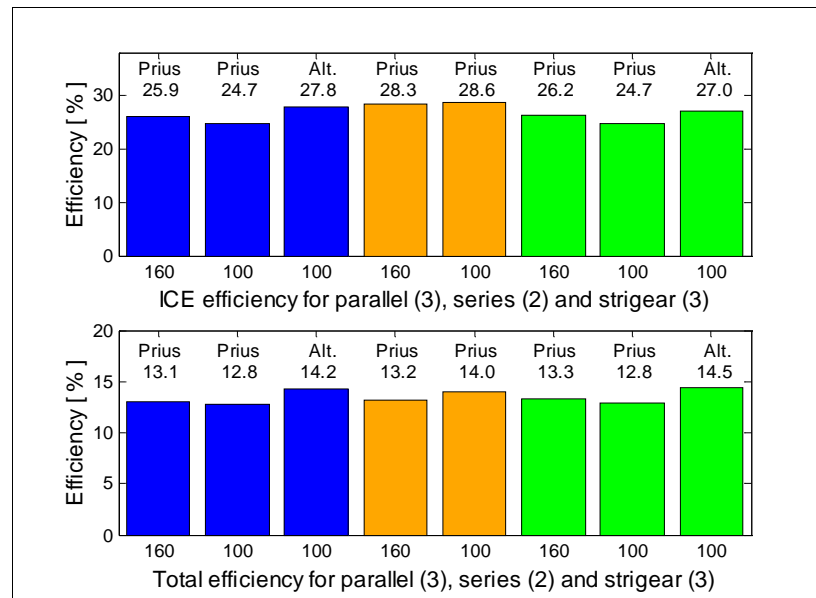Figure 5-25: The graphs show the ICE- and the total efficiency when the maximal vehicle speed has been varied (160 and 100 km/h) while driving ECE 15. The simulations have been carried out for parallel- (3), series- (2) and strigear (3) topology. The parallel- and strigear topology have also been simulated with the alternative engine/motor design. The efficiency values are corrected to correspond to $SOC_{start} = SOC_{stop}$.

Strigear

The strigear topology has a control algorithm that admits the advantage to chose a control strategy where the over-all losses are as low as possible. This means that the clutch is opened or closed and the topology runs as a parallel or series topology.

The simulated pure parallel topology is designed with a high efficiency. This is due to the choice of two electric motors, instead of one large, in combination with a control algorithm that switches off the ICE and the generator when their efficiency reaches below a stipulated limit. This way of controlling the topology can raise the efficiency, since it is possible to use only one machine at low power.

Switching the strigear does not only imply controlling a clutch. Included in the two different modes are unique speeds and torque for the electric machines and the ICE. Hence a mode change for the strigear implies correction of diverging speed and torque levels for motors and engine. Yet

another important factor that influences the topology is that it is bringing a history, for instance the SOC, which might be the result of "another topology".

Below, Figure 5-26 and Figure 5-27, the motors and ICE behaviour for first the parallel and after that the strigear topology are displayed when driving ECE 15, with no parameter changed from the default design. As previous shown, both topologies consume 0.55 l/10 km with this design.
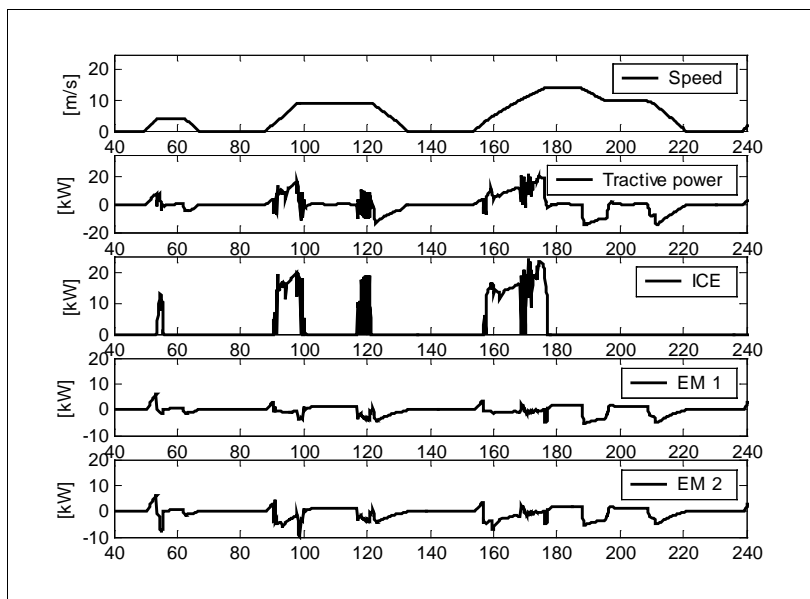
Figure 5-26: The figure shows the engine and motor power supply in the timeslot 40 - 240 seconds, when driving the *parallel* topology in ECE 15.
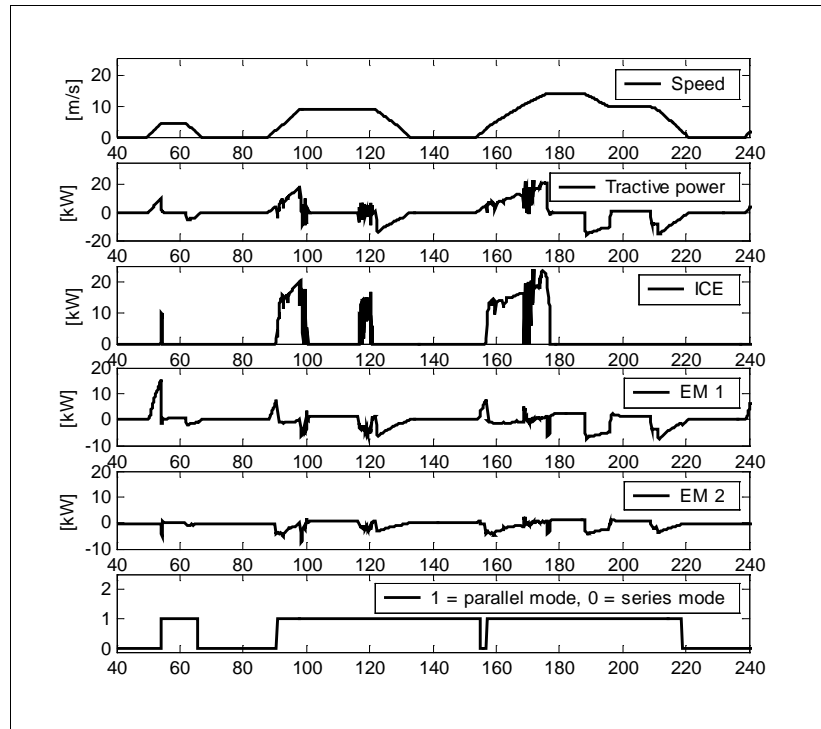
Figure 5-27: The figure shows the engine and motor power supply in the timeslot 40 - 240 seconds, when driving the *strigear* topology in ECE 15.

The parallel topology turns out as the preferred alternative, since the strigear isn't switching very often. The switching behaviour for the entire cycle is shown in Figure 5-28.
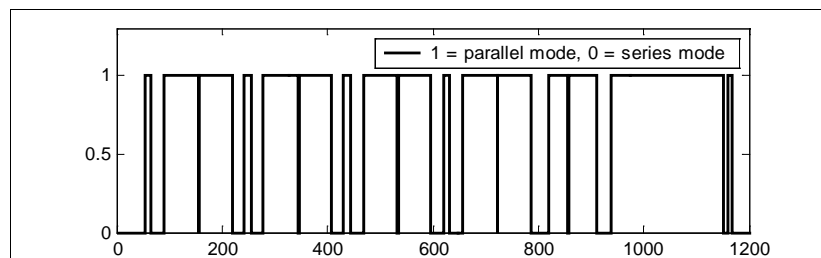
Figure 5-28: The mode switching in ECE 15, 1 = parallel mode and 0 = series mode.

As can be seen in figure above, the predominant mode choice is the parallel mode. The profits made by changing mode, seems to be lost in connection with the adjustment of speed and torque in the new mode. In Figure 5-29 below, speed and torque levels are shown during ECE15, 750 – 1000 seconds, when running the strigear and parallel topologies.
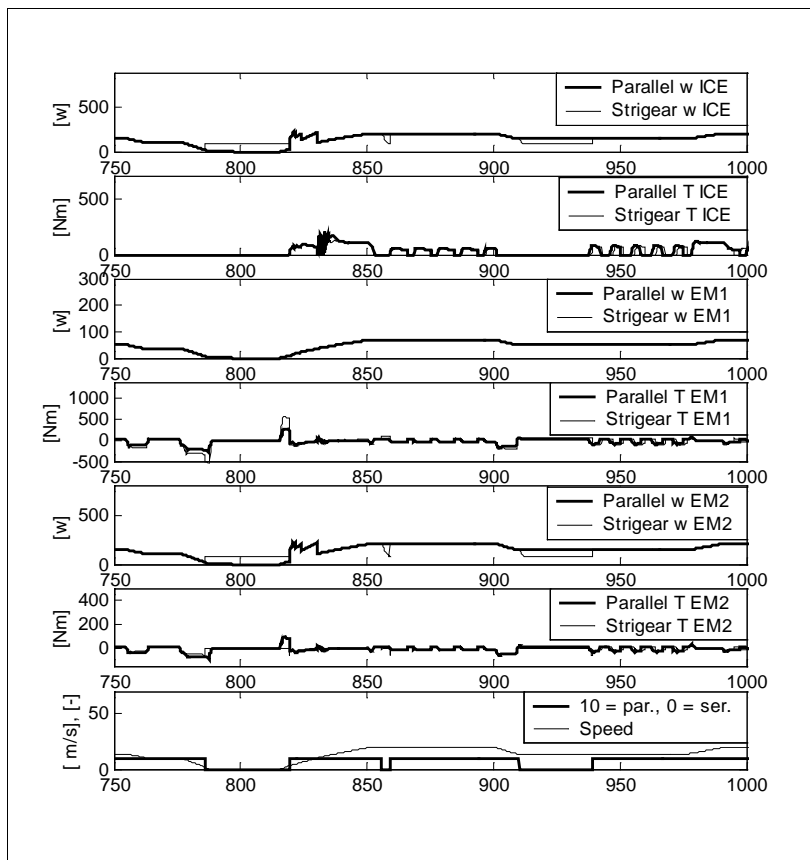
Figure 5-29: The graphs show speed (w) and torque (T) for the strigear (thin line) and the parallel (fat line) when running ECE 15. The figure is chosen for the timeslot 750-1000 seconds. The lowest graphs display the drive cycle (thin line) and the mode changes (fat line). Series mode is displayed as value zero and parallel mode differed from zero.

The figure above shows that the control of the two topologies differs. It appears distinctly that the parallel mode has the predominantly best efficiency. If the parallel topology instead had been equipped with *one* electric

motor instead of two, the result would have turned out slightly different. The motor sizes are possible to vary to a limited extent. It is not possible to, for instance, choose one motor as 66 kW and the other one as zero, and hereby obtain a pure parallel topology. The choice 65 kW and 1kW is however accepted and would result in slightly increased fuel consumption. The difference in fuel consumption is not large and can be seen in Figure 5-30.
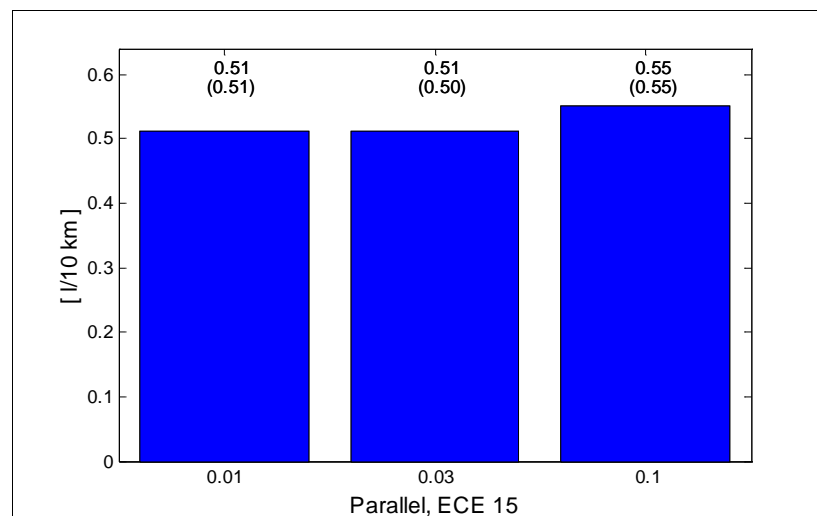
Figure 5-30: The parallel topology simulated with electrical machines of 1 kW and 65 kW. The "almost-one-electrical-machine-design" has been simulated with varied K_{Pice} (0.01, 0.03 and 0.1). These results can be compared to the ones presented in Figure 5-15, the results of which are given in parenthesis in this figure.

The choice of charging gain, K_{Pice}, affects the response from the ICE to a SOC deviation. This has, on its turn, influences on the total losses, that is the mode switching. In Figure 5-31 the switching is displayed for different charging gains.
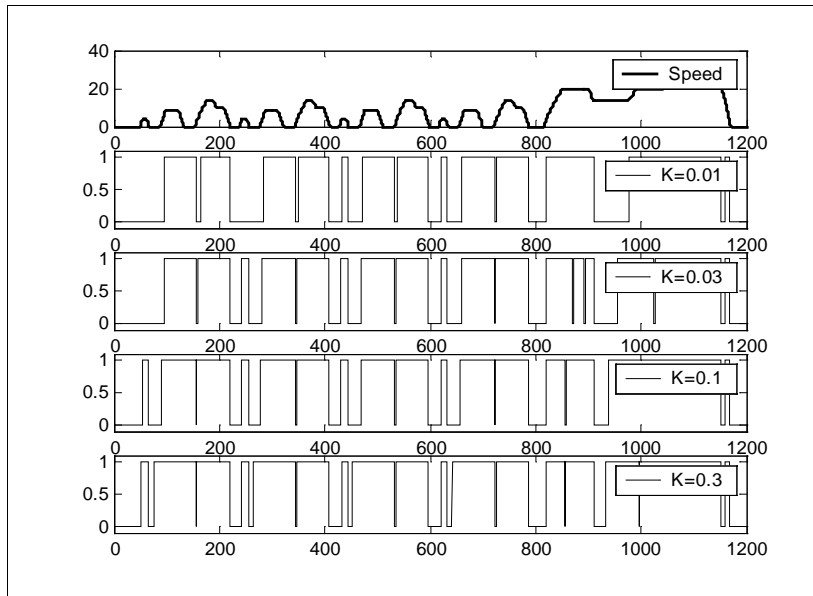
Figure 5-31: The graphs show different mode switching for strigear topology, depending on the chosen charging gain, K_{Pice}. The uppermost graph shows the speed (m/s) for ECE 15. The other graphs show the strigear mode switching. 1 is equal to parallel mode and 0 is equal to series mode.

As can be seen in the figure, a larger charging gain leads to a mainly parallel behaviour. Larger K_{Pice} implies that the ICE has to supply the tractive power demand to a larger extent and the highest efficiency for the ICE power supply is the parallel path.

When the batteries are allowed to compensate the power demand, i.e. K_{Pice} is small, the topology turn more often into the series mode. This is due to that the battery is more dynamically used.
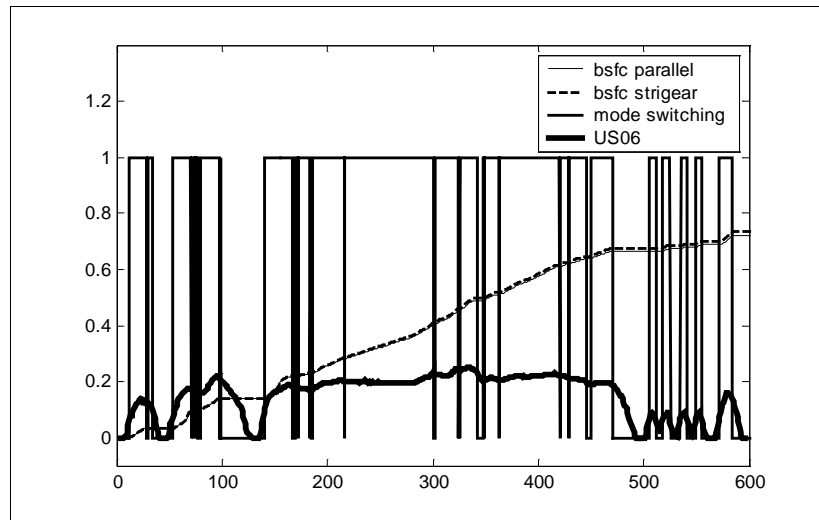
Figure 5-32: The figure displays the fuel consumption for US06, parallel- (solid line) and strigear- (dashed line) topology. The fat line displays the mode switching, 0 = series mode, 1= parallel mode.
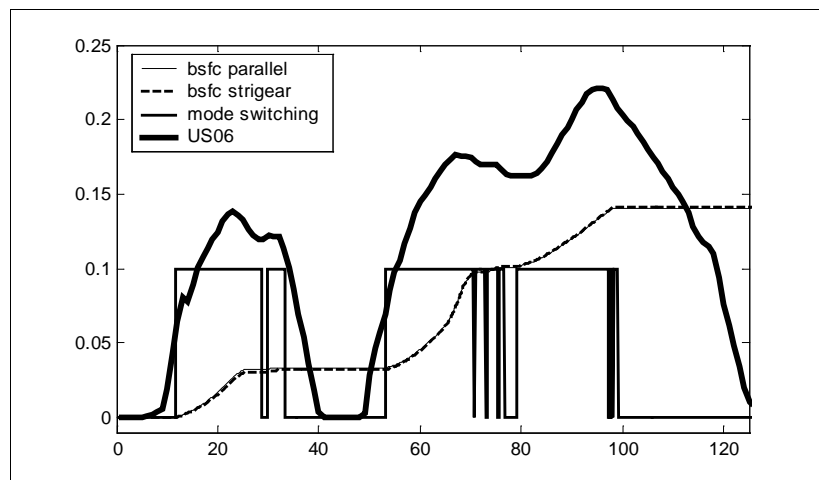
Figure 5-33: This is the fuel consumption for the first 125 seconds for US06, parallel and strigear topology. Mode switching is displayed as the fat line, 0 = series mode, 0.1 = parallel mode.

In Figure 5-32 and Figure 5-33 the fuel consumption are displayed for the parallel and strigear HEV. In the heaviest accelerations the strigear consumes

slightly more fuel then the pure parallel hybrid, though it is working in
parallel mode.

In Figure 5-34 speed vs torque are displayed for both strigear and parallel
HEV. It can be compared with the results of the parallel running ECE 15, see
Figure 5-9.
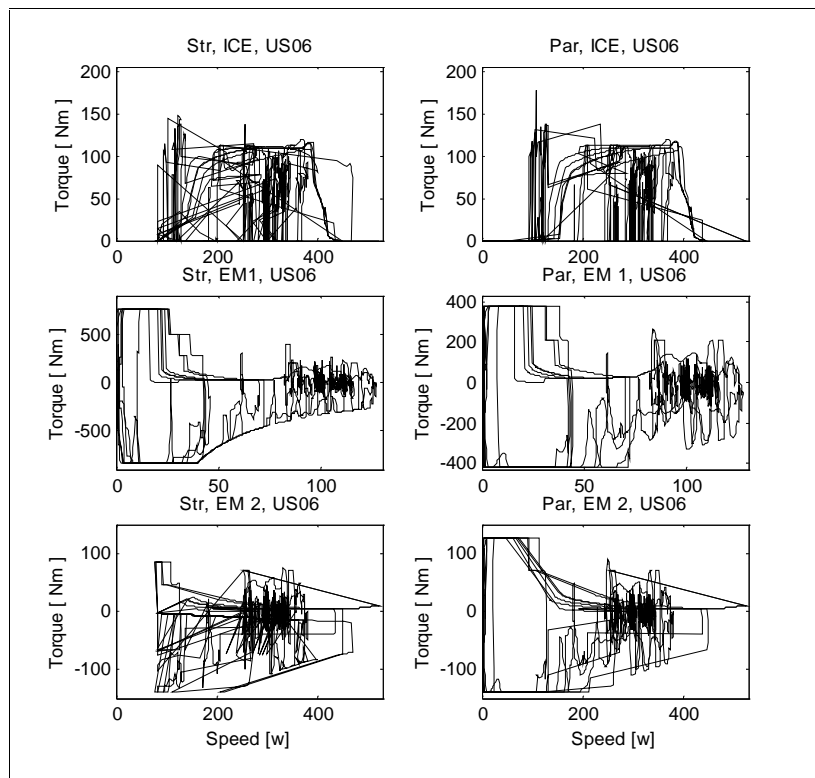
Figure 5-34: The graphs display the speeds and torques when driving parallel and
strigear topology in US06.

As can be seen, in Figure 5-34, the hybrids are not identically equipped.
The control algorithms of the hybrids differ too, which is clearly visible in the
figure above. Figure 5-35 shows the choice of torque and speed for the ICE
and electrical machines for the first 250 seconds of US06.
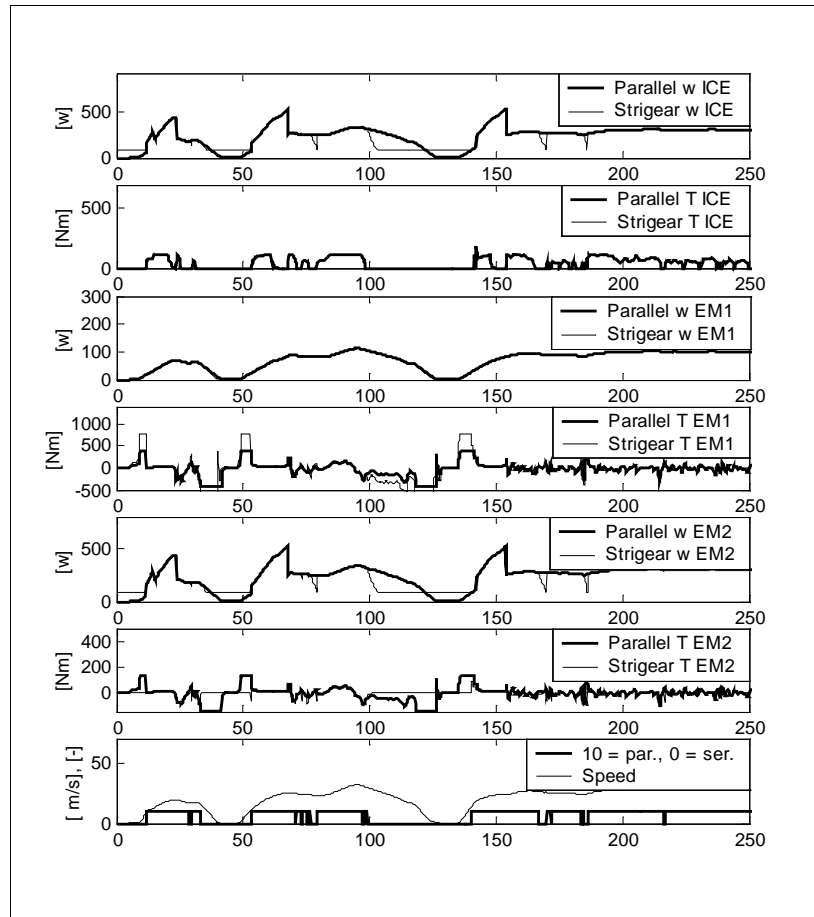
Figure 5-35: The graphs show torques and speed for the ICE and the electrical machines for parallel (fat line) and strigear (thin line) while driving US06, 0-250 seconds. The lowest graph also displays the strigear mode switching.

As can be seen the speed and torque choices are not identical. When the strigear is switching this affects its torque and speed choices clearly. The most distinct difference between the topologies is the torque demand of the electric machines. The electric machine 1 supplies the entire torque demand, when strigear runs in series mode, while the parallel at the same time distributes the torque demand to both machines.

If the strigear is run with the *exact* configuration as the parallel topology, the fuel consumption, while running US06, is reduced less than 1%. The

speed and torque choices turn out quite differently. See Figure 5-36. If this
redesigned strigear runs ECE 15, there will be no impact on the fuel
consumption.
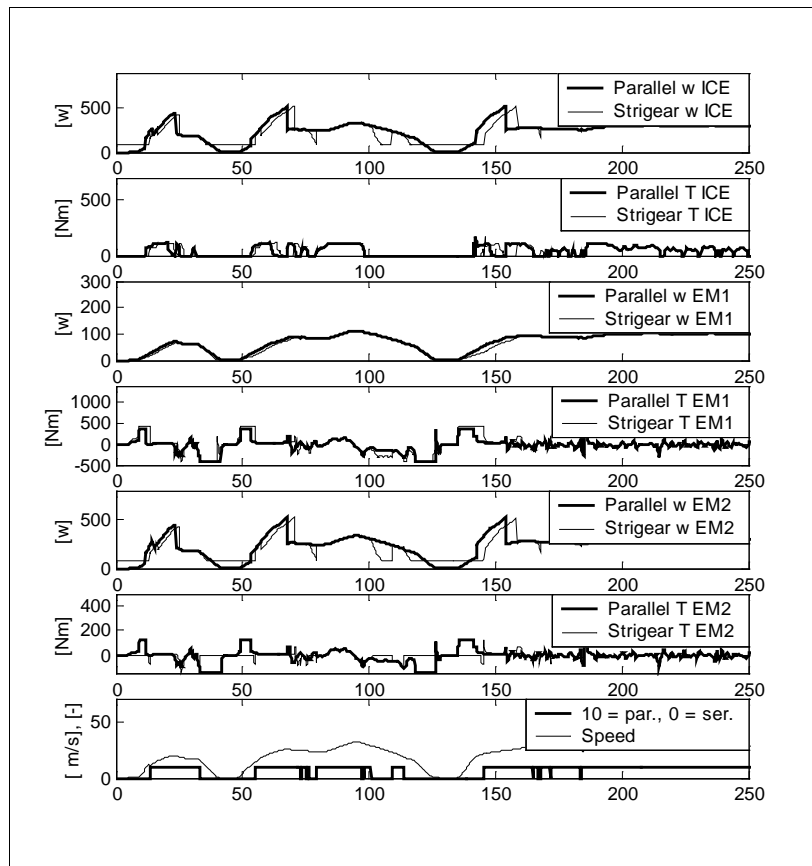
Figure 5-36: The graphs show torques and speed for the ICE and the electrical
machines for parallel (fat line) and strigear *exact* equal to the parallel
(thin line) while driving US06, 0-250 seconds.

Criteria

The received simulation results can be evaluated with help of different
criteria. According to the criteria presentation in Chapter 2, the fuel
consumption and emissions will be valued. For this purpose simulation
results, including the original values of parameters, have been used.

For pricing the emissions, the prices for urban driving, set by Friedrich and Bickel (Friedrich- Bickel, 2002), will be utilized.

Table 11 displays the cost/10 km for fuel and emissions, according to criteria 1.

Table 11: Comparison table using the criteria 1. Lowest result figure gives "the best" topology, when using criteria 1. All prices are set in Euro.

Topology	Bsfc [l/10 km]	NO_x [g/10 km]	CO [g/10 km]	HC [g/10 km]	Drive cycle	Result Criteria 1 [Euro]
Price [Euro]	1.02	0.0587	$2.13 *10^{-5}$	0.0157		
Parallel	0.55	2.37	0.60	0.25	ECE 15	0.71
Series	0.55	1.11	2.45	0.29	ECE 15	0.64
Strigear	0.54	2.41	0.58	0.24	ECE 15	0.70
Power split	0.58	2.59	0.60	0.28	ECE 15	0.75

This is only one way of pricing the simulation results. In Table 12 the mutual comparison is used as judgement. This procedure gives a slightly different result and should be look at as an example.

Table 12: Comparison table using the criteria 2. Lowest result figure gives "the best" topology, when using criteria 2.

Topology	Bsfc [l/10 km]	NO_x [g/10 km]	CO [g/10 km]	HC [g/10 km]	Drive cycle	Result Criteria 2
Weight factor	1	1/3	1/3	1/3		
Parallel	2	2	2	2	ECE 15	4.0
Series	2	1	4	4	ECE 15	5.0
Strigear	1	3	1	1	ECE 15	2.67
Power split	4	4	2	3	ECE 15	7.0

When the size of the emissions or the fuel consumption is not important, more than for ranking, extreme values will not have large influence. On the other hand small differences will be given a larger weight. This is what occurs while using criteria 2.

Chapter 6 Conclusions

Four generic hybrid electric topologies have been simulated in two drive cycles with as equal conditions as possible. This is done with the aim to study the performance, losses, fuel consumption and emissions of the topologies. The investigated topologies are parallel-, series-, strigear- and power split HEV.

6.1   Influences of parameters

The influences of six different parameters have been investigated. The parameters have been varied one by one, to illustrate its influence on the topology. The investigated parameters are: charging time constant for power demand (τ_{ICE}), battery inner resistance (R_{inner}), battery size, charging gain (K_{Pice}), engine and motor sizes and finally maximum vehicle speed.

Time constant, τ_{ICE}

The time constant is related to the low pass filtering of the total power demand, which thereafter will be requested from the ICE. Fast ICE dynamics, i.e. a short time constant, τ_{ICE}, load the battery less, and require faster dynamic response from the ICE. This implies lower battery losses and facilitates a smaller battery. It also leads to lower fuel consumption, even though in some cases hardly visible. That means also that the vehicle efficiency is higher with a faster time constant, but the time constant should not be so short that the ICE is forced to supply the immediate power demand, including the power transients. The speed of the ICE response has to be related to the emissions. In the extreme case with a very small time constant the ICE has to respond faster and the risk for transient emissions will increase.

The vehicle is equipped in a way that better suits the rapid US06 cycle. This results in higher efficiencies for the highway cycle.

Battery inner resistance, R_{inner}

To investigate the sensitivity of the model to battery efficiency, the battery inner resistance has been raised from its default value of 100% to 500%. This resulted in a reduced total efficiency and an increased fuel consumption of 7-11%. The ICE efficiency was hardly affected by the raised level of R_{inner}. This is due to that the control law of the ICE is decoupled from the battery efficiency.

Battery size

The battery has been reduced to half the size to stress its impact on the fuel consumption and vehicle efficiency. This resulted in a larger deviation of the SOC, but no, or negligible, increase in the fuel consumption. The ΔSOC is still less than 20%, which implies that even smaller battery could be used.

The energy density is high enough even with reduced size battery, but the power density may be a limiting factor. This implies a possible advantage with use of super capacitors.

Charging gain, K_{Pice}

The total power demand is a sum of power demands. One of the contributors is when the SOC diverges from its reference value. The deviation is multiplied with a gain factor, K_{Pice}. A small gain factor permits a large deviation in SOC while a large factor will adjusts the SOC quicker. That means that the hybrid will act more like a pure ICE vehicle when K_{Pice} is large. On the other hand, a large deviation of the SOC leads to a reduced battery lifetime and ought to be avoided.

Reducing the gain factor from 0.03 to 0.01 leads to increasing SOC deviation from 10 to 15 %. This larger SOC deviation leads to increased fuel consumption. This is the reason why a small, but not too small gain factor results in the highest vehicle efficiency.

Size of electric machines and ICE

The simulation vehicle is equipped with the same size of electric machines and ICE as the Toyota Prius. This choice has been examined as well as an

alternative solution. In the alternative solution, the total power is kept constant. This is only a rough simplification when redesigning the engine and motor sizes, but gives an indication of its consequences.

In the alternative solution the electric machine 1 is designed to almost be able to handle the demanded power of the smooth ECE 15. This leads to increased fuel consumption when driving the rapid US06.

The fuel consumption is however reduced when driving ECE 15 with the alternative design. The alternative design was also equipped with the best value of charging gain. This combination was simulated in ECE 15 and turned out to be increasing the efficiency further.

Maximum vehicle speed

The torque/speed distribution in a vehicle is depending on the vehicle speed maximum. The speed maximum affects in its turn the gear ratio of the vehicle. The default design is given a maximum speed of 160 km/h.

Simulations have been carried out when the maximum speed was reduced to 100 km/h. Since the maximum speed of US06 is 130 km/h, only ECE 15 has been investigated.

It turned out that reducing the maximum speed did not increase the total efficiency, rather the contrary. However when the alternative maximum speed was combined with the alternative engine and motor design, the result did surpass the default design.

6.2 Parallel vs strigear

The strigear hybrid has the advantage to choose the most sufficient topology, parallel or series. In the performed simulation, the used switching condition is the total losses. The outcome of the mode changes is that the parallel mode is the dominating, but not the over all prevailing mode. The switching mode is dependent of the charging gain and other control parameters.

However, the benefits with the strigear system are small, if none, and must be compared to the additional complexity.

6.3 Criteria

Depending on chosen criteria, the result will turn out quite differently. For instance, there are variations of prices to choose from when pricing the emissions as well as variations of applied ranking rates. The results stress the

importance of carefully handling the validation criteria, since a criterion is a possible tool to hide design topology weaknesses. The chosen ranking example adjusts transient values and strengthens small differences.

6.4   Preferred choice

When choosing a HEV topology, it is strongly depending on the application. The simulations point to the parallel topology as the predominant choice. It has a lower complexity than the other topologies presented.

The time constant should be chosen rather fast ($\tau_{ICE} = 1$) and the charging gain should be rather small ($K_{Pice} = 0.03$).

Chapter 7 Future work

To put a full stop to this comparison has not been easy. There are yet further questions that are interesting to investigate. The most essential questions, which are of particular interest for additional efforts, are;

1. Diesel engine
2. Faster ICE, introduction of super capacitors
3. State of the art ICE, assisted by a turbo charger
4. 4QT according to KTH[4]

In Strandh's thesis there is, besides the gasoline engine, a diesel engine. To replace the naturally aspirated gasoline engine in the simulation models with this diesel engine model is the natural continuation of this study. The diesel engine has a higher total efficiency. It is therefore of interest to investigate the impact of improved engine efficiency.

Introducing super capacitors in the HEV model facilitate a faster ICE. Power density may be a limiting factor and the super capacitor will make it possibly to decrease the charging time constant.

The simulated vehicle is the Toyota Prius. There are engines available on the market, and are further improved than the Prius engine. An interesting comparison would therefore be to supply the simulation model with a state of the art ICE, equipped with an electrically assisted turbo charger.

The four-quadrant transducer (4QT) is a HEV concept developed at KTH. The concept claims to combine the advantages from series- and parallel HEV and to results in reduced fuel consumption. To compare this solution with the other simulated HEV would therefore be an interesting continuation of this comparison.

---

[4] Kungliga Tekniska Högskolan, Stockholm

Chapter 8 References

Andersson, Christian et al (2000), Simulation and verification of a hybrid bus, *Norpie* /2000, Aalborg, Denmark.

Andersson, Christian (2001), *Observations on electric hybrid bus design*, Techn. Licentiate thesis, Department of Industrial Electrical Engineering and Automation, Lund University, Lund, Sweden.

Banverket, (1992), Beräkningshandledning, BVH 106, (in Swedish), Planneringsavdelningen, Borlänge, Sweden.

Baretta, Joseph (1998), New classification on electric-thermal hybrid vehicles, *Electric Vehicle Symposium 15*, Brussels, Belgium.

Bäckström, Thomas (2000), *Integrated Energy Transducer Drive for Hybrid Electric Vehicles,* PhD-Thesis, Department of Electric Power Engineering, Electrical Machines and Power Electronics, Royal Institute of Technology, Stockholm, Sweden.

California Air resources Board (2002-03-06), http://www.arb.ca.gov/msprog/ levprog /test_proc.htm.

Dieselnet (2001-03-14), http://www.dieselnet.com/standards/cycles/ece_ eudc.html.

Duoba, Michael et al (2001), Characterization and comparison of two hybrid electric vehicles (HEVs) – Honda Insight and Toyota Prius, 2001-01-1335, *SAE 2001 World Congress*, Detroit, USA.

Eiraku, Akira et al (1998), An application of hardware in the loop simulation to hybrid electric vehicle, *Electric Vehicle Symposium 15*, Brussels, Belgium.

Emissiontrading (2002-02-19), http://www.emissionstrading.com.

European Commission (1999), ExternalE – Externalities of Energy, Vol. 9, Fuel cycles for emerging and end-use technologies, transport & waste, Office for official publications of the European Communities, Luxembourg.

Friedrich, Rainer - Bickel, Peter (2002), Aktueller Stand der externen Kosten und Gesundheitsrisiken durch Energienutzung – Entwurf, (in German), Institute für

Energiewirtschaft und Rationelle Energieanwendung, Univesity of Stuttgart, Stuttgart, Germany.

Harbolla, B. (1992), Analyses of hybrid drive systems with new electric components – morphology, evaluation and optimisation, Institut für Kraftfahrwesen, RWTH Aachen, P-030 out of summary report Advanced electric drive systems for buses, vans and passenger cars to reduce pollution, EDS study, Dec. 1992, Maggetto, Gaston et al.

Heywood, John B. (1988), *Internal combustion engine fundamentals*, McGraw-Hill int. Editions, Automotive Techn. Series, Singapore.

Heilig, Mates (1985), *Kolvmaskiner AK*, (in Swedish), Department of Turbo machines, Lund University, Lund, Sweden.

Hellman, Karl H. et al (1998), Evaluation of a Toyota Prius hybrid system (THS), Technical Report EPA 420-R-98-006, United States Environmental Protection Agency, USA.

Hemmingsson, Morten (1999), *A powerflow control strategy to minimize energy losses in hybrid electric vehicles*, Techn. Licentiate thesis, Department of Industrial Electrical Engineering and Automation, Lund University, Lund, Sweden.

How stuff works, (2001-10-11a), http://www.howstuffworks.com/hybrid-car.htm.

How stuff works, (2001-10-11b), http://www.howstuffworks.com/question66.htm.

INEEL (2002-02-02), http://ev.inel.gov/fop/general_info/aux2.html.

Johansson, Bengt (1999), *Förbränningsmotorer AK*, (in Swedish), Department of Heat and Power Engineering, Combustion Engines, Lund University, Lund, Sweden.

Johnson, Valerie H et al (2001), Development and validation of a temperature-dependent resistance/capacitance battery model for ADVISOR, *Electric Vehicle Symposium 18*, Berlin, Germany.

Karlsson, Hua Lu (2000), Emission test of a Toyota Prius electric vehicle, Report No MTC6017, MTC AB, Haninge, Sweden.

Maggetto, Gadton - Kahlen, Hans (1997), Electric and hybrid vehicles, *EPE –97*, Norway.

Van Mierlo, Joeri et al (1998), Comparison of power control algorithms in hybrid vehicles, *Electric Vehicle Symposium 15*, Brussels, Belgium.

Van Mierlo, Joeri (2000), *Simulation software for comparison and design of electric, hybrid and internal combustion vehicles with respect to energy, emissions and performances*, PhD-thesis, Department of Electrical Engineering, Vrije Universiteit Brussel, Brussels, Belgium.

Miller, John M - Nicastri, Paul R (1998), The next generation automotive electrical power system architecture: issues and challenges, *The AIAA/IEEE/SAE Digital Avionics Systems Conference*, Seattle, USA.

Powertrain (2001-07-11), http://www.powertrain.se.

Preem (2002-02-20), http://www.preem.se.

Toyota Motor Corporation (2000), *PRIUS New Car Features*, May 2000, Pub. No. NCF 184E, Overseas service division, Toyota Motor Corporation, Japan.

SIKA 1999:6, (1999), Översyn av samhällsekonomiska kalkylprinciper och kalkylvärden på transportområdeet – ASEK, (in Swedish), SIKA Rapport 1999:6, Stockholm, Sweden.

SIKA 2000:3, (2000), ASEK kalkylvärden i sammanfattning, (in Swedish), SIKA Rapport 2000:3, Stockholm, Sweden.

Steen, Bengt (1999), A Systematic Approach to Environmental Priority Strategies in Product Development (EPS), Version 2000 - Models and data of the default method, CPM Report 1999:5, Department of Environmental System Analysis, Chalmers University of Technology, Göteborg, Sweden.

Steen, Bengt – Ryding, Sven-Olof (1992), The EPS enviro-accounting method, an application of environmental accounting principles for evaluation and validation of environmental impact design, Swedish environmental Research Institute (IVL), Göteborg, Sweden.

Strandh, Petter – Egnell, Rolf (2001), Modelling SI-engines for hybrid vehicles, SAE 2001-01-0575, *SAE 2001 World Congress*, Detroit, USA.

Strandh, Petter (2002), *Combustion Engine Models for Hybrid Vehicle System Development*, Techn. Licentiate thesis, Department of Heat and Power Engineering, Combustion Engines, Lund University, Lund, Sweden.

Stridsberg, Lennart (1998), Dual electric motor hybrid power train, *Electric Vehicle Symposium 15*, Brussels, Belgium.

U.S. Department of energy, Energy efficiency and renewable energy network (EREN) (2001-10-09), http://www.ott.doe.gov/hev/what.html.

Vedmar, Lars (1998), *Transmissioner*, (in Swedish), Department of Machine Elements, Lund University, Lund, Sweden.

Your dictionary (2001-10-09), http://www.yourdictionary.com/cgi-bin/mw.cgi.

Årzén, Karl-Erik (2000), *Real time control systems*, Department of Automatic Control, Lund University, Lund, Sweden.

Chapter 9 Appendix

9.1   Appendix A; Data according to Toyota Prius

The input data originate from Toyota (Toyota Motor Corporation, 2000) and are used as parameters in the simulation models. The main data are presented in Table 13.

Table 13: Data for Toyota Prius, used as parameters in the simulation models.

Property	Value
Vehicle mass (total) [kg]	1645
Front area [m^2]	2.52
Max power em1 [kW]	33
Max torque em1 [Nm]	350
Max speed em1 [rad/s]	585
Max power em2 [kW]	33
Max torque em2 [Nm]	68
Max speed em2 [rad/s]	471
Max power ICE [kW]	53
Max torque ICE [Nm]	115
Gear ratio ring wheel/wheel axis	3.5
Battery type	NiMH
Maximum charge [kWh]	1.7
Maximum speed [km/h]	160
Battery inner resistance [Ω][5]	0.49-0.56

---

[5] $R_{inner} = f(SOC)$ (Johnson et al, 2001)

9.2   Appendix B; Measurements of Toyota Prius (MTC)

MTC AB is a research, development and test company in Sweden, focusing on engines, vehicles and their environmental effects.

MTC AB has carried out investigations of exhaust emissions from a Toyota Prius marketed in Sweden. For this purpose two driving cycles have been used; the EU2000 Driving Cycle (NEDC) and US06 Supplemental Federal Test Procedure (US06). Both hot and cold tests have been performed (+22°C and -7°C). In the test CO, HC, NO_x and fuel consumption were measured. Some unregulated emissions were measured such as ethylene, propylene, benzene and yet other ones.

In the report, the MTC AB results have not been adjusted for deviation in state of charge of the battery (ΔSOC) at start and stop. The fuel consumption therefore includes possible variations in SOC. For further details, see (Karlsson, 2000).

The investigated vehicle is the Toyota Prius sold in Sweden 2000. That means it is equipped with an engine of 53 kW, an electric machine of 33 kW and a generator of 33 kW.

MTC has used a variant of ECE15 that includes a peak at 120 km/h instead of at 90 km/h. The drive cycle, used by MTC, can be seen in Figure 9-1. In Figure 9-2 and Figure 9-3 are some of the MTC results presented.
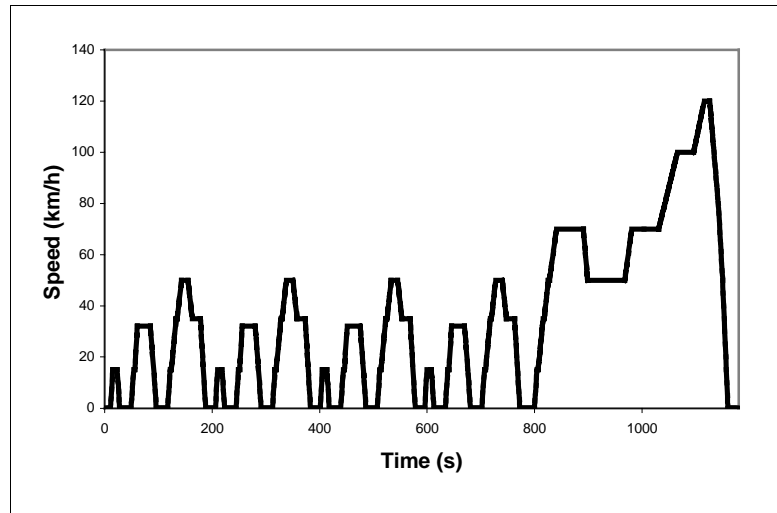
Figure 9-1:   MTC has used a slightly different variant of ECE15. The last
               acceleration has its peak at 120 km/h instead of 90 km/h.
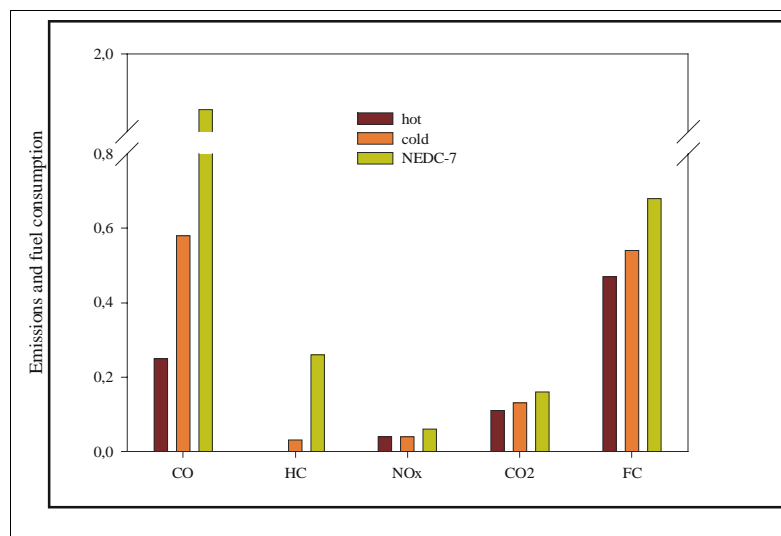
Figure 9-2:   CO, HC, NO_X and CO_2 emissions (g/km) and fuel consumption (l/10
               km) in test-driving the variant of ECE15 viewed in figure XX. The tests
               shown have been hot and cold started at 22°C and cold started at -7°C
               (NEDC-7).
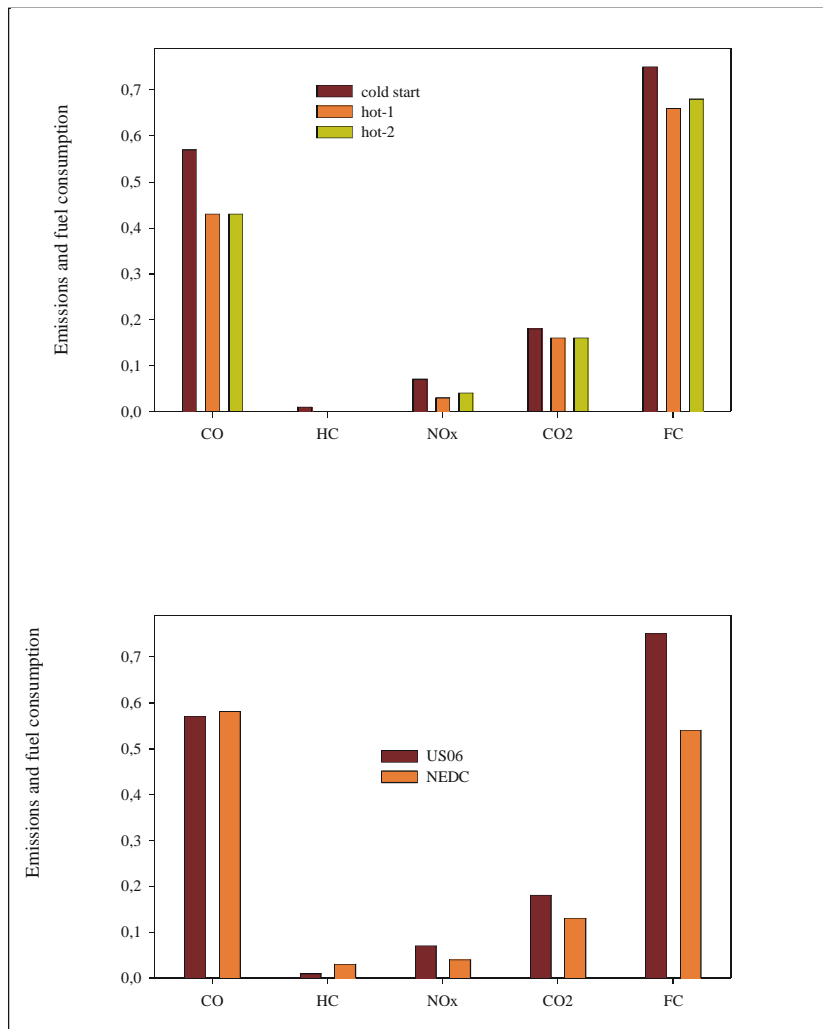
Figure 9-3:   The figure shows the CO, HC and NO_X and CO_2 emission (g/km) and the fuel consumption (FC) (l/10km). The upper graph shows the US06 cycle. The lower graph shows US06 cycle and a variant of ECE15, called NEDC and viewed in figure XX, cold started at 22°C.

9.3   Appendix C; Measurements of Toyota Prius (EPA)

The United States Environmental Protection Agency (EPA) has also carried out tests and measurement of a Toyota Prius. The Prius tested is a Japan-market production vehicle, which is designed for the Japanese market, slightly different from the European one.

The investigated Prius has an engine with a maximum power of 43 kW at 4000 rpm. On an inquiry about the size of the electric machines the author answers by referring to another paper (Duoba et al, 2001). In this paper the Prius, sold at the Japanese market, is investigated and the sizes of the electric machines are accounted to 30 kW at 6000 rpm for the traction motor and 15 kW at 4800 rpm for the generator.

For further details about the measurements see the EPA report (Hellman et al, 1998). The test includes more emission than what is accounted for in the Table 14.

Table 14: Consecutive test over US06 schedule.

| Battery Mode:	HC [g/km]:	CO [g/km]:	NO$_x$ [g/km]:	Fuel Consumption [l/100 km]:	Net Charge [Amp hrs][6]:
"A" [7]	0.019	0.31	0.056	6.35	0.265
"A"	0.019	0.37	0.056	6.42	0.058
"A"	0.019	0.37	0.044	6.42	0.302
"B" [8]	0.019	0.44	0.056	7.31	-0.854
"B"	0.019	0.56	0.044	7.15	-0.554
"B"	0.025	0.44	0.056	7.12	-0.405

EPA includes measurements made upon other vehicles with about the same fuel economy as Toyota Prius, as a comparison. This is made with the interest of compare the emissions of the other vehicles. The results of this comparison are shown in Table 15 and Table 16, and all emission data derive from low mileage data.

---

[6] Negative values relate to net battery-pack charging over the test cycle; position values relate to net battery-pack discharge over cycle.

[7] "A" denotes normally charged battery pack prior to first US06, then followed by two additional US06 tests in succession.

[8] "B" denotes deep discharge of battery pack, evidenced by dashboard warning indicator, prior to test over US06 cycle.

Table 15: Comparison of emissions from high fuel economy vehicles.

Vehicle:	Car Class:	Weight [kg]:	HC [g/km]:	CO [g/km]:	NO_x [g/km]:
Suzuki Metro	Sub-compact	964	0.02	0.19	0.02
VW New Beetle	Sub-compact	1417	0.04	0.06	0.43
VW Passat	Mid-size	1531	0.14	0.31	0.38
VW Jetta	Compact	1417	0.06	0.25	0.37
Toyota Prius	Sub-compact	1361	0.04	0.31	0.03
Toyota Corolla	Compact	1247	0.11	0.75	0.07

Table 16: Continuation of Table 15.

Vehicle:	Fuel Consumption [l/100 km]:	Transmission:
Suzuki Metro	4.32	M5[9]
VW New Beetle	4.56	M5
VW Passat	4.67	M5
VW Jetta	4.62	M5
Toyota Prius	4.84	THS[10]
Toyota Corolla	6.44	M5

9.4 Appendix D; The California Air Resources Board Low-Emission Vehicle Regulations

The California Air Resources Board administrates the California low-emission vehicle (LEV) regulations. The regulations are available on the net (California Air Resources Board, 2002). The LEV regulations were originally

---

[9] Manual 5-speed gearbox.
[10] Toyota Hybrid System.

adopted in a 1990-91 rulemaking and became generally applicable in the 1994 model year. The program also includes requirements for the introduction of zero-emission vehicles (ZEVs).

Following a hearing 1998 in the *LEV II* regulations were adopted and they will become applicable with the 2004 model year. The original LEV standards are now referred as the *LEV I standards*.

The LEV I standards are contained primary in § 1960.1. This section includes all of the California exhaust emission standards for 1981 trough 2003 model year passenger cars (PC), light duty trucks (LDT) and medium duty vehicles (MDV).

Section § 1960.1(g) describes the standards for the LEV I, TLEV (transitional LEV), and ULEV (ultra LEV) for passenger cars and light-duty trucks. The sections claims that the exhaust emissions from new 1992 through 2003 model-year LEV I transitional low-emission vehicles, and new 1992 through 2006 model-year LEV I low-emission vehicles and ultra-low-emission vehicles, in the passenger car and light-duty truck classes shall not exceed the emission values shown in Table 17.

Table 17: LEV I exhaust emission standards for transitional low-emission vehicles, low-emission vehicles, ultra-low-emission vehicles and zero-emission vehicles in passenger car and light duty truck vehicle classes. The table shows an extract from the standard, concerning passenger cars and all light-duty trucks.

Vehicle weight [kg]:	Durability vehicle Basis [km]:	Vehicle Emission Category:	HC [g/km]:	CO [g/km]:	NO$_x$ [g/km]:
0-1700	80000	TLEV	0.078	2.1	0.2
0-1700	80000	LEV	0.046	2.1	0.1
0-1700	80000	ULEV	0.025	1.1	0.1
0-1700	160000	TLEV	0.097	2.6	0.4
0-1700	160000	LEV	0.056	2.6	0.2
0-1700	160000	ULEV	0.034	1.3	0.2

The Supplemental Federal Test Procedure (SFTP) exhaust emission standards for 2001 and subsequent model LEVs and ULEVs in the passenger cars and light-duty truck classes, and 2003 and subsequent LEVs, ULEVs, and SULEVs (super ULEVs) in the medium-duty classes shall not exceed the levels stated in § 1960.1(r) (Table 18). They are applicable for both LEV I and LEV II vehicles.

Table 18: SFTP exhaust emission standards for low-emission vehicles, ultra-low-emission vehicles and super-ultra-low-emission vehicles in the passenger car, light-duty truck and medium-duty vehicle classes. The table shows an extract of the standard.

Vehicle Type:	Loaded Vehicle Weight [kg]:	US06 Test [g/km]:	
		$NMHC^{11} + NO_x$:	CO:
PC	All	0.09	5.0
LDT	0-1700	0.09	5.0
LDT	1700-2600	0.16	6.5
MDV	1700-2600	0.25	6.5
MDV	2600-3900	0.37	7.3

For further information about the tables, its calculations and regulations see the web site for California Air Resources Board, where the figures are explained in detail.

---

[11] NMHC + NO_x means non-methane hydrocarbon plus oxides if nitrogen emissions.

Chapter 10 Abbreviations

A_v	vehicle front area
$C_{batt\_thermal}$	thermal capacity
C_d	air resistance
C_r	rolling resistance
CO	carbon monoxide
CHR	combustion hybridisation rate
EHR	electric hybridisation rate
ELU	environmental load unit
EPA	Environmental protection agency
EPS	environmental priority strategies
F^*_{tot}	total requested force
HEV	hybrid electric vehicles
HC	hydrocarbon
ICE	internal combustion engine
J	moment of inertia
K_{Pice}	charging gain
K_s	speed regulation device gain
$K_{\omega_{r\_to\_speed}}$	gain factor, used in the PSH to obtain the velocity
LEV	low-emission vehicle
M_v	vehicle mass
$NiMH$	nickel metal hydride
NO_X	nitrogen oxide
P_{aux}	auxiliary power
P_{batt}	battery power
P_{el}	electric power
P_{em1}	power, electric machine 1
P_{em2}	power, electric machine 2
P^*_{ice}	ICE power reference value
P_{loss}	power losses
P_{max}	maximum power

P_r resistance power

P_{th} thermal power

$P_{tractive}$ tractive power

PE power electronics

PSH power split hybrid

$R_{batt\_thermal}$ battery thermal resistance

R_{inner} battery inner resistance

R_{planet} radius of planet wheel

RH rate of hybridisation

S_v vehicle speed

$SFTP$ supplemental federal test procedure

SOC state of chart

SOC^* state of chart reference

SOC_{start} state of chart at start

SOC_{stopp} state of chart at stop

$SULEV$ super ultra low-emission vehicle

TWC tree-way catalytic converter

T torque

T^*_{em1} torque reference value, electric machine 1

T^*_{em2} torque reference value, electric machine 2

T_{emp} battery temperature

T^*_{ice} ICE torque reference

T_{outer} outdoor temperature

T^*_{tot} total requested torque

T^*_{wheel} wheel torque reference

$TLEV$ transitional low-emission vehicle

UDC urban driving cycle

$ULEV$ ultra low-emission vehicle

ZEV zero-emission vehicle

$W_{batt,\,max}$ maximum battery energy

$bsfc$ brake specific fuel consumption

c carrier wheel

c_p specific heat of a gas at constant pressure

c_v specific heat of a gas at constant volume

e electric power

$em1$ electric machine 1

$em2$ electric machine 2

g a radius (see Figure 2-12)

gr_1 gear ratio, gear box 1

gr_2	gear ratio, gear box 2
i	current
m	mass
n	grasping of teeth with the planet wheel(s)
p	planet wheel
p_f	mean pressure to overcome the mechanical friction losses
p_i	indicated mean pressure of a ICE
r	ring wheel
r_{wheel}	wheel radius
s	sun wheel
strigear	sequentially run, triple gearbox connected engine/motor hybrid
u	actuator output
u_{batt}	battery voltage
v	velocity
v^*	velocity reference
z	number of tooth
ΔP	sum of electric power, flowing out of the battery
ε	compression rate of an ICE
η_{batt}	battery efficiency
η_{em1}	efficiency of electric machine 1
η_{em2}	efficiency of electric machine 2
η_{ice}	ICE efficiency
η_m	mechanical efficiency of an ICE
η_t	theoretical efficiency of a piston engine
κ	adiabatic exponent ($=c_p/c_v$)
λ	ratio between the amount of actual and stoichiometric fuel-to-air mixture
ρ	radius on which the circumferential forces, $n*T$, acts
ρ_a	air density
τ_i	integrator time constant
τ_{ICE}	ICE time constant, low pass filtering the P^*_{ice}
τ_t	tracking time constant
ω	speed
$\omega_{carrier}$	speed of carrier wheel
ω_{em1}	speed of electric machine 1
ω^*_{em1}	speed reference of electric machine 1
ω^*_{ice}	ICE speed reference

ω_{ring} speed of ring wheel
ω_{solar} speed of sun wheel
4QT   four-quadrant transducer